STUDIES ON AMYLOID AGGREGATION AND CROSS-SPECIES PRION TRANSMISSION

A Dissertation
Presented to
The Academic Faculty

by

Aditi Sharma

In Partial Fulfillment
of the Requirements for the Degree
Doctorate of Philosophy in Bioengineering

Georgia Institute of Technology
May 2018

STUDIES ON AMYLOID AGGREGATION AND CROSS-SPECIES PRION TRANSMISSION

Approved by:

Dr. Andreas S. Bommarius, Advisor
School of Chemical and Biomolecular Engineering
Georgia Institute of Technology

Dr. Julie A. Champion
School of Chemical and Biomolecular Engineering
Georgia Institute of Technology

Dr. Yury O. Chernoff, Advisor
School of Biology
Georgia Institute of Technology

Dr. M. G. Finn
School of Chemistry and Biochemistry
Georgia Institute of Technology

Dr. Sven H. Behrens, Advisor
School of Chemical and Biomolecular Engineering
Georgia Institute of Technology

Date Approved: [February 05, 2018]

ACKNOWLEDGEMENTS

I would like to begin by thanking my advisor Dr. Andreas S. Bommarius for giving me the opportunity to work on this project and be a part of his lab. His positive outlook, enthusiasm, immense knowledge of his field, excellent communication skills, and an energetic personality made him a great role model and advisor. His support and encouragement helped me get through periods of slow research progress. I am especially grateful for the freedom he gave to me to shape this thesis and to develop into an independent researcher. I would also like to thank my co-advisors Dr. Yury O. Chernoff and Dr. Sven H. Behrens for the help and guidance that they provided over the years. I have always been astounded by and have greatly admired the depth of their knowledge in their respective fields. Their advisement was certainly irreplaceable in improving this thesis work. I am truly honored to work alongside this trio of brilliant scientists and engineers. I also thank my committee members, Dr. Julie A. Champion and Dr. M. G. Finn for their invaluable feedback. I appreciate their thoughtful questioning which tested and improved my understanding, and suggestions which helped make this work better.

I would also like to thank all the present and former members of the Bommarius lab for making my life in the lab memorable and enjoyable. I really appreciate the interest everyone took in my project and I am grateful for the ingenious suggestions and help that I received. It was a privilege to be a part of such a brilliant and intellectual lab group. I am thankful to Dr. Jonathan Rubin for introducing me to my project, training me, and getting me started on my thesis project. I thank Harrison Rose for taking a special interest in my project and for his contribution to the computational modeling aspect of my project. Dr.

Bettina Bommarius for the help, support, and advice that she provided. I would also like to thank Dr. Samantha Au for being a good friend and colleague and I cherish the time spent with her in lab. I feel privileged to have worked alongside many other great colleagues – Past members: Dr. Marietou Paye, Dr. Jonathan Park, Dr. Yuzhi Kang, Dr. Lizzette M. Gómez Ramos, Dr. Ryan Clairmont, and Dr. Michael Rood: thank you welcoming me to the lab and for all the help and support; Current members: Dr. Mick Robbins, Thomas Kwok, Robbie Franklin, Matt McDonald, Adam Caparco, Michael Stellato, and Nick Kruyer: thank you for all the fun and entertainment that you provided over the years that made it a pleasure to come to lab. I thank my undergraduate students - Victoria Ratte, Farida Jariwala, and Zhe Liu for their contributions to different aspects of my thesis project. I am also grateful to have been a part of the Chernoff lab group. I thank Kathryn Bruce for her contributions to the species barrier work and Zack Deckner for the help he provided over the years. I especially thank Pavithra Chandramowlishwaran for being a great friend and mentor. I appreciate the interest she took in my project as well as all the help she provided. It was a delight to have her company during my stay here at Georgia Tech.

I would also like to thank my friends in Atlanta and other parts of the US who made my life outside of lab enjoyable. It was always a great pleasure to visit friends back in India during my yearly vacations: thank you for making each vacation in India extremely memorable and joyous, spending time with you all refreshed and recharged me for another year of hard work.

Finally, I would like to thank my family for their never-ending love and support. I thank my parents and brother for always believing in me: just knowing that you are there to help and support me has always been enough. I also thank my in-laws for the love and

affection that they have given me and I am truly grateful to have them in my life. Last but not the least, I would like to thank my loving husband, Pratik Mital, for being my pillar of strength and my constant source of support and encouragement: thank you for being my partner in everything and for always being there for me.

.

TABLE OF CONTENTS

LIST OF TABLES

LIST OF FIGURES

SUMMARY

Proper folding of protein molecules into their native structure is necessary to maintain function. Misfolding of proteins can reduce functionality as well as result in the formation of amorphous aggregates or ordered aggregates like amyloids. Amorphous aggregate formation during production, transport, and storage of protein-based biologics is a cause of concern in the biopharmaceutical industry as it results in a reduction in the efficacy or activity of the active pharmaceutical ingredient. On the other hand, ordered aggregation of proteins into amyloids (and their transmissible versions, prions) has been shown to result in several neurodegenerative diseases in humans and other mammals. While the effect of co-solutes including ions has been extensively studied in the context of measuring the stability of protein formulations and formation of disordered aggregates, there is limited information available on the effect of ions on the formation of ordered amyloid aggregates. In this thesis, we have investigated in detail the effect of presence of ionic co-solutes on the aggregation of amyloids.

Here, we have studied the efficiency of cross-transmission of the NM fragment of Sup35 protein, from three closely related species of the *Saccharomyces sensu stricto* group, namely *S. cerevisiae*, *S. bayanus* and *S. paradoxus*, amongst each other. Using ions of the Hofmeister series, we discerned the relative effects of protein sequence, seed conformation, and environment on the cross-species transmission of this protein. Further, investigation of the fibrillation of Amyloid beta-42 ($A\beta_{42}$) and Sup35NM in the presence of anions of the Hofmeister series at pH above and below their isoelectric points uncovered interesting differences in their aggregation behavior pointing to key differences in the aggregation

mechanism and the biophysical/biochemical properties of these proteins. Lastly, we developed a computational model for amyloid aggregation kinetics and used it for global fitting of Sup35NM amyloid aggregation data. In all, this thesis expands the current knowledge of ion-specific effects on aggregation of amyloid proteins as well as of the mechanisms of amyloid aggregation.

CHAPTER 1. INTRODUCTION

Proteins are an important class of biomolecules which carry out a variety of biological functions like biocatalysis, transport, storage, motility, regulation or signal transduction, etc. The functionality of proteins depends on proper folding into a three-dimensional structure. If a protein is not correctly folded into its native functional conformation, then its ability to perform its function is compromised. Reasons for improper or incomplete folding of a protein include mutations in the gene encoding the protein, mistakes by the translation machinery or ribosome, and external stresses such as high temperature, oxidative stresses, etc. Misfolding of proteins can result in aggregation as a consequence of minimizing the energetic penalty of exposing certain amino acid residues or due to attractive forces between some regions on the protein. Living organisms have mechanisms in place to ensure proper folding and prevent aggregation of proteins. Chaperones are a class of 'helper' proteins which constitute the biological machinery that assists in the protein folding process. Chaperones act through different mechanisms such as providing a favorable local environment for folding, preventing collapse and aggregation of partially unfolded regions, and catalyzing folding. Misfolded and aggregated proteins can be detrimental to cellular function and are targeted for degradation by the ubiquitin-proteasome system or through vacuolar proteolysis so that the amino acid precursors can be recycled and to rid the cells of damaged and dysfunctional proteins. Thus, chaperones and protein degradation machinery are central to maintaining protein quality control *in vivo* and ensuring that cellular proteins are functional which in turn is crucial for proper cellular functioning.

1.1 Protein folding, misfolding, and aggregation

The process of protein folding consists of three steps. First step is the fast collapse or the burst phase, during which the polypeptide chain folds into a molten globule which has a secondary structure and some super secondary structure. This process typically occurs on the time scale of milliseconds. The burst phase is followed by intermediate folding where a tertiary structure is formed on the order of milliseconds to seconds. Finally, the protein folds to the final native state in less than a second. The dynamics of protein folding is depicted by the folding funnel diagram shown below in Figure 1.1.

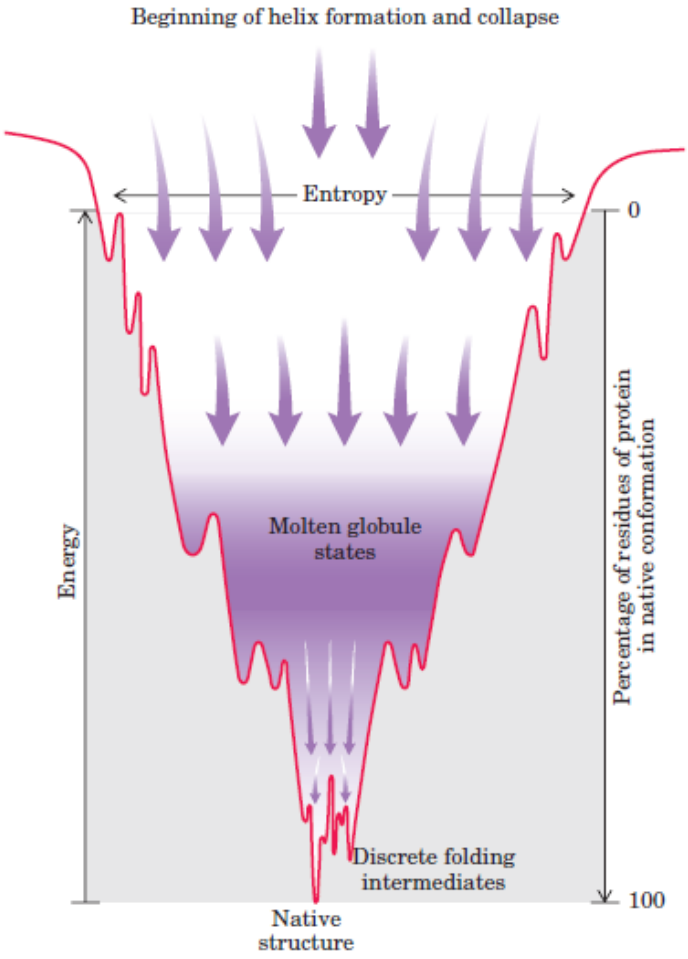

Figure 1.1 – Thermodynamics of protein folding depicted as a free-energy funnel [1]

Protein folding to the lower free-energy native state is a thermodynamically favorable reaction. However, the protein molecule can get trapped in any of the states which correspond to the various local minima along the free energy folding landscape to the native state. Such partially folded or misfolded states often tend to form aggregates which can be amorphous or ordered in nature.

The various fates of a newly synthesized protein are depicted in Figure 1.2

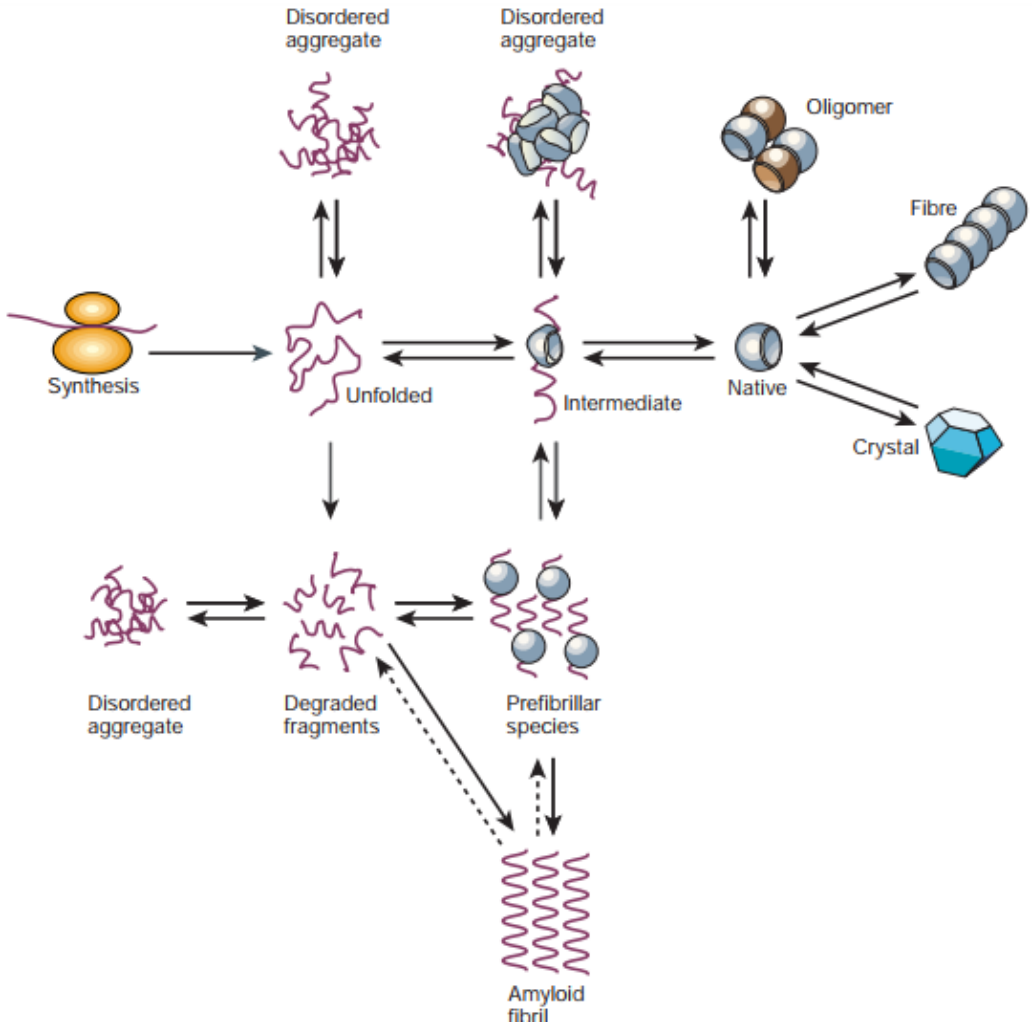

Figure 1.2 – A unified view of some of the types of structure that can be formed by polypeptide chains [2]

1.1.1 Amorphous and Ordered Protein Aggregation

Amorphous aggregates are generally formed by misfolded or partially folded proteins with exposed hydrophobic residues. The protein molecules try to minimize the energetic penalty due to exposure of these residues in an aqueous polar environment by associating together and hiding the hydrophobic residues inside the aggregate mass. Disordered or amorphous aggregation can occur as a consequence of denaturation of proteins by denaturing agents such as urea, high temperature, acidic or basic conditions etc.

While most proteins have been shown to form amorphous aggregates, only a special class of proteins can form ordered, amyloid-like fibrous aggregates under moderate conditions. These amyloidogenic proteins can undergo a conformation change into an alternate, stable, and self-transmissible β-sheet rich configuration [3-6]. The amyloid conformation lends the protein molecules a tendency to associate with other protein molecules through β-sheet interactions and form ordered fibrous aggregates. The aggregation process is generally considered to proceed via a monomer addition mechanism where the incoming non-amyloid monomer undergoes a conformational conversion to the amyloid form as it adds to the amyloid polymer. While amyloids form a unique class of proteins which form these ordered fibrous aggregates under moderate conditions, many other proteins have been also shown to form amyloid-like aggregates under extreme conditions like very high or low pH or temperature [2].

A more inclusive depiction of the folding landscape shows how proteins can get trapped as amorphous or ordered aggregates which represent alternate stable minima besides the native state (see Figure 1.2).

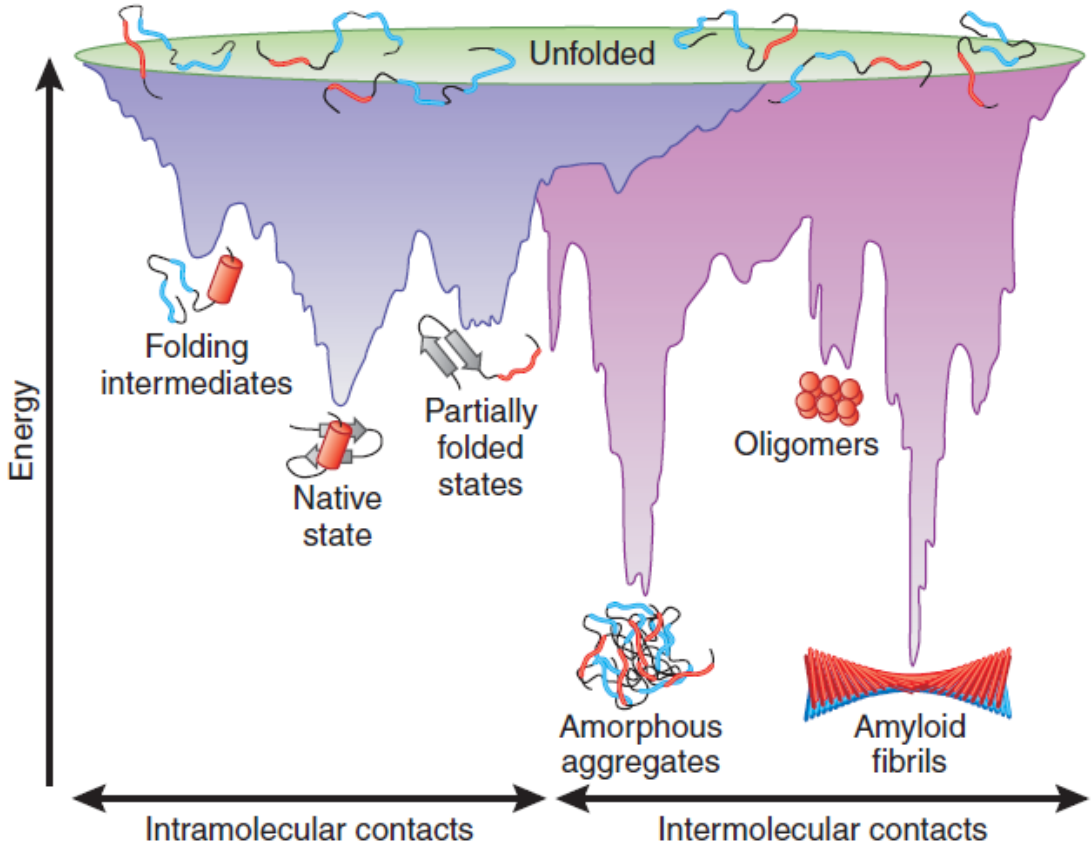

Figure 1.3 – Energy landscape scheme of protein folding and aggregation [7]

In addition to being an energetically unfavorable occurrence *in vivo*, protein aggregation can also be highly toxic to the cells. For example, the formation of amyloid aggregates can result in a number of diseases in mammals. Protein aggregation is also an undesirable occurrence during the synthesis, purification, formulation, and storage of

protein based biopharmaceuticals, such as enzymes, antibodies, etc. Aggregates are detrimental because they reduce efficacy or activity of the desired protein, are aesthetically undesirable, and, most importantly, may incite an immunogenic response within the patient [8-10].

1.2 Amyloids/Prions

Amyloids which have been shown to be transmissible from one organism to another are called prions (Proteinaceous Infectious Particles). The nature of these infectious agents and their mechanism of transmission had evaded scientists for a long time until they were identified to be proteins [11, 12]. There are about 40 genetic or sporadic amyloid diseases in humans. Amyloids and prions are involved in several neurodegenerative diseases in mammals, namely Alzheimer's disease, Parkinson's disease, Creutzfeldt-Jakob disease, kuru, bovine spongiform encephalopathy, scrapie, chronic wasting disease etc. as well as other diseases such as diabetes mellitus type-II, atherosclerosis, etc. [13-18]. Nevertheless, it is important to note that not all amyloids cause diseases. Self-assembled amyloids or amyloid-like protein assemblies also perform biological roles such as in scaffolding of covalent polymers e.g. in melanin, spider and insect silk, and long term memory in Drosophila [19, 20]. Consequently, there is a lot of interest in studying the aggregation properties of this curious class of proteins.

Several prions have also been identified in yeast. However, whether yeast prions cause disease like mammalian prions is a topic of debate in the scientific community [21, 22]. It is widely believed that yeast prions act as non-Mendelian elements of inheritance

[23-26]. Yeast prions have been extensively studied and the “protein only” model for prion transmission was proven in yeast [27].

1.2.1 Methods for studying amyloid aggregation

The most common and straightforward techniques for monitoring amyloid aggregation involve the use of dyes such as Thioflavin T, Congo red, ANS, and oligothiophenes, which bind to protein molecules present in the amyloid state and exhibit enhanced fluorescence or birefringence [28, 29]. Fluorescence/absorbance data obtained using dyes for simple non-seeded amyloid aggregation generally follows a sigmoidal behaviour as shown in Figure 1.4

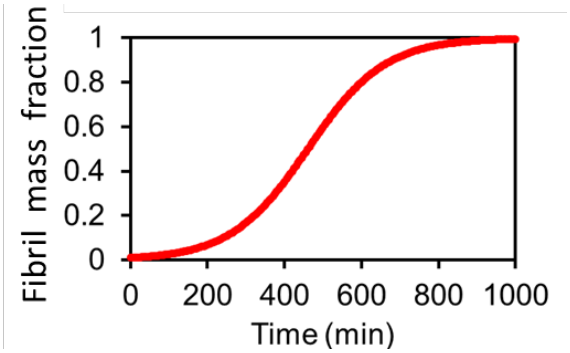

Figure 1.4 – Typical sigmoidal amyloid aggregation curve

Other methods that track the fiber/aggregate fraction include direct absorbance or turbidity measurements. Light scattering is generally used to monitor the size of the aggregates but runs into the issue of the sample becoming highly polydisperse as more and more aggregates are formed. Microscopic techniques such as transmission electron microscopy, atomic force microscopy and fluorescence microscopy of labelled proteins/peptides are widely used to image aggregates. Other qualitative techniques include

analysing the insolubility of aggregate sample in the presence of detergents like SDS, analysing protease resistance, and electrophoresis techniques such as SDS-PAGE, SDD-AGE (Semi-Denaturing Detergent Agarose Gel Electrophoresis), and capillary electrophoresis, etc [30].

1.2.2 Factors affecting amyloid aggregation

The main factors which affect the amyloid aggregation process are the primary sequence of the protein and environmental conditions such as temperature, pH, presence of co-solutes, or agitation. [31-34]. Rubin et al. 2013 demonstrated ion-specific effects on the aggregation process of the prion domain containing fragment of Sup35 protein from *Saccharomyces cerevisiae* [32]. It was shown that ions influenced both the aggregation kinetics as well as the structure of the aggregates as observed by AFM and TEM analysis. Further, aggregates formed in the presence of different ions resulted in phenotypically different characteristics when transfected into yeast cells. Sup35NM has also been shown to form different strains of [*PSI+*] when nucleation occurs at different temperatures [34-36]. Tanaka et al. 2004 studied the effect of temperature on aggregation of Sup35NM from *Saccharomyces cerevisiae* and found that a lower temperature (4°C) resulted in faster kinetics and phenotypically “strong” variant while a high aggregation temperature (37°C) resulted in slower kinetics and a phenotypically “weak” variant when transfected into *Saccharomyces cerevisiae* [34].

1.2.3 Hofmeister Series

The effect of ions on protein solubility and conformation was first studied by the Czech scientist, Franz Hofmeister, in the 1888. He arranged anions and cations based on

their ability to salt out (precipitate) hen egg white lysozyme. This arrangement of ions is termed as the Hofmeister series [37]. The complete series as discovered in Hofmeister's original work is given below [38].

Hofmeister series of anions

$SO_4^{2-} > HPO_4^{2-} > CH_3CO_2^- > C_3H_5O(CO_2)_3^{3-} > C_4H_4O_6^{2-} > HCO_3^- > CrO_4^{2-} > Cl^- > NO_3^- > ClO_4^-$

Hofmeister series of cations:

$Li^+ > Na^+ > K^+ > NH_4^+ > Mg^{2+}$

A lower concentration of the ions on the left of both the series were required to precipitate the protein while a higher concentration of the ions on the right was required for precipitation. Today, these series have been extended to other ions and the ions are usually arranged as per the ability to stabilize the native structure of proteins. In general, the ions which are larger in size, weakly hydrated, less polarized, decrease surface tension, and increase protein solubility are called 'chaotropes' while the smaller, strongly hydrated ions which increase surface tension and decrease protein solubility, favoring the most compact conformation are called 'kosmotropes'. While the underlying mechanism of how ions stabilize/destabilize protein structure is not completely know, two main hypotheses have been considered. The first is based on the ability of ions to make and break hydrogen bonds (hence the terms 'chaotropes' or 'water structure breakers' and 'kosmotropes' or 'water structure makers'). However, this idea has been challenged by studies that reveal that influence of salts beyond the second solvation shell is not enough to account for their

effects on protein structure [39-41]. The second hypothesis suggests that dispersion forces play a significant role in ion effects [42, 43].

Previous work from our group has shown that the effect of ions on the aggregation kinetics and the structure of the amyloid aggregates formed by the prion domain containing NM fragment of the protein Sup35 from *Saccharomyces cerevisiae* at a pH of 7.4 correlates very well with their position in the Hofmeister series [31, 32].

1.3 Proteins in this Study

In this study, we have mainly worked with two proteins namely, yeast prion protein, Sup35 and human Amyloid beta$_{42}$ (Aβ_{42}).

1.3.1 Sup35p

Prions act as protein-based elements of inheritance in yeast. [*PSI*$^+$] is one such yeast prion which results from the conformational change of cellular Sup35 protein to the prion form [44-46]. Sup35 is a subunit of the eukaryotic translation termination factor, eRF3. The conversion to [*PSI*$^+$] causes loss of functionality resulting in reduced translational termination fidelity and nonsense read through. Since its discovery Sup35, has served as a model for studying the formation and propagation of amyloid aggregates [25, 47].

Sup35 can be divided into 3 segments –N (N-terminal domain), M (middle domain), and C (C-terminal domain). The N fragment is responsible for the prion characteristics of Sup35, the C fragment is responsible for its translation termination function and the function of the middle domain is not known yet.

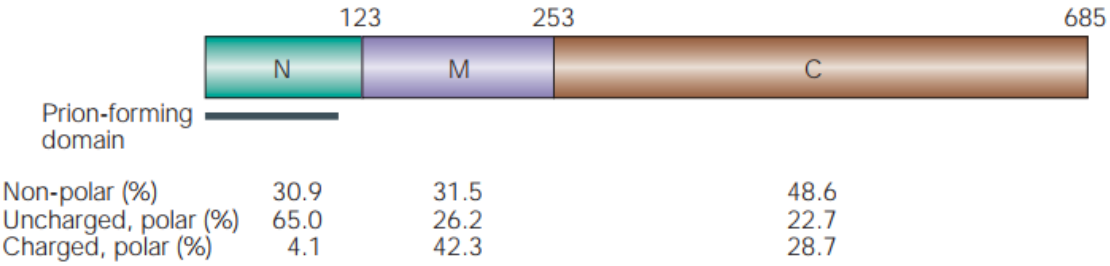

Figure 1.5 – Domains of Sup35 and their amino acid compositions [45]

The NM fragment of Sup35 is widely used to study amyloid formation *in vitro* since the N fragment alone is difficult to express and purify, is insoluble and aggregates too fast. Here, we have used Sup35NM as a model protein in all the sub aims of this thesis.

1.3.2 Amyloid beta$_{42}$ (Aβ$_{42}$)

Aβ$_{42}$ is a 42 amino acid-long peptide formed by the proteolytic cleavage of amyloid precursor protein (APP). It is considered to be the causal factor for Alzheimer's disease [48-51]. It forms fibrillar aggregates which associate together resulting in the formation of amyloid plaques in the central nervous system of the patient and lead to neuronal cell death and degeneration. Recent work on demonstrating the structure of Aβ$_{42}$ fibers has shown that in the fibrillar form the peptide buries its hydrophobic residues in the core of symmetrical dimers that are stacked perpendicular to the axis of the fiber [52, 53].

1.4 Map of this Dissertation

This thesis is organized in the following manner. Chapter 2 describes studies done to understand the main factors affecting the cross-species transmission of Sup35NM between three closely related *Saccharomyces* species. The environment of aggregation and

the seed 'strain' were modulated with the help of ions to investigate the relative impact of the protein sequence, strain, and environment on co-aggregation. Chapter 3 looks at the specific effects of ions on the aggregation kinetics of Sup35NM and $A\beta_{42}$ *in vitro* at pH values above and below the isoelectric points of the two proteins. Electrophoretic mobility measurements were also done to determine how ions interact with the proteins and understand the relative differences in the aggregation behavior of these two proteins. Chapter 4 discusses the development of a simulation-based computational model for amyloid aggregation kinetics. The model is compared with existing models that have been used for fitting aggregation data collected for other proteins.

1.5 References

1. Boyle, J., *Lehninger principles of biochemistry (4th ed.): Nelson, D., and Cox, M*. Biochemistry and Molecular Biology Education. Vol. 33. 2005: John Wiley & Sons Inc. 74-75.

2. Dobson, C.M., *Protein folding and misfolding.* Nature, 2003. **426**(6968): p. 884-890.

3. Prusiner, S.B., *Prions.* Proceedings of the National Academy of Sciences, 1998. **95**(23): p. 13363-13383.

4. Pan, K.-M., M. Baldwin, J. Nguyen, M. Gasset, A. Serban, D. Groth, I. Mehlhorn, Z. Huang, R.J. Fletterick, and F.E. Cohen, *Conversion of alpha-helices into beta-sheets features in the formation of the scrapie prion proteins.* Proceedings of the National Academy of Sciences, 1993. **90**(23): p. 10962-10966.

5. Nguyen, J., M.A. Baldwin, F.E. Cohen, and S.B. Prusiner, *Prion Protein Peptides Induce. alpha.-Helix to. beta.-Sheet Conformational Transitions.* Biochemistry, 1995. **34**(13): p. 4186-4192.

6. Ross, E.D., A. Minton, and R.B. Wickner, *Prion domains: sequences, structures and interactions.* Nature cell biology, 2005. **7**(11): p. 1039-1044.

7. Hartl, F.U. and M. Hayer-Hartl, *Converging concepts of protein folding in vitro and in vivo.* Nat Struct Mol Biol, 2009. **16**(6): p. 574-81.

8. Wang, W., S.K. Singh, N. Li, M.R. Toler, K.R. King, and S. Nema, *Immunogenicity of protein aggregates—concerns and realities.* International journal of pharmaceutics, 2012. **431**(1): p. 1-11.

9. Hermeling, S., D.J. Crommelin, H. Schellekens, and W. Jiskoot, *Structure-immunogenicity relationships of therapeutic proteins.* Pharmaceutical research, 2004. **21**(6): p. 897-903.

10. Rosenberg, A.S., *Effects of protein aggregates: an immunologic perspective.* The AAPS journal, 2006. **8**(3): p. E501-E507.

11. Prusiner, S.B., *Novel proteinaceous infectious particles cause scrapie.* Science, 1982. **216**(4542): p. 136-144.

12. Kocisko, D.A., J.H. Come, S.A. Priola, B. Chesebro, G.J. Raymond, P.T. Lansbury, and B. Caughey, *Cell-free formation of protease-resistant prion protein.* 1994.

13. Chiti, F. and C.M. Dobson, *Protein misfolding, functional amyloid, and human disease.* Annu. Rev. Biochem., 2006. **75**: p. 333-366.

14. Eisenberg, D., R. Nelson, M.R. Sawaya, M. Balbirnie, S. Sambashivan, M.I. Ivanova, A.Ø. Madsen, and C. Riekel, *The structural biology of protein aggregation diseases: Fundamental questions and some answers.* Accounts of chemical research, 2006. **39**(9): p. 568-575.

15. Gregersen, N., P. Bross, S. Vang, and J.H. Christensen, *Protein misfolding and human disease.* Annu Rev Genomics Hum Genet, 2006. **7**: p. 103-24.

16. Jackson, G.S. and A.R. Clarke, *Mammalian prion proteins.* Current opinion in structural biology, 2000. **10**(1): p. 69-74.

17. Höppener, J.W., M.G. Nieuwenhuis, T.M. Vroom, B. Ahrén, and C.J. Lips, *Role of islet amyloid in type 2 diabetes mellitus: consequence or cause?* Molecular and cellular endocrinology, 2002. **197**(1): p. 205-212.

18. Westermark, P., G. Mucchiano, T. Marthin, K.H. Johnson, and K. Sletten, *Apolipoprotein A1-derived amyloid in human aortic atherosclerotic plaques.* The American journal of pathology, 1995. **147**(5): p. 1186.

19. Fowler, D.M., A.V. Koulov, W.E. Balch, and J.W. Kelly, *Functional amyloid–from bacteria to humans.* Trends in biochemical sciences, 2007. **32**(5): p. 217-224.

20. Maury, C., *The emerging concept of functional amyloid.* Journal of internal medicine, 2009. **265**(3): p. 329-334.

21. McGlinchey, R.P., D. Kryndushkin, and R.B. Wickner, *Suicidal [PSI+] is a lethal yeast prion.* Proceedings of the National Academy of Sciences, 2011. **108**(13): p. 5337-5341.

22. Shorter, J. and S. Lindquist, *Prions as adaptive conduits of memory and inheritance.* Nature Reviews Genetics, 2005. **6**(6): p. 435-450.

23. Wickner, R.B., H.K. Edskes, M.-L. Maddelein, K.L. Taylor, and H. Moriyama, *Prions of yeast and fungi Proteins as genetic material.* Journal of Biological Chemistry, 1999. **274**(2): p. 555-558.

24. Wickner, R.B., H.K. Edskes, F. Shewmaker, and T. Nakayashiki, *Prions of fungi: inherited structures and biological roles.* Nature reviews microbiology, 2007. **5**(8): p. 611-618.

25. Liebman, S.W. and Y.O. Chernoff, *Prions in yeast.* Genetics, 2012. **191**(4): p. 1041-1072.

26. Halfmann, R., D.F. Jarosz, S.K. Jones, A. Chang, A.K. Lancaster, and S. Lindquist, *Prions are a common mechanism for phenotypic inheritance in wild yeasts.* Nature, 2012. **482**(7385): p. 363-368.

27. King, C.Y. and R. Diaz-Avalos, *Protein-only transmission of three yeast prion strains.* Nature, 2004. **428**(6980): p. 319-23.

28. Nilsson, M.R., *Techniques to study amyloid fibril formation in vitro.* Methods, 2004. **34**(1): p. 151-160.

29. Hawe, A., M. Sutter, and W. Jiskoot, *Extrinsic fluorescent dyes as tools for protein characterization.* Pharm Res, 2008. **25**(7): p. 1487-99.

30. Pryor, N.E., M.A. Moss, and C.N. Hestekin, *Unraveling the early events of amyloid-beta protein (Abeta) aggregation: techniques for the determination of Abeta aggregate size.* Int J Mol Sci, 2012. **13**(3): p. 3038-72.

31. Yeh, V., J.M. Broering, A. Romanyuk, B. Chen, Y.O. Chernoff, and A.S. Bommarius, *The Hofmeister effect on amyloid formation using yeast prion protein.* Protein Science, 2010. **19**(1): p. 47-56.

32. Rubin, J., H. Khosravi, K.L. Bruce, M.E. Lydon, S.H. Behrens, Y.O. Chernoff, and A.S. Bommarius, *Ion-specific effects on prion nucleation and strain formation.* J Biol Chem, 2013. **288**(42): p. 30300-8.

33. Klement, K., K. Wieligmann, J. Meinhardt, P. Hortschansky, W. Richter, and M. Fandrich, *Effect of different salt ions on the propensity of aggregation and on the structure of Alzheimer's abeta(1-40) amyloid fibrils.* J Mol Biol, 2007. **373**(5): p. 1321-33.

34. Tanaka, M., P. Chien, N. Naber, R. Cooke, and J.S. Weissman, *Conformational variations in an infectious protein determine prion strain differences.* Nature, 2004. **428**(6980): p. 323-328.

35. Toyama, B.H., M.J. Kelly, J.D. Gross, and J.S. Weissman, *The structural basis of yeast prion strain variants.* Nature, 2007. **449**(7159): p. 233-7.

36. Sharma, J. and S.W. Liebman, *Variant-specific prion interactions.* Cell Logistics, 2013. **3**: p. e25698.

37. Hofmeister, F., *On the understanding of the effects of salts.* Arch. Exp. Pathol. Pharmakol.(Leipzig), 1888. **24**: p. 247-260.

38. Kunz, W., J. Henle, and B.W. Ninham, *'Zur Lehre von der Wirkung der Salze' (about the science of the effect of salts): Franz Hofmeister's historical papers.* Current Opinion in Colloid & Interface Science, 2004. **9**(1): p. 19-37.

39. Turton, D.A., J. Hunger, G. Hefter, R. Buchner, and K. Wynne, *Glasslike behavior in aqueous electrolyte solutions.* J Chem Phys, 2008. **128**(16): p. 161102.

40. Wachter, W., W. Kunz, R. Buchner, and G. Hefter, *Is there an anionic Hofmeister effect on water dynamics? Dielectric spectroscopy of aqueous solutions of NaBr, NaI, NaNO3, NaClO4, and NaSCN.* J Phys Chem A, 2005. **109**(39): p. 8675-83.

41. Tielrooij, K.J., N. Garcia-Araez, M. Bonn, and H.J. Bakker, *Cooperativity in ion hydration.* Science, 2010. **328**(5981): p. 1006-9.

42. Salis, A. and B.W. Ninham, *Models and mechanisms of Hofmeister effects in electrolyte solutions, and colloid and protein systems revisited.* Chem Soc Rev, 2014. **43**(21): p. 7358-77.

43. Zhang, Y. and P.S. Cremer, *Interactions between macromolecules and ions: the Hofmeister series.* Current Opinion in Chemical Biology, 2006. **10**(6): p. 658-663.

44. Chien, P., J.S. Weissman, and A.H. DePace, *Emerging principles of conformation-based prion inheritance.* Annual review of biochemistry, 2004. **73**(1): p. 617-656.

45. Tuite, M.F. and B.S. Cox, *Propagation of yeast prions.* Nature Reviews Molecular Cell Biology, 2003. **4**(11): p. 878-890.

46. Tuite, M.F. and B.S. Cox, *The [PSI^+] prion of yeast: A problem of inheritance.* Methods, 2006. **39**(1): p. 9-22.

47. Derkatch, I.L., Y.O. Chernoff, V.V. Kushnirov, S.G. Inge-Vechtomov, and S.W. Liebman, *Genesis and variability of [PSI] prion factors in Saccharomyces cerevisiae.* Genetics, 1996. **144**(4): p. 1375-1386.

48. Hardy, J.A. and G.A. Higgins, *Alzheimer's disease: the amyloid cascade hypothesis.* Science, 1992.

49. Selkoe, D.J., *The molecular pathology of Alzheimer's disease.* Neuron, 1991. **6**(4): p. 487-498.

50. Selkoe, D.J., *Cell biology of the amyloid beta-protein precursor and the mechanism of Alzheimer's disease.* Annual review of cell biology, 1994. **10**(1): p. 373-403.

51. Walter, J., C. Kaether, H. Steiner, and C. Haass, *The cell biology of Alzheimer's disease: uncovering the secrets of secretases.* Current opinion in neurobiology, 2001. **11**(5): p. 585-590.

52. Colvin, M.T., R. Silvers, Q.Z. Ni, T.V. Can, I. Sergeyev, M. Rosay, K.J. Donovan, B. Michael, J. Wall, S. Linse, and R.G. Griffin, *Atomic Resolution Structure of Monomorphic Abeta42 Amyloid Fibrils.* J Am Chem Soc, 2016. **138**(30): p. 9663-74.

53. Walti, M.A., F. Ravotti, H. Arai, C.G. Glabe, J.S. Wall, A. Bockmann, P. Guntert, B.H. Meier, and R. Riek, *Atomic-resolution structure of a disease-relevant Abeta(1-42) amyloid fibril.* Proc Natl Acad Sci U S A, 2016. **113**(34): p. E4976-84.

CHAPTER 2. CONTRIBUTION OF THE PRION PROTEIN SEQUENCE, STRAIN, AND ENVIRONMENT TO THE SPECIES BARRIER

This chapter is adapted from a research article bearing the same title published in the Journal of Biological Chemistry in November 2015. Kathryn L. Bruce, Buxin Chen, Stefka Gyoneva, Sven H. Behrens, Andreas S. Bommarius, and Yury O. Chernoff contributed to this work.

2.1 Abstract

Amyloid propagation requires high levels of sequence specificity so that only molecules with very high sequence identity can form cross-β-sheet structures of sufficient stringency for incorporation into the amyloid fibril. This sequence specificity presents a barrier to transmission of prions between two species with divergent sequences, termed a species barrier. Here, we study the relative effects of protein sequence, seed conformation, and environment on the species barrier strength and specificity for the yeast prion protein, Sup35p, from three closely related species of the *Saccharomyces sensu stricto* group, namely *S. cerevisiae*, *S. bayanus* and *S. paradoxus*. Through *in vivo* plasmid shuffle experiments we show that the major characteristics of the transmission barrier and conformational fidelity are determined by the protein sequence rather than cellular environment. *In vitro* data confirm that kinetics and structural preferences of aggregation of the *S. paradoxus* and *S. bayanus* proteins are influenced by anions in accordance to their positions in the Hofmeister series, as previously observed for *S. cerevisiae*. With the help of *in vitro* aggregation experiments, we show that the specificity of the species barrier is primarily affected by the sequence and the type of anion present during the formation of the initial seed, while anions present during the seeded aggregation process typically

influence aggregation kinetics rather than the specificity of prion conversion. Thus, our work shows that the protein sequence and the conformation variant (strain) of prion seed are the primary determinants of cross-species prion specificity both *in vivo* and *in vitro*.

2.2 Introduction

Amyloidogenic proteins form ordered self-seeding fibrous aggregates which are known to be associated with a variety of neurodegenerative diseases in humans and other mammals, such as Alzheimer's disease, Parkinson's disease, and prion diseases, including sheep scrapie, mad cow disease, elk and deer chronic wasting disease, and human Creutzfeldt-Jakob disease, kuru and fatal familial insomnia [1-5]. The amyloid/prion form of an amyloidogenic protein can convert the cellular form of a protein of the same or very similar amino acid sequence into an amyloid conformation, usually via cross-β interactions [6-9]. Transmissible amyloids, called prions, can spread the amyloid state between organisms.

2.2.1 Species barrier

Cross-species transmission of the prion state is impaired by sequence divergence within the prion proteins, resulting in a "species barrier" to transmission of a prion from one species to another [10]. However, the species barrier can be overcome in some species combinations. For example, bovine spongiform encephalopathy (BSE), which possibly originated from transmission of a scrapie prion from sheep to cattle, resulted in the widely known 'mad cow' disease epidemic which greatly affected the United Kingdom in the 1990s [11, 12]. BSE was also found to be transmitted from cattle to humans, manifesting itself as a new variant of Creutzfeldt-Jakob disease, vCJD [13-16]. Therefore,

understanding of the determinants of species barrier and cross-species prion transmission is crucial for preventing future outbreaks of prion diseases. However, the rules governing species barriers as well as effects of the physiological and environmental conditions on the barrier are poorly understood to date. In this work we, study the contribution of protein sequence, prion strain, and environment of cross-species transmission of a yeast prion protein from the *Saccharomyces* genus.

2.2.2 Yeast Prion Sup35p

Yeast prions are cytoplasmic elements heritable in a non-Mendelian fashion [17, 18]. As many of them control phenotypically detectable traits, yeast prions provide a useful model for studying molecular basis of prion phenomena. One of the best studied yeast prion proteins is a translation termination factor Sup35. Prion formation by Sup35 causes translational readthrough (nonsense-suppression), a phenotypically detectable trait in specifically designed yeast strains [17, 18]. Previously, we [19, 20] and others [21] have reported observations of the species barrier and cross-species prion transmission between Sup35 proteins of three closely related yeast species - *S. cerevisiae, S. paradoxus*, and *S. bayanus*, containing Sup35p with high levels of sequence similarity. Sup35 protein can be divided into three segments: 1) N-terminal prion domain (Sup35N); 2) linker middle domain (Sup35M); and 3) functional C-terminal domain (Sup35C) responsible for translation termination and cell viability. Levels of similarity between the Sup35N fragments of the Sup35 proteins from the *Sachharomyces sensu stricto* are close to those observed among mammalian prion proteins [22, 23], which renders this system a useful model for studying species barrier. The Sup35N domain alone is difficult to express, as it is poorly soluble and aggregates too rapidly, whereas the addition of Sup35M domain

resolves all the above mentioned issues. Therefore, Sup35NM is widely used as a model protein for studying amyloid aggregation *in vitro*, and is shown to transmit prion properties to full-size Sup35 after transfection into the yeast cells [24, 25]. Amino acid similarities between the Sup35NM regions of the three different species are respectively 95% and 93% (*S. cerevisiae* / *S. paradoxus* combination), 85% and 78% (*S. cerevisiae* / *S. bayanus* combination), 85% and 79% (*S. paradoxus* / *S. bayanus* combination) [19, 20]. Sequence alignment of the N domains of Sup35 from the three yeast species is shown in Appendix A. Previous experiments performed by us with divergent Sup35 proteins (or proteins containing divergent or chimeric Sup35N domains) in *S. cerevisiae* cells have demonstrated that the prion species barrier depends on the level of divergence of Sup35N sequences, and that different sub-regions (modules) of Sup35N play a primary role in determining the barrier in different cross-species combinations [19, 20, 26]. A prion species barrier was also observed with divergent Sup35NM fragments *in vitro* [19].

2.2.3 Prions "strains" or "variants"

Prion proteins, including mammalian PrP and yeast Sup35 not only can fold into alternative prion and non-prion forms, but can also adopt multiple distinct amyloid conformations, known as "strains" or "variants" [17, 27-33]. Different strains are associated with distinct disease patterns in mammals and different stringencies of phenotypic effects in fungi (because of this, yeast prion strains could be termed "strong", "intermediate", "weak" etc.). Once formed, the prion strain is typically faithfully reproduced, although strain "mutations" may occur with a low frequency [34-38]. In both mammals and yeast, prion strain properties influence species barrier [26, 39]. For example, transmission of the specific "strong" prion strain from *S. cerevisiae* to *S. paradoxus* Sup35

prion domain (PrD) in *S. cerevisiae* cells is relatively efficient, while transmission of the specific "weak" prion strain in the same direction is rare [20]. Notably, underlying *S. cerevisiae* prion "strain" patterns were maintained during propagation through *S. paradoxus* protein, but irreversibly altered during propagation through *S. bayanus* protein, that could be detected as a "switch" of prion strain after reverse transmission back to the *S. cerevisiae* sequence [20]. This shows that not only efficiency of prion transmission but also fidelity of reproduction of prion conformation during transmission is controlled by the level of identity of interacting protein sequences.

2.2.4 Ion-specific Effects on Sup35NM Prion Formation

Previous work from our group has also demonstrated that the ion present in solution greatly influences not only processes such as deactivation of enzymes [40-42] but also the *in vitro* amyloid formation by *S. cerevisiae* Sup35NM, and that ion-specific effects are determined by their position in the Hofmeister series in the fashion of "inverse" Hofmeister effect. Specifically, strongly hydrated anions (kosmotropes) initiate nucleation quickly and promote rapid fiber elongation, while poorly hydrated anions (chaotropes) slow down the aggregation kinetics [43, 44]. A similar effect of kosmotropes has also been observed by another group for the mammalian prion protein, PrP [45]. Moreover, amyloid formation by Sup35NM in the presence of different anions resulted in the generation of a different spectrum of prion strains, with kosmotropes favoring the formation of "strong" strains (characterized by smaller aggregate size and higher frangibility and proliferation), and chaotropes favoring the formation of "weak" strains (characterized by larger aggregate size and lower frangibility and proliferation) [43, 44].

In this work, we specifically address the contribution of the cellular composition and the conditions of the aggregation reaction to the specificity of prion transmission. *In vitro* aggregation experiments are performed to determine if anions of Hofmeister series influence cross-species specificity of prion transmission. Further, results of *in vivo* experiments are compared in the cells of different yeast species, to determine whether species specific patterns of intracellular environment influence the parameters of the prion species barrier. Our results are consistent with the notion that protein sequence and conformation remain the primary determinants of cell specificity, while environmental conditions influence specificity primarily via favoring the formation of different prion strains.

2.3 Materials and Methods

2.3.1 In vitro Techniques

2.3.1.1 Expression and purification of Sup35NM

Plasmid constructs containing the SUP35NM coding regions of different origins with the attached C-terminal His_6 tags were generated as described previously [46] and expressed in *E. coli* host strain HMS174 (DE3) pLysS (Novagen) in order to produce the Sup35NM-(His_6) proteins. The cell pellets were stored at −80°C until purification. Purification of Sup35NM proteins from E. coli was carried out as described previously [47]. The purified protein was precipitated using methanol at -20°C and stored at -80°C in 80% methanol.

2.3.1.2 Kinetic assays using thioflavin T

Protein pellet stored at -80°C was collected by centrifugation. The supernatant was discarded and the protein was re-suspended in 8 M urea. Sup35NM was then concentrated by 10 kDa centrifugal filter and diluted 100 folds with PBS pH 7.4. The samples were boiled for about 10 min before starting the aggregation experiments to break down any preformed aggregates. 1 mM thioflavin T (ThT; Sigma Aldrich) solution was prepared fresh in PBS. Aggregation experiments were conducted in triplicates in a 96 well plate with final ThT and Sup35NM concentrations of 100 μM and 10 μM, respectively, and containing 0.4 M sodium salt. The seeded experiments contained 5% by volume of sonicated amyloid aggregates. Polymerization was carried out at 25°C in a 96-well plate with linear shaking at 18Hz in a BioTek Synergy H4 Hybrid Multi-Mode Microplate Reader (Winooski, VT). Fluorescence readings were taken every minute for about 16 hours using an excitation wavelength of 440 nm and emission wavelength of 480 nm.

2.3.1.3 Preparation of amyloid seeds

The respective sodium salt was added to Sup35NM, purified and prepared as described above, to a final concentration of 0.5 M salt and 10 μM protein in a micro-centrifuge tube. The samples were allowed to rotate at 20 rpm at room temperature for 2 days. After polymerization the amyloid samples were stored at -80 ^{0}C until use.

2.3.2 Yeast Cultivation and Genetic Techniques.

2.3.2.1 Cultivation

Standard yeast media and growth conditions were employed [48]. Yeast cultures were incubated at 30°C. Standard procedures [49] were used for [*PSI*$^{+}$] detection,

characterization, and curing by GuHCl. All strains have an *ade1-14* nonsense mutation in the *ADE1* gene that contains a premature UGA stop codon, allowing detection of [*psi*$^-$] and [*PSI*$^+$] through the read-through or nonsense suppression assay [49].

2.3.2.2 Yeast transformation and transfection

Standard techniques for yeast transformation were employed [48, 49]. For transfection with yeast extracts, cells of the [*PSI*$^+$] donor strain were disrupted via a standard glass-bead lysis procedure, and resulting lysate was transfected into the spheroplasts of the [*psi*$^-$] *S. paradoxus* strain GT1320-36A using a modified protocol described by Rubin et al. 2013 [44] and originally adapted from Tanaka et al. 2004 [24]. To prepare spheroplasts, the cell wall of a [*psi*$^-$] recipient cell was fragmented with zymolase. An empty *URA3* vector was co-transfected into the recipient cells as an indicator of that material has passed across the cell membrane (see Figure 2.1A).

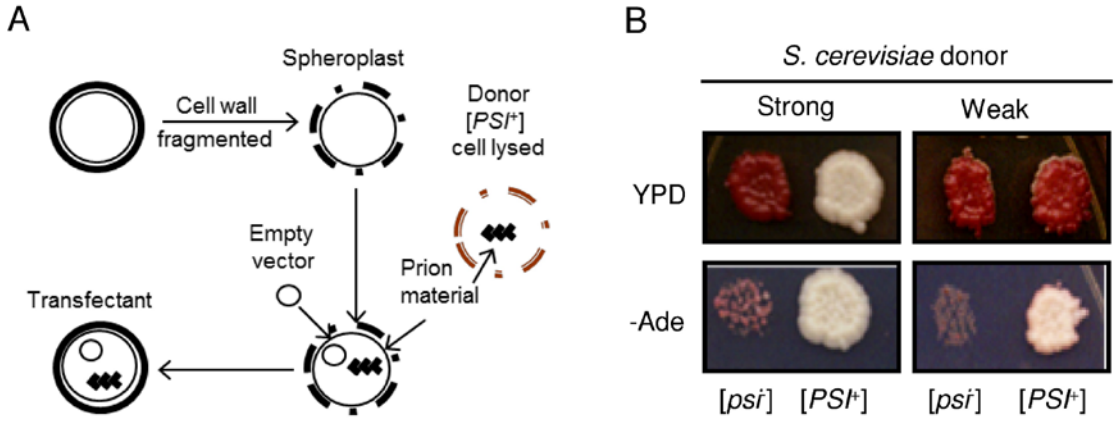

Figure 2.1 – Cross-species prion transfection. (A) Summary of the transfection procedure. (B) Cellular extract was transfected from either a strong or weak [*PSI*$^+$] *S. cerevisiae* strain into a [*psi*$^-$] *S. paradoxus* strain, expressing the Sup35 protein from *S. cerevisiae*. Representative [*PSI*$^+$] *S. paradoxus* transfectants obtained from either the strong (left) or weak (right) [*PSI*$^+$] donor strains are shown. Yeast cells were

grown on YPD (for color assay) and on –Ade medium (for suppression assay) at 30°C for 8 days.

Transfectants were obtained on the medium counter-selecting against the Trp- donor strain (-Ura-Trp) in order to avoid contamination by donor cells. Both small and large colonies were observed on –Ura-Trp. Only large colonies contained the *URA3* plasmid, smaller colonies (from cells without the plasmid) resulted from background growth, possibly due to a low concentration of YPD present in the transfectant selection medium. The large Ura+ colonies were tested on –Ade medium to check for [PSI^+] (see Figure 2.1B). Transfection of *in vitro* generated aggregates into *S. cerevisiae* strains GT797 and GT987 was performed as previously described [44], with sonication in order to increase frequency of transfection, and using an empty plasmid with the *LYS2* marker for selection of transfectants.

2.3.2.3 Direct and reverse shuffle procedures

The *SUP35* genes of various origins were exchanged in the *S. paradoxus* strain (please refer Sharma et al. 2015 [50] for details), by using a plasmid shuffle procedure (Figure 2.2) performed as previously described for *S. cerevisiae* [19, 20], except that *LYS2* and *URA3* markers were used on plasmids, instead of *LEU2* and *URA3*. For direct shuffle, cells containing a $SUP35_{SC}$ *LYS2* plasmid were transformed with a plasmid containing the *SUP35* gene of the same or different origin, and *URA3* marker, followed by loss of the original *LYS2* plasmid (direct shuffle). From each individual [PSI^+] transformant, only a single Ura+ Lys- colony was analyzed. To perform a reverse shuffle, cells obtained from direct shuffle and containing the $SUP35_{SP}$ *URA3* plasmid were transformed with the $SUP35_{SC}$ *LYS2* plasmid, and cured of the original *URA3* plasmid.

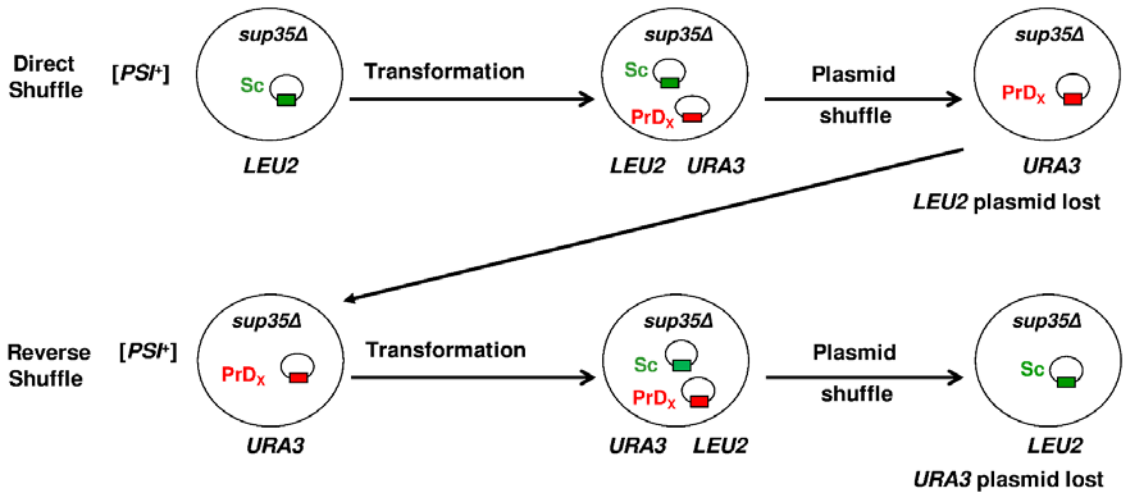

Figure 2.2 – Plasmid shuffle scheme: Scheme of direct and reverse plasmid shuffle. "Sc" refers to SUP35 from *S. cerevisiae*. "PrDX" refers to *SUP35* genes of various origins, or chimeric constructs.

2.4 Results

2.4.1 Amyloid Formation by Sup35NM from S. bayanus and S. paradoxus in the Presence of Different Salts along the Hofmeister Series

To obtain materials for studying the cross-species prion transmission *in vitro*, we have first examined the unseeded amyloid formation of $Sup35NM_{Sb}$ and $Sup35NM_{Sp}$ in the presence of the salts (Figure 2.3, A and B), and compared results to our previous data for $Sup35NM_{Sc}$ [44]. We have determined that the parameters of *in vitro* aggregation of $Sup35NM_{Sb}$ and $Sup35NM_{Sp}$ are influenced by anions of the Hofmeister series in the same way as previously observed for $Sup35NM_{Sc}$. For both proteins, the lag time of amyloid formation was shortened in the presence of sulfate (strong kosmotrope) and prolonged in the presence of perchlorate (strong chaotrope), compared to chloride (mild chaotrope). This establishes the generality of the inverse Hofmeister effect on the amyloid formation by

each of three Sup35NM proteins from the *Saccharomyces* species used in this work.

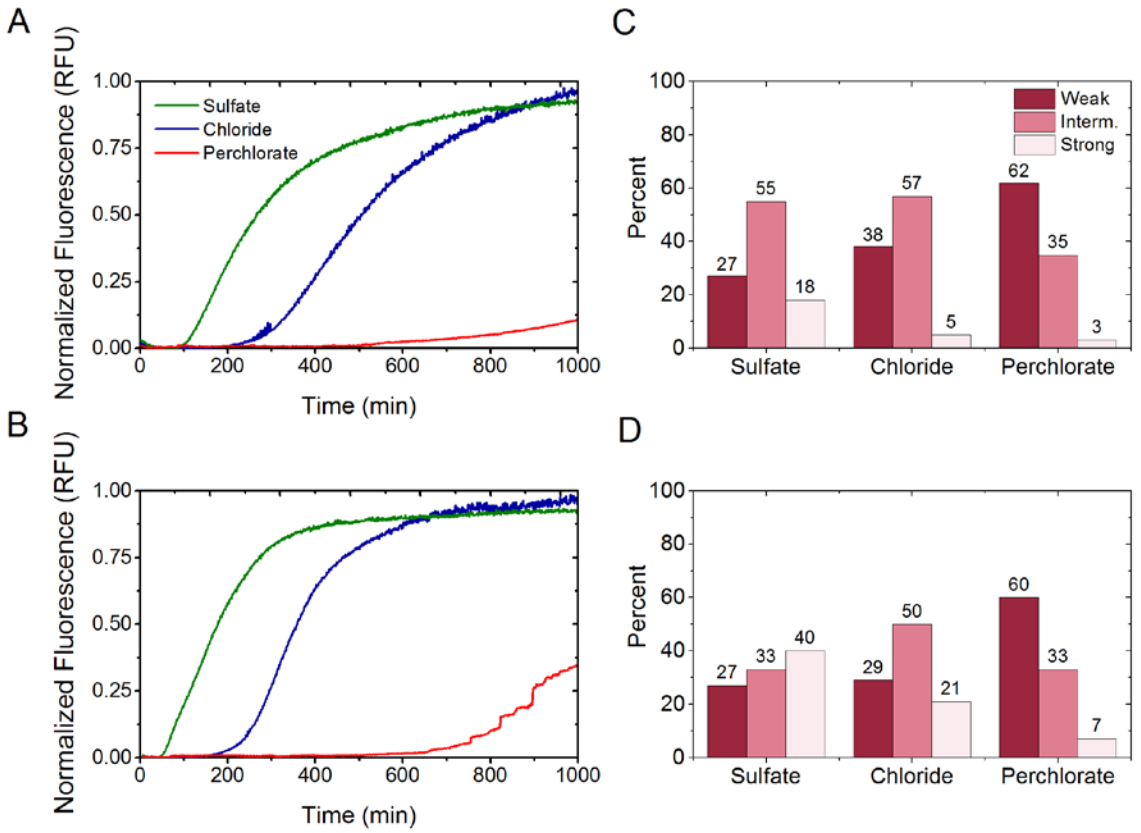

Figure 2.3 – Aggregation profiles of Sup35NM$_{Sb}$ and Sup35NM$_{Sp}$ in the presence of 0.4 M salts monitored by Thioflavin T fluorescence assay and phenotypic characterization of Sup35NM$_{Sb}$ and Sup35NM$_{Sp}$ prion strains. (A, B) Amyloid formation by Sup35NM$_{Sb}$ (A) and Sup35NM$_{Sp}$ (B) in the presence of 0.4M sulfate, chloride or perchlorate are presented to show the effect of Hofmeister ions on their aggregation. In the presence of a strong kosmotrope (sulfate), the lag times are short and elongation rates are fast. The opposite is true of aggregation in a chaotropic solution (perchlorate) while the aggregation plots show intermediate lag times and elongation rates in the presence of the mildly chaotropic chloride ions. (C, D) Distribution of weak, intermediate and strong [*PSI*$^{+}$] colonies obtained after the transfection of the yeast strains GT987 (expressing Sup35$_{Sb}$) and GT797 (expressing Sup35$_{Sp}$) with Sup35NM$_{Sb}$ (C) and Sup35NM$_{Sp}$ (D) amyloids, respectively, obtained in the presence of sulfate, chloride or perchlorate salts. For both the proteins, amyloids formed in sulfate resulted in higher number of strong strains, which appeared white or faintly pink in color on YPD, than the amyloids formed in perchlorate which formed more weak strains appearing dark pink on YPD. Amyloids formed in chloride showed intermediate strain patterns to those formed in sulfate and perchlorate.

We have also determined if patterns of amyloids generated by Sup35NM$_{Sp}$ and Sup35$_{Sb}$ *in vitro* are influenced by ionic composition. Amyloids generated by Sup35NM$_{Sp}$ or Sup35NM$_{Sb}$ in the presence of various salts were transfected into the [*psi*$^{-}$] *S. cerevisiae* strain bearing either Sup35$_{Sp}$ or Sup35$_{Sb}$ protein instead of Sup35$_{Sc}$. For both proteins, higher proportion of "weaker" [*PSI*$^{+}$] isolates was detected after transfection with amyloids obtained in the presence of chloride or perchlorate, compared to amyloids obtained in the presence of sulfate (Figure 2.3, C and D). This confirms that a kosmotrope favours formation of "stronger" prion strains, while a chaotrope favours formation of "weaker" prion strains by Sup35NM$_{Sp}$ and Sup35NM$_{Sb}$, similar to what has been described for Sup35NM$_{Sc}$ [44].

2.4.2 Cross-Species Amyloid Seeding in the Presence of a Mild Chaotrope.

Next, we have investigated the impact of sequence divergence on the species barrier between Sup35NM proteins from the three species. For this purpose, we studied cross-species amyloid seeding in an "intermediate" environment, that is, in the presence of mild chaotrope (chloride) which is positioned between sulfate and perchlorate in the Hofmeister series. Amyloids used as seeds were also formed in the presence of chloride. The monomeric proteins (referred to as "monomers") and the sonicated amyloid fibers (referred to as "seeds") used as seeds for the aggregation assays, can be considered as *in vitro* analogues of the *in vivo* [*psi*$^{-}$] recipients and [*PSI*$^{+}$] donors, respectively (see section 2.4.5 below). Our results (Figure 2.4) show that Sup35NM$_{Sc}$ and Sup35NM$_{Sp}$ are highly efficient in seeding each other in the presence of chloride, as we detect zero (or near zero) lag times for cross-seeding of Sup35NM$_{Sc}$ with Sup35NM$_{Sp}$, and vice versa. In contrast, Sup35NM$_{Sb}$ is less efficient in seeding the other two proteins or being seeded by them, and thus exhibits

a stronger species barrier (Figure 2.4). This generally agrees with *in vivo* data ([19, 20] and below), and can be explained by a higher degree of homology between the prion domains (PrDs) of Sup35NM$_{Sc}$ and Sup35NM$_{Sp}$, and a lower degree of homology between the PrDs of any of these proteins and Sup35NM$_{Sb}$.

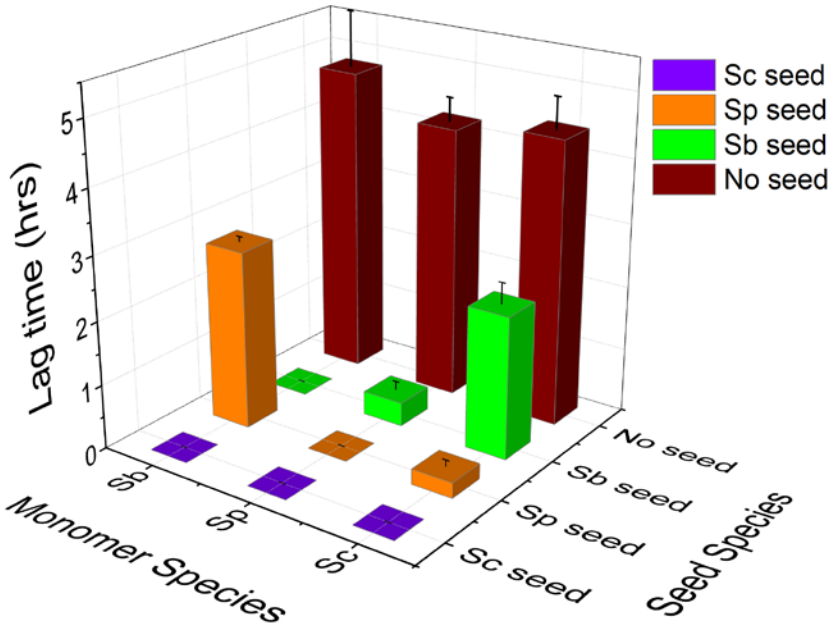

Figure 2.4 – Lag time in hours for seeding experiments performed in 0.4 M sodium chloride. The seeds were formed in the presence of chloride salt. Homologous seeding is highly efficient with zero lag times. Sc/Sp combination results in zero or close to zero lag times. Larger lag times are observed in some cases involving Sb as a seed or monomer.

Also, in accordance with previous reports, we observe an asymmetry in the species barrier [19, 20, 34, 51]. For example, seeding of Sup35NM$_{Sc}$ monomer with the Sup35NM$_{Sb}$ seeds results in a lag time of 2.22 hrs, while seeding of Sup35NM$_{Sb}$ monomer with the Sup35NM$_{Sc}$ seed shows essentially no lag time. A similar asymmetric effect is seen in the Sp/Sb heterologous seeding combination.

Notably, the asymmetry pattern observed in the presence of chloride was different from the asymmetry patterns observed *in vivo*, as well as in the previous *in vitro* data [19]. Those results uncovered a stronger barrier for the $Sup35NM_{Sb}$ seeding with the $Sup35NM_{Sc}$ seeds, rather than in the opposite direction. To further investigate this discrepancy, we have attempted both seed formation and cross-seeding in PBS, as in our previous work. Indeed, the asymmetry pattern observed in PBS resembled *in vivo* data and our previous *in vitro* results, rather than the asymmetry pattern observed in chloride (see Figure 2.5). Thus, the addition of chloride appears to reverse an asymmetry pattern of the species barrier, indicating that the ionic composition of the solution influences the barrier. To decipher the mechanism of this phenomenon, we have performed a more systematic study aimed at determining whether ionic composition acts via influencing "seed" properties or directly affects cross-seeding interactions.

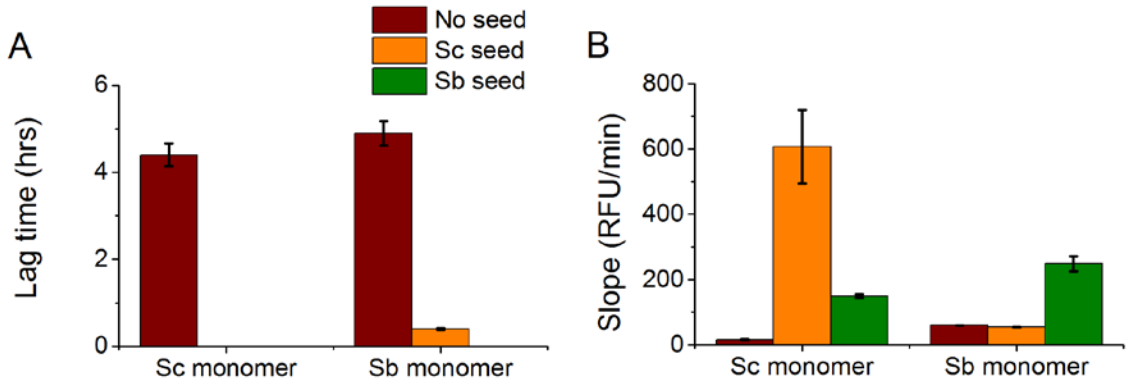

Figure 2.5 – Cross-seeding in the presence of a mild chaotrope. Lag time (A) and Slope in RFU/min (B) for unseeded and cross -seeding aggregation reactions between *S. cerevisiae* and *S. bayanus* in PBS. The seeds were also formed in PBS. Seeding $Sup35NM_{Sc}$ monomer with $Sup35NM_{Sb}$ seeds is more efficient (zero lag time and higher slope) than seeding $Sup35NM_{Sb}$ monomer with $Sup35NM_{Sc}$ seeds (non-zero lag time and lower slope).

2.4.3 Comparison of the Cross-Seeding Capabilities of Seeds Obtained in the Presence of Different Salts.

First, we determined if cross-seeding is influenced by conditions in which a "seed" is generated. Hofmeister ions have been shown to affect both kinetics of amyloid aggregation and structural parameters of resulting aggregates, reflecting distinct protein conformations [43, 44]. Kosmotropic ions such as sulfate lead to faster kinetics and "stronger" strains and chaotropic ions such as perchlorate lead to slower kinetics and "weaker" strains [43, 44, 47, 52]. We have confirmed this for $Sup35NM_{Sp}$ and $Sup35NM_{Sb}$ (see above). As strain patterns influence cross-species prion conversion [20, 23], we have compared cross-seeding by seeds obtained in different salts. In all the reactions, we saw that amyloid seeds of the same protein formed in different salts have different lag times and slopes depending on the salt they are formed in (Figure 2.6 and Figure 2.7). Interestingly, seeds formed in sulfate do not always result in the shortest lag times, and seeds formed in perchlorate do not always lead to the longest lag times. Figure 2.8 shows the effect of salt present during seed formation on the species barrier in combinations $Sup35NM_{Sc}$/$Sup35NM_{Sb}$ and $Sup35NM_{Sp}$/$Sup35NM_{Sb}$.

In the case of $Sup35NM_{Sc}$/$Sup35NM_{Sb}$ (Figure 2.8A), the seed obtained in chloride shows the shortest lag time in one of the combinations, while the seed obtained in perchlorate shows the shortest lag time in the other combinations. This agrees with our previous observation that for the $Sup35_{Sc}$/$Sup35_{Sb}$ combination *in vivo*, the species barrier is more severe for the "strong" strain, compared to the "weak" strain. The combination $Sup35NM_{Sp}$/$Sup35NM_{Sb}$ shows an even stronger trend in this direction, exhibiting the longest lag period for the sulfate-generated seeds in both reciprocal combinations (Figure

2.8B). Overall, our data demonstrate that salts of Hofmeister series influence species barriers via altering the structural parameters of the seed produced in the presence of the respective salt.

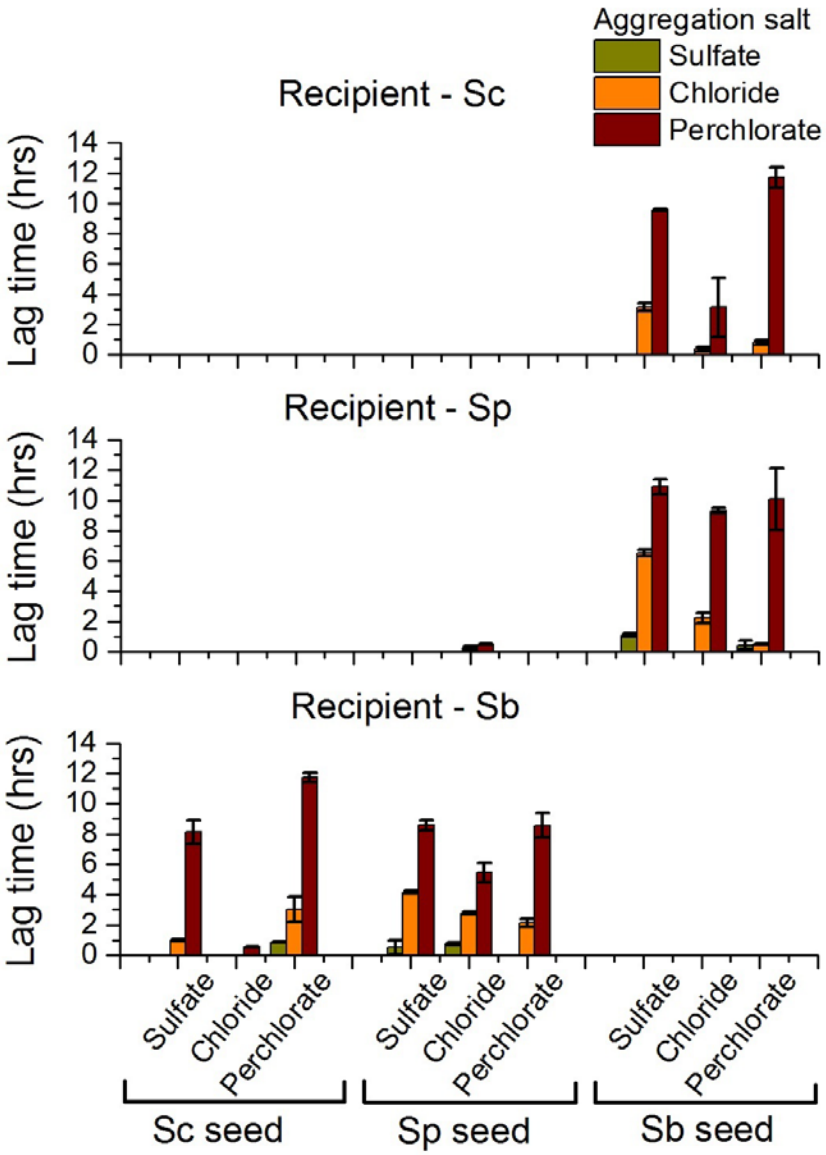

Figure 2.6 – Lag times in hours for unseeded and seeded aggregation reactions. Homologous aggregation is more efficient than heterologous aggregation. Heterologous aggregation of Sup35NM$_{Sc}$ and Sup35NM$_{Sp}$ is very efficient with close to zero lag times while heterologous aggregation of Sup35$_{Sb}$ with the other two proteins is less efficient. Co-aggregation in the presence of sulfate leads to the shortest lag times and aggregation in perchlorate results in the longest lag times.

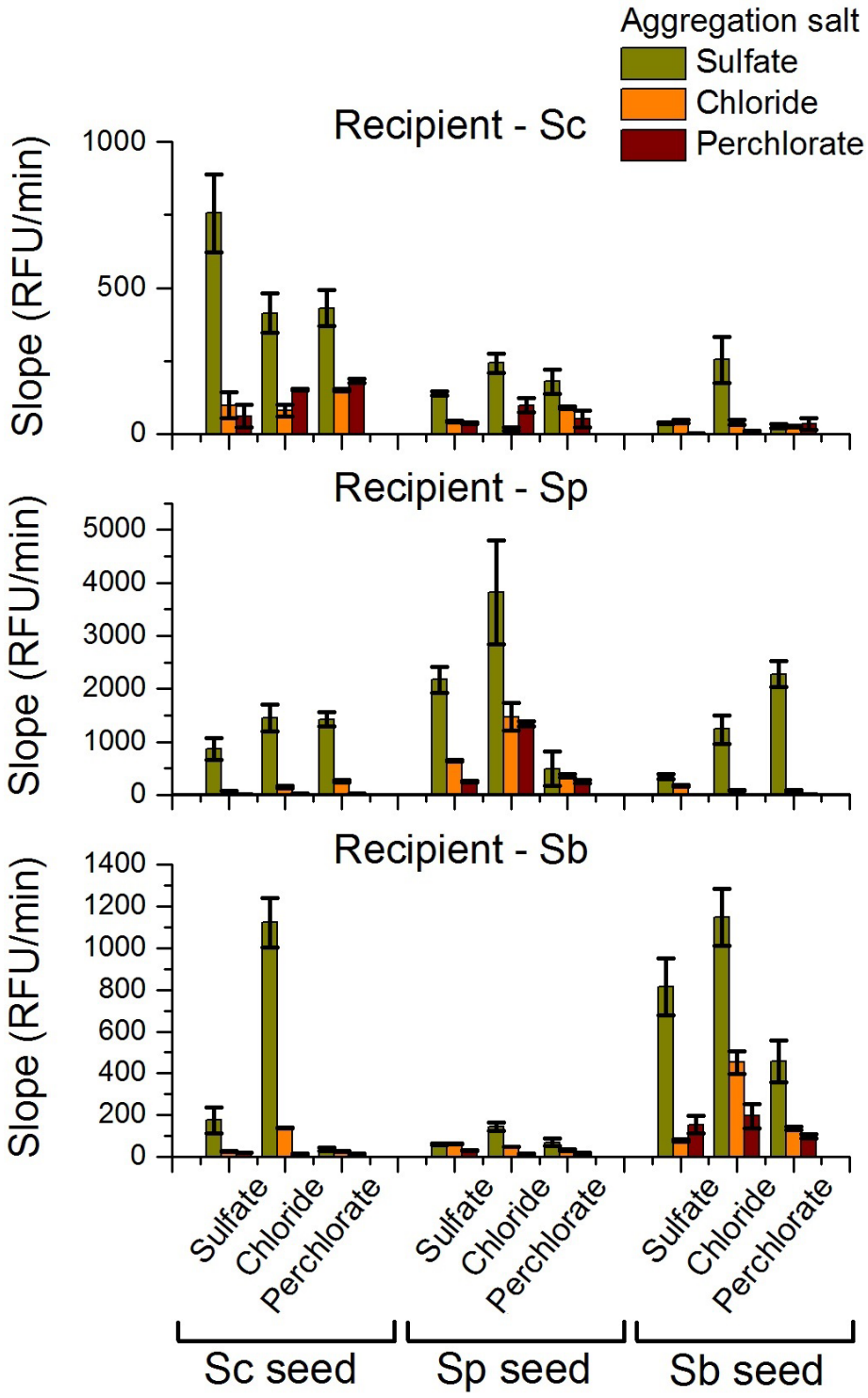

Figure 2.7 – Slope in RFU/min for unseeded and seeded aggregation reactions. Homologous aggregation is more efficient than heterologous aggregation. Co-aggregation in the presence of sulfate leads to the highest slopes and aggregation in perchlorate results in the smallest slopes.

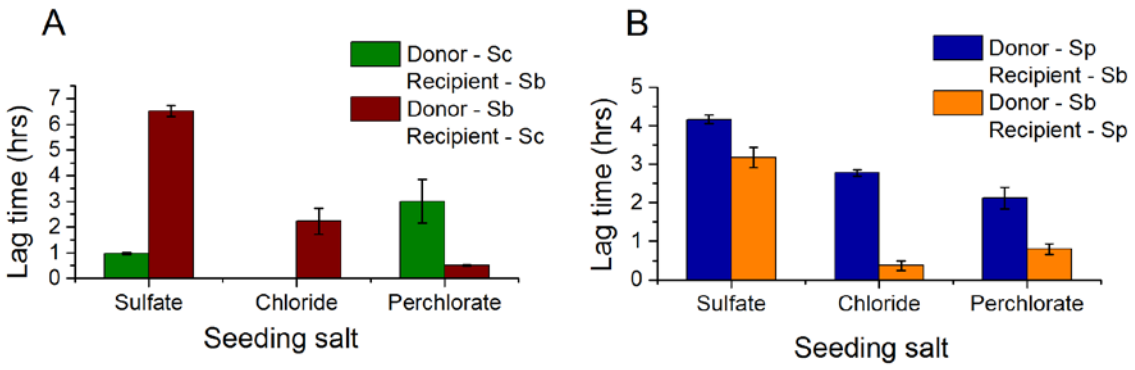

Figure 2.8 – Effect of seeding salt on heterologous co-aggregation Sc/Sb (A) and Sp/Sb (B). Amyloid seeds were formed in the presence of sulfate, chloride and perchlorate salts and aggregation was carried out in the presence of chloride salt. Salts present during seed formation affect co-aggregation kinetics as seen in a variation of the lag time.

2.4.4 Comparison of Cross-Seeding Reactions Performed in the Presence of Different Salts

To determine if the environment of the *in vitro* reaction influences the specificity of cross-seeding, we then investigated the effect of salts present in the aggregation medium on cross-seeding in the $Sup35NM_{Sb}$/$Sup35NM_{Sc}$ and $Sup35NM_{Sb}$/$Sup35NM_{Sp}$ combinations (Figure 2.9). Aggregation in sulfate, which is a strong kosmotrope, resulted in faster aggregation kinetics with shorter lag times and steeper slopes. On the other hand, aggregation in perchlorate, which is a strong chaotrope, resulted in longer lag times and smaller slopes. Aggregation kinetics in the slightly chaotropic chloride salt fell in between the kinetics observed for sulfate and perchlorate as the aggregation salts.

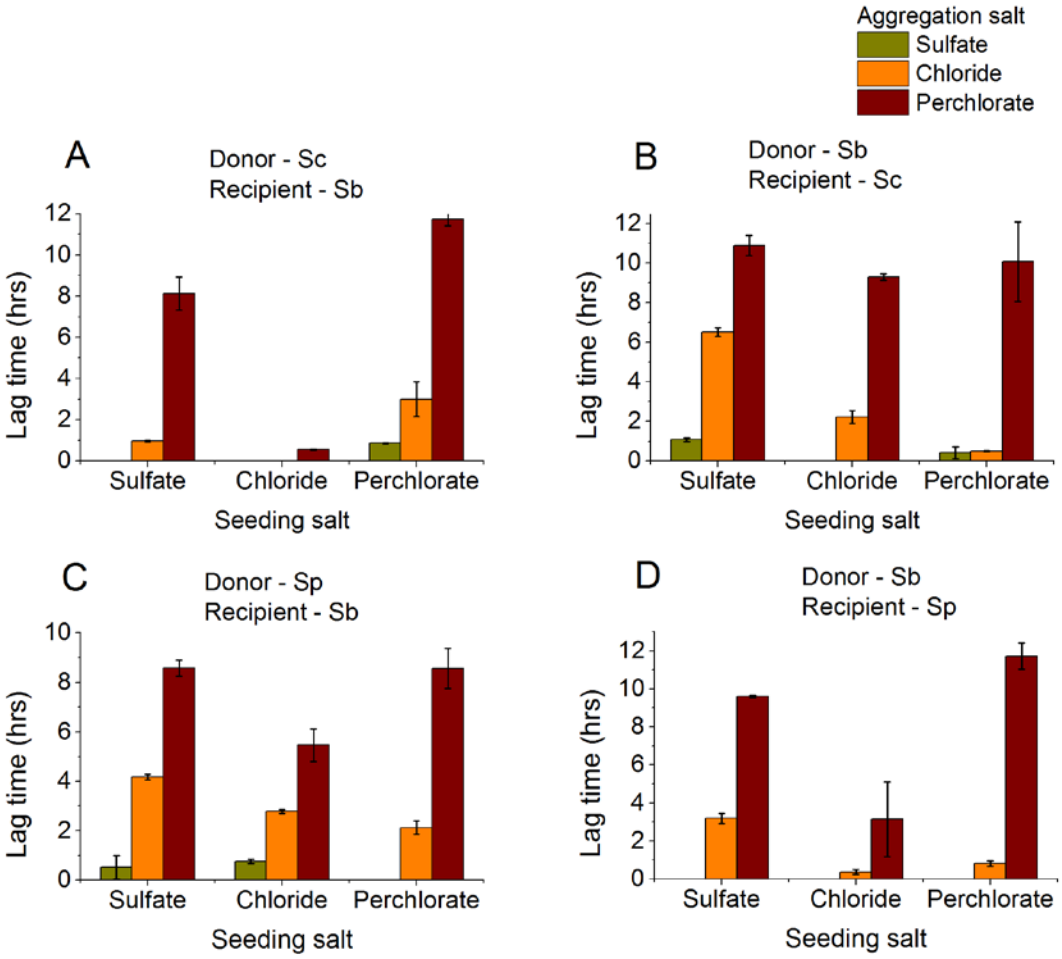

Figure 2.9 – Effect of aggregation salt on heterologous co-aggregation. (A) Sc monomer seeded with Sb amyloids seeds. (B) Sb monomer seeded with Sc amyloids seeds. (C) Sp monomer seeded with Sb amyloids seeds. (D) Sb monomer seeded with Sp amyloids seeds. Amyloid seeds were formed in the presence of sulfate, chloride and perchlorate salts. Irrespective of the salt-dependent seed, aggregation is the fastest in the presence of the strongly kosmotropic sulfate and slowest in the presence of the strongly chaotropic perchlorate.

Despite numerical differences, this overall pattern was detected independently of the salt in which the initial seed was obtained (for more data and for the effect on slope as well as on the lag time, see Figure 2.6 and Figure 2.7). Hence, the salt in which the cross-seeding reaction is performed has a strong and systematic influence on the kinetics of cross-

seeding reaction but does not affect the specificity of reaction, in contrast to the salt in which the initial seed is generated.

2.4.5 [PSI$^+$] Transfection into Saccharomyces paradoxus Cells

To transfer a *S. cerevisiae* prion into the cell of a different *Saccharomyces* species, was transfected the *S. paradoxus* strain bearing the *SUP35$_{Sc}$* gene, with the extracts of [*PSI*$^+$] *S. cerevisiae* cells (Figure 2.1A). The Ade+ colonies were identified among transfectants and shown to be curable of Ade+ phenotype by GuHCl, an agent eliminating yeast prions. Thus, we have shown that the prion formed in the *S. cerevisiae* donor species can be transfected into a different recipient species, *S. paradoxus*. Moreover, the major properties of specific prion variants were maintained independently of the cell environment (Figure 2.1B). For example, transfection with the cellular extract from the "strong" [*PSI*$^+$] *S. cerevisiae* strain GT256-23C generated "strong" [*PSI*$^+$] isolates in *S. paradoxus*, as can be seen from growth on –Ade medium, color in YPD medium (Figure 2.1B) and almost entire lack of spontaneous [*PSI*$^+$] loss in mitotic divisions (only 3 out of 1624 colonies, obtained from 5 independent cultures, lost [*PSI*$^+$]). In contrast, transfection with the cellular extract from the "weak" [*PSI*+] *S. cerevisiae* strain GT988-1A generated "weak" [*PSI*$^+$] isolates in *S. paradoxus* (Figure 2.1B), Therefore, we were able to use the *S. paradoxus* cells containing the same "strong" [*PSI*$^+$] strain that was previously studied in the *S. cerevisiae* cell environment for our shuffle experiments, that allowed a direct assessment of the effect of cell environment onto the species barrier.

2.4.6 Comparison of Cross-Species Prion Transmission in S. cerevisiae and S. paradoxus Cells

To study the extent of influence of cell environment on the species barrier, cross-species prion transmission of a "strong" $Sup35_{Sc}$ [PSI^{+}] strain to *S. paradoxus* cells containing Sup35 proteins with PrD of different origin, or with a chimeric PrD was determined by using a plasmid shuffle procedure (Figure 2.2) and compared to previous results obtained in the *S. cerevisiae* cells [20]. Constructs with chimeric Sup35 PrDs were produced by reshuffling modules I (positions 1-33 in *S. cerevisiae* nomenclature), II (positions 34-96) and III (positions 97-123) in all possible combinations as described earlier [20]. Modules I and II roughly correspond to the QN-rich stretch and region of oligopeptide repeats, respectively. These are sub-regions of Sup35 PrD that were previously shown to influence the specificity and fidelity of cross-species prion transmission [20]. Results and comparison to the previous data are shown in Figure 2.10A.

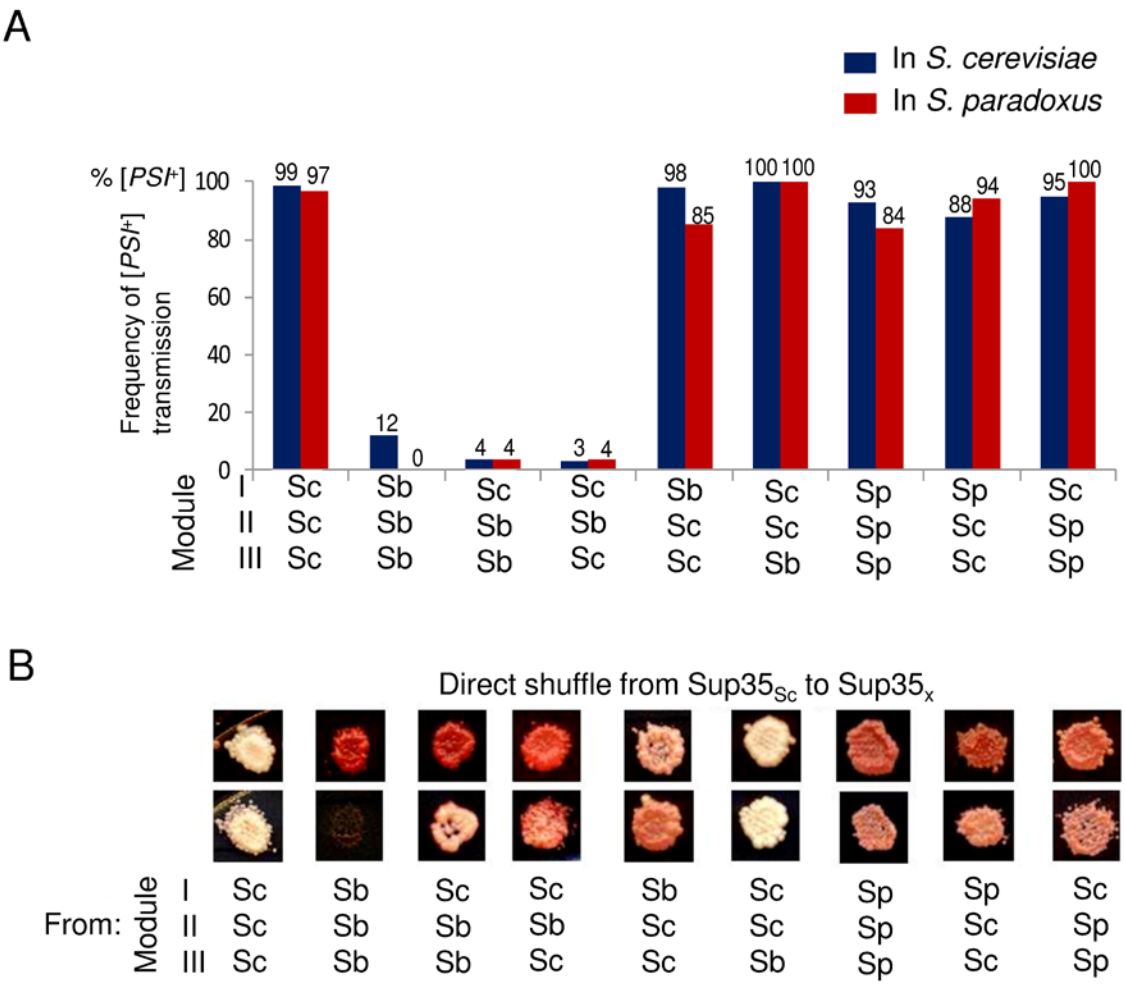

Figure 2.10 – Comparison of direct cross-species prion transmission in the *S. cerevisiae* and *S. paradoxus* cell environments. (A) Frequency of [*PSI*$^+$] transmission from *S. cerevisiae* Sup35 proteins to the proteins with divergent or chimeric prion domains (as indicated) is shown. Data obtained from the *S. cerevisiae* cell environment (shown in blue) were previously published in Chen et al, 2010. Numerals I, II, and III refer to the exchangeable modules of the PrD. "Sc", "Sp", and "Sb" refer to *S. cerevisiae*, *S. paradoxus*, and *S. bayanus*, respectively. (B) Phenotypes of [*PSI*$^+$] produced from direct transmission in *S. paradoxus*. Numerals I, II, and III refer to the exchangeable modules of the PrD. "Sc", "Sp", and "Sb" refer to *S. cerevisiae*, *S. paradoxus*, and *S. bayanus*, respectively. YPD (top) and –Ade (bottom) plates were photographed after 8 days.

Overall, similar patterns of transmission were observed in both *S. cerevisiae* and *S. paradoxus* cells, although some numerical differences were found. In both cases, the strongest barrier was detected between the *S. cerevisiae* and *S. bayanus* PrDs (in the *S. paradoxus* cells, no transmission was detected for this combination at all). By contrast, there was only a slight decrease in prion transmission from $Sup35_{Sc}$ to proteins with *S. paradoxus* PrD or its QN-rich stretch (module I). Previously described constructs with chimeric PrDs [20] were used to determine the roles of various regions of Sup35 in the species barrier. Similar to the experiments in *S. cerevisiae* cells, the region of oligopeptide repeats (module II) was a primary determinant of species-specificity of prion conversion in the combination of *S. cerevisiae* and *S. bayanus*. Notably, transmission of the prion state from $Sup35_{Sc}$ to any protein with the QN-rich stretch (module I) and/or the region of oligopeptide repeats (module II) coming from the species other than *S. cerevisiae* resulted in the appearance of a phenotypically weaker prion (Figure 2.10B), as previously observed in *S. cerevisiae* [20].

In further experiments, prions generated by transmission from $Sup35_{Sc}$ to proteins with divergent or chimeric PrDs were transmitted back to $Sup35_{Sc}$ by using reverse shuffle (Figure 2.11).

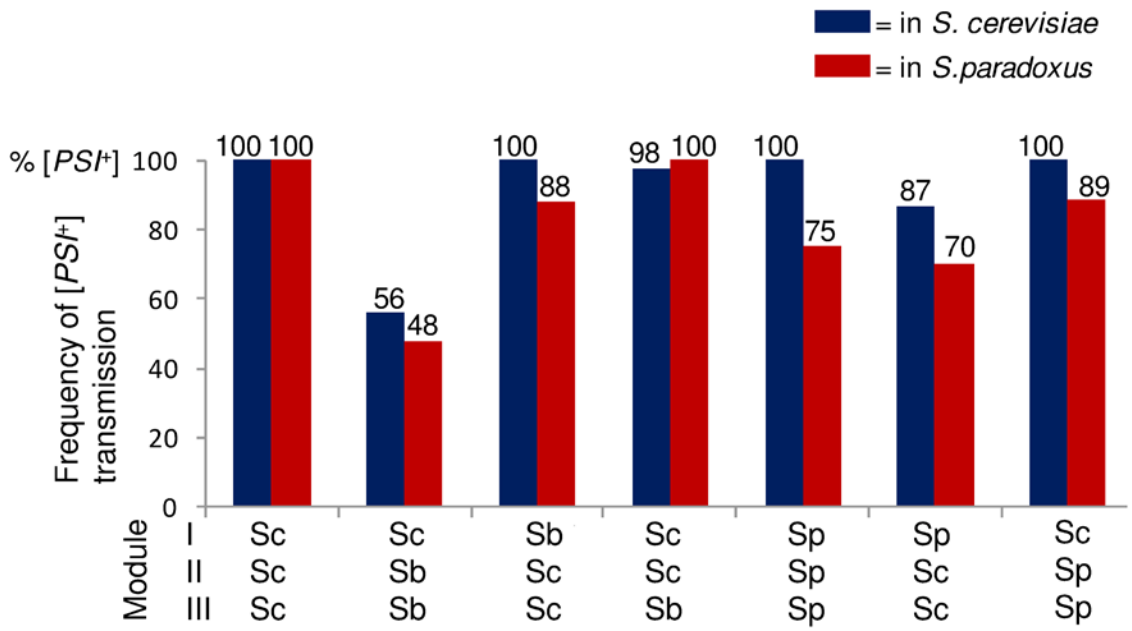

Figure 2.11 – Comparison of reverse cross-species prion transmission in *S. cerevisiae* and *S. paradoxus*. Frequencies of [*PSI*$^+$] transmission from the divergent or chimeric prion domains (as indicated) to the *S. cerevisiae* protein are shown. Designations are the same as in Figure 2.10. Notably, the reverse shuffle constructs containing the *S. paradoxus* PrD or its module I restored the original strong [*PSI*$^+$] variant. In contrast, reverse shuffle from constructs containing module II of *S. bayanus* produced weak [*PSI*$^+$] variants.

In most cases, results followed the same pattern as previously detected in *S. cerevisiae* [20]. As in *S. cerevisiae*, reverse transmission of prion state to Sup35$_{Sc}$ from the constructs containing the module II of *S. bayanus* was high in *S. paradoxus*, confirming the asymmetry of the species barrier in the *S. cerevisiae* – *S. bayanus* combination. On the other hand, while proteins containing *S. paradoxus* PrD or at least its module I transmitted the [*PSI*$^+$] state to Sup35$_{Sc}$ efficiently, a noticeable decrease was detected in *S. paradoxus*, compared to the *S. cerevisiae* cells.

For most combinations, the "strong" [*PSI*$^+$] phenotype has been restored after reverse transmission to Sup35$_{Sc}$, confirming that to the extent detectable by the resolution of our

approach, prion "weakening" during its propagation by a divergent or chimeric protein was due to changes in its phenotypic expression rather than in the molecular "properties" of prion strain. However, the $Sup35_{Sc}$ prion strain became "weak" after the reverse transmission from the protein containing at least module II from *S. bayanus* (Figure 2.12). Therefore, the underlying properties of the prion variant were irreversibly changed in this combination, once again confirming previous observations made in *S. cerevisiae* cells [20].

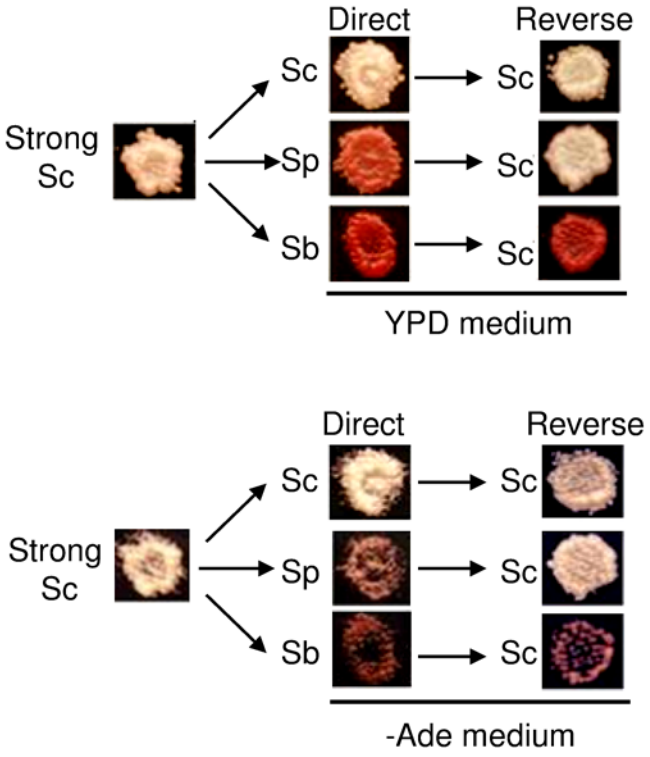

Figure 2.12 – Reproduction and switch of prion variants in cross-species transmission in the *S. paradoxus* cell environment on reverse shuffle. Representatives of direct shuffle experiment where [*PSI*$^{+}$] isolates obtained from a strong *S. cerevisiae* prion variant in the *S. paradoxus* cell environment went through direct shuffle to the control *S. cerevisiae* Sup35 protein or chimeric proteins with either *S. paradoxus* PrD or *S. bayanus* Module II PrDs, followed by reverse shuffle back to *S. cerevisiae* Sup35. (Top: YPD medium; Bottom: -Ade medium.)

Overall, our data show that the major rules of a transmission barrier, applying to both efficiency of prion transmission and fidelity of the reproduction of prion "strain" patterns by a divergent protein, are generally invariant in *S. cerevisiae* and *S. paradoxus* host cells, even though some quantitative differences were detected.

2.5 Discussion

We have previously reported that anions of the Hofmeister series influence kinetics and strain preference during *in vitro* amyloid formation by $Sup35NM_{Sc}$ [44, 47], and now we show that Sup35NM proteins from the other species of the *Saccharomyces sensu stricto* group, $Sup35NM_{Sb}$ and $Sup35NM_{Sp}$, also respond to the presence of kosmotropic or chaotropic ions in the same way as $Sup35NM_{Sc}$. We have confirmed previous data by showing that *in vitro,* in agreement with previous research, the more similar Sc/Sp proteins exhibit a relatively low barrier in the transmission of prion state, while the more divergent Sb protein shows a high barrier with the other two proteins [19]. We also performed systematic studies of the effects of the Hofmeister series anions on cross-species prion transmission. Overall, our data show that the salt present during amyloid formation can alter parameters of the species barrier. The most plausible explanation for this result is that the salts present during seed formation determine the seed conformation, which in turn influences the efficiency of conformational adaptation of a new monomer to the preformed nuclei provided by this seed. This agrees with our previous *in vivo* data showing that the prion strain pattern controls the specificity of transmission of the prion state to the newly immobilized protein [20]. In contrast, salts present during the process of cross-seeding exhibit a strong and systematic influence on the kinetics of cross-species aggregation in

accordance with the inverse Hofmeister trend that has been previously reported for homologous aggregation [44], but they do not alter the transmission specificity.

Interestingly, we observed that the seeds formed in chloride are more efficient in promoting both homologous and cross-species aggregation than the seeds formed in sulfate or perchlorate (Figure 2.6 and Figure 2.7). We hypothesize that this might be because seeded nucleation in chloride produces a very diverse mix of various prion strains. This diversity helps in providing a pool of seed conformations some of which more amenable for the monomer to template onto. Thus, there always exists a fraction of strains which can act as highly efficient templates in any given conditions. By contrast, aggregation in the presence of either highly kosmotropic (e. g. sulfate) or highly chaotropic (e.g. perchlorate) salt exhibits a more pronounced bias toward one particular strain, thus the type of the strain "pre-adopted" to the changed environment may not exist for certain conditions.

Previous work by the Weissman group has shown that temperature can be used to affect the specificity of the species barrier between *Saccharomyces cerevisiae* and *Candida albicans*. Tanaka et al. [24] observed that when $Sup35NM_{Sc}$ is aggregated at low (4ºC) temperature, more "promiscuous" aggregates with a stronger phenotype and higher seeding capabilities can be generated, compared to aggregates produced at high (37ºC) temperature. Tanaka et al. [53] had shown that the seeds of the *S. cerevisiae* Sup35NM protein formed at different temperatures show variable ability to cross-seed the Sup35NM protein from *Candida albicans*. Chien et al. [54] had shown that polymerization of a chimeric protein, combining the regions from the Sup35 prion domains of both *S. cerevisiae* and *C. albicans* can produce distinct prion strains with different seeding specificities, depending on temperature. These results agree with our observations that the differences in ionic

composition influence species barrier via promoting formation of different strains. However, our work represents the first systematic comparison of the effects of aggregation conditions at the stages of initial aggregate formation and cross-species seeding. Our data confirm that protein sequence and conformation play a central role in determining specificity of prion transmission, and show that external factors influence transmission specificity primarily via altering the nature of the initial seed, whereas the conditions of the actual cross-seeding reaction itself have an impact only on the kinetics of the process.

Further, by constructing a unique set of *S. paradoxus* strains allowing for prion detection and using the transfection protocol, we were able to obtain the *S. cerevisiae* and *S. paradoxus* cultures with one and the same "strain" of prion that helped us differentiate the effects of prion protein properties and intracellular environment on cross-species prion conversion. Our data show that both transmission barrier and conformational fidelity *in vivo* are primarily determined by the protein itself rather than by the environment. Thus, differences between the *S. cerevisiae* and *S. paradoxus* intracellular environments do not affect major rules of [*PSI*$^+$] transmission, although they might influence the quantitative characteristics of the process.

2.6 Conclusions and future work

Chapter 2 presents a detailed systematic study of species barrier in closely related species of the *Saccharomyces sensu stricto* group and demonstrates that the most important factor in determining the efficiency of cross-species transmission is the similarity in the sequences of the donor and recipient proteins both *in vivo* and *in vitro*, followed by the type of prion strain, while the effect of the environment is very systematic and only determines

the efficiency of co-transmission. Since the sequence similarity and identity levels of this system are similar to that of mammalian prion proteins, cross-species transmission of mammalian prion proteins can also be expected to behave in a similar fashion. This suggests that cross-species transmission is more likely between mammalian prion proteins which share high levels of sequence similarity and identity with each other. On the other hand, certain prion strains can possess a conformation which makes them more infectious and easily transmissible perhaps due to ease of conformational templating and addition of monomer onto their active surface. And finally, we can expect the environmental conditions that promote amyloid formation to promote cross-seeding or cross-species transmission while conditions which obstruct amyloid aggregation to hinder transmission of prions between different species.

An extension of this work would be to investigate if cross-transfection of aggregates produced *in vitro* in the presence of different salts results in similar patterns of transmission as seen in the *in vitro* cross-seeding experiments. For example, $Sup35NM_{Sc}$ seeds formed in the presence of a particular salt can be transfected into *S. bayanus* and *S. paradoxus* and the efficiency of transmission can be determined. Such a study can provide a direct comparison between *in vitro* and *in vivo* cross seeding indicating how well the *in vitro* cross-seeding experiments mirror cross-transmission of a prion *in vivo*.

Further, it will also be interesting to study the relative contribution of the environment and the seed strain on the final conformation of the aggregates formed. To do so, aggregates formed in the presence of a particular salt for example sodium sulfate can be used to seed Sup35NM in the presence of a salt of the opposite effect like sodium perchlorate and the structure of the final aggregate formed can be studied by TEM and/or AFM. Similarly, a

combination of seeding and aggregation salts can be used to further understand the relative influence of the seeding conditions and the environment on the conformation of the resulting aggregate and how faithfully the amyloid template is reproduced when the conditions of aggregation are altered.

It is interesting to note that Tanaka et. al. [24] had observed that Sup35NM strains with a 'strong' phenotype were formed at a low temperature (4ºC) while strains with a 'weak' phenotype were formed at a high temperature (37ºC). The aggregates formed at 4ºC showed lower thermal stability than the ones formed at 37ºC. Although the aggregation kinetics and the structure of the fibers formed were not determined in this work, we and others have observed that amyloid aggregation is faster at higher temperatures and slower at low temperatures [55]. So, interestingly while the aggregates formed at 4ºC have lower stability and result in strong phenotypes on transfection just like the ones formed in the presence of kosmotropes, the aggregation kinetics in the two cases are very different. Therefore, the phenotype on transfection and possibly the amyloid structure may not depend directly on the aggregation kinetics. This may be explained by the fact that while high temperature and the presence of kosmotropes both result in faster kinetics the driving force behind each effect is different. Crowding and depletion interactions due to the presence of kosmotropes result in bringing the species in solution closer to each other and hence, result in faster aggregation. On the other hand, it is the increase in the average kinetic energy and the number of collisions that overcome the activation energy barrier between the species in solution caused by a rise in temperature, which results in faster kinetics. This suggests that perhaps kinetics does not dictate amyloid strain conformation. It would be fruitful to look at the effect of other environmental conditions to further

evaluate the role of kinetics in strain formation. For example, the effect of agitation or other co-solutes on aggregation kinetics, stability, structure, and phenotype of the amyloid strains formed can be studied and compared to the effect of ions and temperature.

Finally, we can also investigate if the effect of ions on the surface tension of water results in the observed effect on amyloid aggregation or if it is some other ion-specific property. In this work, we have shown that the anion present during aggregation affects the kinetics of seeded aggregation similar to unseeded aggregation. To test if this is caused by changes in surface tension or some other ion-specific property, other additives which affect surface tension in a similar fashion could be added as co-solutes. For example, osmolytes such as sugars (e.g. sucrose) increase the surface tension of water by exerting a crowing effect similar to kosmotropes and their presence as a co-solute can be expected to result in faster aggregation kinetics. On the other hand, surfactants such as SDS reduce the surface tension like chaotropes and can be expected to result in slower aggregation kinetics. Hence, crowding agents and surfactants can be added as co-solutes to unseeded and seeded reactions and their effect on the kinetics of aggregation can be investigated.

2.7 Author contributions

In vitro aggregation experiments and transfection of yeast with amyloid aggregates generated *in vitro* were performed by Aditi Sharma. *In vivo* experiments were done by Kathryn L. Bruce. The strains used in this study were constructed by Buxin Chen, Stefka Gyoneva, and Kathryn L. Bruce.

2.8 References

1. Chiti, F. and C.M. Dobson, *Protein misfolding, functional amyloid, and human disease.* Annu. Rev. Biochem., 2006. **75**: p. 333-366.

2. Eisenberg, D. and M. Jucker, *The amyloid state of proteins in human diseases.* Cell, 2012. **148**(6): p. 1188-1203.

3. Eisenberg, D., R. Nelson, M.R. Sawaya, M. Balbirnie, S. Sambashivan, M.I. Ivanova, A.Ø. Madsen, and C. Riekel, *The structural biology of protein aggregation diseases: Fundamental questions and some answers.* Accounts of chemical research, 2006. **39**(9): p. 568-575.

4. Gregersen, N., P. Bross, S. Vang, and J.H. Christensen, *Protein misfolding and human disease.* Annu Rev Genomics Hum Genet, 2006. **7**: p. 103-24.

5. Jackson, G.S. and A.R. Clarke, *Mammalian prion proteins.* Current opinion in structural biology, 2000. **10**(1): p. 69-74.

6. Prusiner, S.B., *Prions.* Proceedings of the National Academy of Sciences, 1998. **95**(23): p. 13363-13383.

7. Pan, K.-M., M. Baldwin, J. Nguyen, M. Gasset, A. Serban, D. Groth, I. Mehlhorn, Z. Huang, R.J. Fletterick, and F.E. Cohen, *Conversion of alpha-helices into beta-sheets features in the formation of the scrapie prion proteins.* Proceedings of the National Academy of Sciences, 1993. **90**(23): p. 10962-10966.

8. Nguyen, J., M.A. Baldwin, F.E. Cohen, and S.B. Prusiner, *Prion Protein Peptides Induce. alpha.-Helix to. beta.-Sheet Conformational Transitions.* Biochemistry, 1995. **34**(13): p. 4186-4192.

9. Ross, E.D., A. Minton, and R.B. Wickner, *Prion domains: sequences, structures and interactions.* Nature cell biology, 2005. **7**(11): p. 1039-1044.

10. Pattison, I., *Experiments with scrapie with special reference to the nature of the agent and the pathology of the disease.* Slow, latent and temperate virus infections, NINDB Monograph, 1965. **2**: p. 249-257.

11. Prusiner, S.B., *Prion diseases and the BSE crisis.* Science, 1997. **278**(5336): p. 245-251.

12. Wilesmith, J.W., J. Ryan, and M. Atkinson, *Bovine spongiform encephalopathy: epidemiological studies on the origin.* The veterinary record, 1991. **128**(9): p. 199-203.

13. Ghani, A.C., C.A. Donnelly, N.M. Ferguson, and R.M. Anderson, *The transmission dynamics of BSE and vCJD.* Comptes rendus biologies, 2002. **325**(1): p. 37-47.

14. Hill, A.F., M. Desbruslais, S. Joiner, K.C. Sidle, I. Gowland, J. Collinge, L.J. Doey, and P. Lantos, *The same prion strain causes vCJD and BSE.* Nature, 1997. **389**(6650): p. 448-450.

15. Hueston, W.D., *BSE and variant CJD: Emerging science, public pressure and the vagaries of policy-making.* Preventive veterinary medicine, 2013. **109**(3): p. 179-184.

16. Ferguson, N.M., C.A. Donnelly, A.C. Ghani, and R.M. Anderson, *Predicting the size of the epidemic of the new variant of Creutzfeldt-Jakob disease.* British Food Journal, 1999. **101**(2): p. 86-98.

17. Liebman, S.W. and Y.O. Chernoff, *Prions in yeast.* Genetics, 2012. **191**(4): p. 1041-1072.

18. Chernova, T.A., K.D. Wilkinson, and Y.O. Chernoff, *Physiological and environmental control of yeast prions.* FEMS microbiology reviews, 2014. **38**(2): p. 326-344.

19. Chen, B., G.P. Newnam, and Y.O. Chernoff, *Prion species barrier between the closely related yeast proteins is detected despite coaggregation.* Proc Natl Acad Sci U S A, 2007. **104**(8): p. 2791-6.

20. Chen, B., K.L. Bruce, G.P. Newnam, S. Gyoneva, A.V. Romanyuk, and Y.O. Chernoff, *Genetic and epigenetic control of the efficiency and fidelity of cross-species prion transmission.* Mol Microbiol, 2010. **76**(6): p. 1483-99.

21. Afanasieva, E.G., V.V. Kushnirov, M.F. Tuite, and M.D. Ter-Avanesyan, *Molecular basis for transmission barrier and interference between closely related prion proteins in yeast.* Journal of Biological Chemistry, 2011. **286**(18): p. 15773-15780.

22. Wopfner, F., G. Weidenhöfer, R. Schneider, A. von Brunn, S. Gilch, T.F. Schwarz, T. Werner, and H.M. Schätzl, *Analysis of 27 mammalian and 9 avian PrPs reveals high conservation of flexible regions of the prion protein.* Journal of molecular biology, 1999. **289**(5): p. 1163-1178.

23. Šandula, J. and A. Vojtková-Lepšíková, *Immunochemical studies on mannans of the genus Saccharomyces.* Folia microbiologica, 1974. **19**(2): p. 94-101.

24. Tanaka, M., P. Chien, N. Naber, R. Cooke, and J.S. Weissman, *Conformational variations in an infectious protein determine prion strain differences.* Nature, 2004. **428**(6980): p. 323-328.

25. Tanaka, M. and J.S. Weissman, *An efficient protein transformation protocol for introducing prions into yeast.* Methods in enzymology, 2006. **412**: p. 185-200.

26. Bruce, K.L. and Y.O. Chernoff, *Sequence specificity and fidelity of prion transmission in yeast.* Seminars in cell & developmental biology, 2011. **22**(5): p. 444-451.

27. Derkatch, I.L., Y.O. Chernoff, V.V. Kushnirov, S.G. Inge-Vechtomov, and S.W. Liebman, *Genesis and variability of [PSI] prion factors in Saccharomyces cerevisiae.* Genetics, 1996. **144**(4): p. 1375-1386.

28. Toyama, B.H., M.J. Kelly, J.D. Gross, and J.S. Weissman, *The structural basis of yeast prion strain variants.* Nature, 2007. **449**(7159): p. 233-7.

29. Stein, K.C. and H.L. True *Prion strains and amyloid polymorphism influence phenotypic variation*. PLoS Pathogens, 2014. DOI: 10.1371/journal.ppat.1004328.

30. Kretzschmar, H. and J. Tatzelt, *Prion disease: a tale of folds and strains.* Brain Pathology, 2013. **23**(3): p. 321-332.

31. Parchi, P., R. Strammiello, A. Giese, and H. Kretzschmar, *Phenotypic variability of sporadic human prion disease and its molecular basis: past, present, and future.* Acta neuropathologica, 2011. **121**(1): p. 91-112.

32. Gambetti, P., I. Cali, S. Notari, Q. Kong, W.-Q. Zou, and W.K. Surewicz, *Molecular biology and pathology of prion strains in sporadic human prion diseases.* Acta neuropathologica, 2011. **121**(1): p. 79-90.

33. Surewicz, W.K. and M.I. Apostol, *Prion protein and its conformational conversion: a structural perspective*, in *Topics in Current Chemistry*. 2011, Springer Berlin Heidelberg. p. 135-167.

34. Bateman, D.A. and R.B. Wickner, *[PSI+] Prion Transmission Barriers Protect Saccharomyces cerevisiae from Infection: Intraspecies' Species Barriers'.* Genetics, 2012. **190**(2): p. 569-579.

35. Bateman, D.A. and R.B. Wickner *The [PSI+] prion exists as a dynamic cloud of variants*. PLoS Genetics, 2013. DOI: 10.1371/journal.pgen.1003257.

36. Li, J., S. Browning, S.P. Mahal, A.M. Oelschlegel, and C. Weissmann, *Darwinian evolution of prions in cell culture.* Science, 2010. **327**(5967): p. 869-872.

37. Mahal, S.P., S. Browning, J. Li, I. Suponitsky-Kroyter, and C. Weissmann, *Transfer of a prion strain to different hosts leads to emergence of strain variants.* Proceedings of the National Academy of Sciences, 2010. **107**(52): p. 22653-22658.

38. Ghaemmaghami, S., J.C. Watts, H.-O. Nguyen, S. Hayashi, S.J. DeArmond, and S.B. Prusiner, *Conformational transformation and selection of synthetic prion strains.* Journal of molecular biology, 2011. **413**(3): p. 527-542.

39. Hill, A.F. and J. Collinge, *Prion strains and species barriers*, in *Prions*. 2004, Karger. p. 33-49.

40. Broering, J.M. and A.S. Bommarius, *Evaluation of Hofmeister effects on the kinetic stability of proteins.* The Journal of Physical Chemistry B, 2005. **109**(43): p. 20612-20619.

41. Broering, J. and A. Bommarius, *Cation and strong co-solute effects on protein kinetic stability.* Biochemical Society Transactions, 2007. **35**(6): p. 1602-1605.

42. Broering, J.M. and A.S. Bommarius, *Kinetic model for salt-induced protein deactivation.* The Journal of Physical Chemistry B, 2008. **112**(40): p. 12768-12775.

43. Hofmeister, F., *On the understanding of the effects of salts.* Arch. Exp. Pathol. Pharmakol.(Leipzig), 1888. **24**: p. 247-260.

44. Rubin, J., H. Khosravi, K.L. Bruce, M.E. Lydon, S.H. Behrens, Y.O. Chernoff, and A.S. Bommarius, *Ion-specific effects on prion nucleation and strain formation.* J Biol Chem, 2013. **288**(42): p. 30300-8.

45. Diaz-Espinoza, R., A. Mukherjee, and C. Soto *Kosmotropic anions promote conversion of recombinant prion protein into a PrPSc-like misfolded form*. PloS one, 2012. **7**, DOI: 10.1371/journal.pone.0031678.

46. Allen, K.D., R.D. Wegrzyn, T.A. Chernova, S. Müller, G.P. Newnam, P.A. Winslett, K.B. Wittich, K.D. Wilkinson, and Y.O. Chernoff, *Hsp70 Chaperones as Modulators of Prion Life Cycle Novel Effects of Ssa and Ssb on the Saccharomyces cerevisiae Prion [PSI+]*. Genetics, 2005. **169**(3): p. 1227-1242.

47. Yeh, V., J.M. Broering, A. Romanyuk, B. Chen, Y.O. Chernoff, and A.S. Bommarius, *The Hofmeister effect on amyloid formation using yeast prion protein.* Protein Science, 2010. **19**(1): p. 47-56.

48. Kaiser, C., S. Michaelis, and A. Mitchell, *"Methods in yeast genetics"* 1994, Cold Spring Harbor Laboratory, Cold Spring Harbor, NY.

49. Chernoff, Y.O., S.M. Uptain, and S.L. Lindquist, *Analysis of prion factors in yeast.* Methods in enzymology, 2002. **351**: p. 499-538.

50. Sharma, A., K.L. Bruce, B. Chen, S. Gyoneva, S.H. Behrens, A.S. Bommarius, and Y.O. Chernoff, *Contributions of the Prion Protein Sequence, Strain and Environment to the Species Barrier.* Journal of Biological Chemistry, 2015.

51. Edskes, H.K., L.M. McCann, A.M. Hebert, and R.B. Wickner, *Prion variants and species barriers among Saccharomyces Ure2 proteins.* Genetics, 2009. **181**(3): p. 1159-1167.

52. Klement, K., K. Wieligmann, J. Meinhardt, P. Hortschansky, W. Richter, and M. Fandrich, *Effect of different salt ions on the propensity of aggregation and on the structure of Alzheimer's abeta(1-40) amyloid fibrils.* J Mol Biol, 2007. **373**(5): p. 1321-33.

53. Tanaka, M., P. Chien, K. Yonekura, and J.S. Weissman, *Mechanism of cross-species prion transmission: an infectious conformation compatible with two highly divergent yeast prion proteins.* Cell, 2005. **121**(1): p. 49-62.

54. Chien, P., A.H. DePace, S.R. Collins, and J.S. Weissman, *Generation of prion transmission barriers by mutational control of amyloid conformations.* Nature, 2003. **424**(6951): p. 948-51.

55. Sabaté, R., A. Villar-Piqué, A. Espargaró, and S. Ventura, *Temperature dependence of the aggregation kinetics of Sup35 and Ure2p yeast prions.* Biomacromolecules, 2011. **13**(2): p. 474-483.

CHAPTER 3. ION-SPECIFIC EFFECTS ON AGGREGATION OF AMYLOID BETA-42 AND SUP35NM

3.1 Abstract

The amyloid aggregation process is influenced by the presence of co-solutes *in vitro.* Ion-specific effects on the stability, solubility, and precipitation of proteins can generally be correlated to their position in the Hofmeister series. Here, we have studied the effect of anions on fiber formation by Amyloid beta$_{42}$ (Aβ_{42}) and Sup35NM at pH above and below their isoelectric points. We find interesting differences in the aggregation kinetics of Aβ_{42} and Sup35NM in the presence of ions. Further, the electrophoretic mobilities of Aβ_{42} and Sup35NM were measured in the presence of anions at pH above and below the isoelectric points to understand how the respective anions interact with these proteins when they are positively or negatively charged. We find that while ion-protein interactions generally follow expectations as per their position in the Hofmeister series, there are qualitative differences in the aggregation behaviour of Aβ_{42} and Sup35NM. These differences may be explained by their widely different biochemical and biophysical properties and point towards a difference in their mechanisms of aggregation.

3.2 Introduction

The amyloid aggregation process is dependent on two main factors, namely, the primary sequence of the protein, and environmental conditions. For the same protein sequence, changes in temperature, pH, solvent composition, agitation etc. have a clear impact on the aggregation kinetics and the structure of the fibers formed [1-4]. The fiber

morphology in turn determines strain properties which govern disease patterns in mammals. Therefore, an investigation of the effect of environmental factors on aggregation kinetics can help in understanding the root cause of differences in disease progression.

3.2.1 Ion-specific effects

Ions can be classified on the basis of their effect on protein solubility and conformation. The Hofmeister series, originally developed by the German scientist Franz Hofmeister in the late 1800s from observations on the ability of ions to precipitate hen egg white lysozyme, serves as a guide to the effect of ions on protein stability [5]. The ions in the series are arranged according to their ability to salt out (precipitate) and salt in (solubilize) most proteins. Ions which are larger in size, weakly hydrated, less polarized, decrease surface tension, and increase protein solubility lie towards one end of the series. These ions were originally proposed to interfere with the hydrogen-bonding of water and were termed as ‘chaotropes’ or ‘water structure breakers’. On the other hand, the smaller, strongly hydrated ions which increase surface tension and decrease protein solubility, favoring the most compact conformation lie towards the other end of the series and were called ‘kosmotropes’ or ‘water structure makers’. The presence of ions also affects the viscosity of bulk water and the position of ions in the Hofmeister series has also been shown to correlate with the Jones-Dole viscosity B coefficient in the following equation.

$$\frac{\eta}{\eta_o} = 1 + Ac^{1/2} + Bc \qquad (1)$$

Here, η is the viscosity of aqueous solution of ions, η_o is the viscosity of water, c is concentration of the ion, A is a term to account for electrostatic effects and B is a measure of the strength of ion-water interactions. B is generally negative for the weakly hydrated chaotropes which result in reduction in viscosity with increase in concentration and is positive for the strongly hydrated kosmotropes which result in increase in viscosity with increase in concentration.

3.2.2 Studies on the effect of ions on amyloid formation

Previous work from our group has shown that sodium salts of different anions can alter the aggregation kinetics and the structure of the amyloid aggregates formed by the prion domain containing NM fragment of Sup35 proteins from *Saccharomyces cerevisiae* at a pH of 7.4 [1, 2]. The effect of the anions on Sup35NM aggregation kinetics and amyloid structure correlates very well with their position in the Hofmeister series. In a separate study on species barrier we have also shown that anions can be used to form seed 'strains' or 'variants' with different transmissibility across closely related species of the *Saccharomyces sensu stricto* group [6]. The effect of ions on fiber nucleation and elongation, and conformation has been studied for a few other amyloidogenic proteins such as amylin, α-synuclein, β2-microglobulin, mouse prion protein, $A\beta_{40}$, etc. [3, 7-10]. However, a clear and comprehensive understanding of these effects keeping in consideration the charge on the protein at the experimental conditions has not been presented. Moreover, a careful comparative study of these effects on different proteins has not been done.

In this work, we have investigated and compared the effect of anions of the Hofmeister series on the aggregation kinetics of Sup35NM and $A\beta_{42}$. $A\beta_{42}$ is a 42 amino acid-long peptide formed by the proteolytic cleavage of amyloid precursor protein (APP), and is considered to be the primary protein associated with Alzheimer's disease. It forms fibrillar aggregates which associate together resulting in the formation of amyloid plaques in the central nervous system of the patient and lead to neuronal cell death and degeneration. Recent work by two separate groups on demonstrating the structure of $A\beta_{42}$ fibers has shown that in the fibrillar form the peptide buries its hydrophobic residues in the core of symmetrical dimers that are stacked perpendicular to the axis of the fiber [11, 12]. Sup35NM on the other hand has been shown to form fibers with a single molecule per layer primarily through interactions of glutamine and asparagine residues in the beta sheet rich prion domain of the protein [13]. Both the proteins have been shown to form aggregates composed of parallel in-register beta sheets [13-15].

Ions play a crucial role in many biological functions. Ion-specific effects are usually found to be more pronounced for anions than cations which are generally excluded from protein-water interface and exhibit less pronounced Hofmeister effects. Amongst anions, chloride ions are universally present in living organisms and other anions like phosphate, iodide, fluoride, acetate, citrate, biocarbonate, nitrate, etc. can also be present in different compartments of a cell. Cells, organelles, and body fluids can also have different pH values. While ionic concentration and pH are tightly regulated in the body to ensure proper biological functioning, any variations in the localized ionic concentration and pH can significantly affect the stability of proteins and may promote disordered aggregation as well as amyloid formation. Therefore, an understanding of the effect of ion concentration

and pH on protein stability and aggregation can shed light on the causal factors of amyloid formation in living organisms.

Here, we have studied the aggregation of Sup35NM and $A\beta_{42}$ in the presence of sodium salts at pH of 3.2, 4.5 and, 7.4. The isoelectric points (pI) of Sup35NM and $A\beta_{42}$ are around 5.3. We observe some similarities in the effect of ions on the fibrillation kinetics of the two proteins, pointing to the universal nature of the effect of ions, as well as some differences in the aggregation behavior of these two proteins which can be correlated to the biophysical properties of these proteins and points to differences in the aggregation mechanisms of the two proteins.

3.3 Material and Methods

3.3.1 Expression and purification of Sup35NM

E. coli host strain HMS174 (DE3) pLysS (Novagen) was transformed with pET21b vector containing the NM domain coding region of Sup35p from *Saccharomyces cerevisiae* with an attached C-terminal His_6 tag [16]. Sup35NM was expressed and purified as described previously [2]. Briefly, the cells were transformed with the cloning vector, protein expression was induced using isopropyl β-D-1-thiogalactopyranoside (IPTG), and the cells were harvested after about 4 hours of induction at 37°C. The cell pellets were stored at −80°C until purification and the protein was purified by Ni-NTA His-tag affinity purification under denaturing conditions. The purified protein was precipitated using cold methanol at -20°C, the protein pellet was collected by centrifugation and washed with cold methanol, and finally stored at -80°C in 80% methanol.

3.3.2 Expression and purification of recombinant $A\beta_{42}$

Gene encoding $A\beta_{42}$ peptide was cloned into pET28 vector using restriction enzymes, NcoI and Xho1, and primers (5'-GCGCGCGC CC ATG GAT GCA GAA TTC CGA -3' (forward) and 5'-GCGC CTC GAG TTA CGC TAT GAC AAC ACC-3' (reverse)). *E. coli* host strain BL21 STAR (DE3) (Invitrogen) was transformed with pET28 vector containing the gene encoding $A\beta_{42}$. $A\beta_{42}$ was purified by a modified protocol adapted from Walsh et al. 2009 [17]. Anion exchange chromatography was performed using Q-Sepharose resin (Sigma Aldrich). Fractions containing pure peptide were pooled together and concentrated using a 3kDa centrifugal filter (EMD Millipore) and buffer exchanged into 2mM NaOH, lyophilized, and stored at −80°C.

3.3.3 Fibrillation assays using Thioflavin T

Sup35NM protein pellet stored in 80% methanol at -80°C was collected by centrifugation. The supernatant was discarded and the protein was re-suspended in 8 M urea. Sup35NM was then concentrated by 3 kDa centrifugal filter (EMD Millipore) and diluted 100 folds into the buffer of choice. The samples were boiled for about 10 min before starting the aggregation experiments to break down any preformed aggregates. A stock solution of 1 mM thioflavin T (ThT; Sigma Aldrich) was prepared fresh in the same buffer.

Lyophilized $A\beta_{42}$ was resuspended in HPLC grade water. The peptide was then filtered through a 30kDa centrifugal filter to obtain the low molecular weight fractions and diluted with 10X buffer to make the final concentration of the peptide 20 μM.

Aggregation experiments were conducted in triplicates in a 96 well plate with final ThT, Sup35NM, and $A\beta_{42}$ concentrations of 10 μM, 10 μM, and 20 μM, respectively, containing 0.1M, 0.3M, and 0.5 M sodium salt. Fibrillation assays were carried out at 37°C in a 96-well plate with orbital shaking at 307 rpm (5mm amplitude) in a BioTek Synergy H1 Multi-Mode Microplate Reader. Fluorescence readings were recorded every 10 minutes using an excitation wavelength of 440 nm and emission wavelength of 485 nm.

3.3.4 Electrophoretic mobility measurements

Electrophoretic mobility values of Sup35NM and $A\beta_{42}$ at concentrations of 10 μM and 20 μM, respectively, were measured in solutions at pH of 3.2, 4.5, and 7.4 containing 0.1M, 0.3M and 0.5M sodium salts using Malvern Zetasizer Nano ZS.

3.4 Results

3.4.1 Fibril formation by Sup35NM and $A\beta_{42}$ at pH above pI

Since, the isoelectric points of both Sup35NM and $A\beta_{42}$ are around 5.3, at pH = 7.4, both the proteins are positively charged. We observe that the effect of ions on the fibrillation of Sup35NM at pH 7.4 correlates with the position of the ions along the Hofmeister series with kosmotropic ions such as SO_4^{2-}, IO_3^-, and F^- making the aggregation faster and chaotropic ions such as Cl^-, Br^- and ClO_4^- slowing down the aggregation as the salt concentration is increased (Figure 3.1). This agrees with our previous reports on the effect of ions on the aggregation of Sup35NM at 25ºC [1, 2].

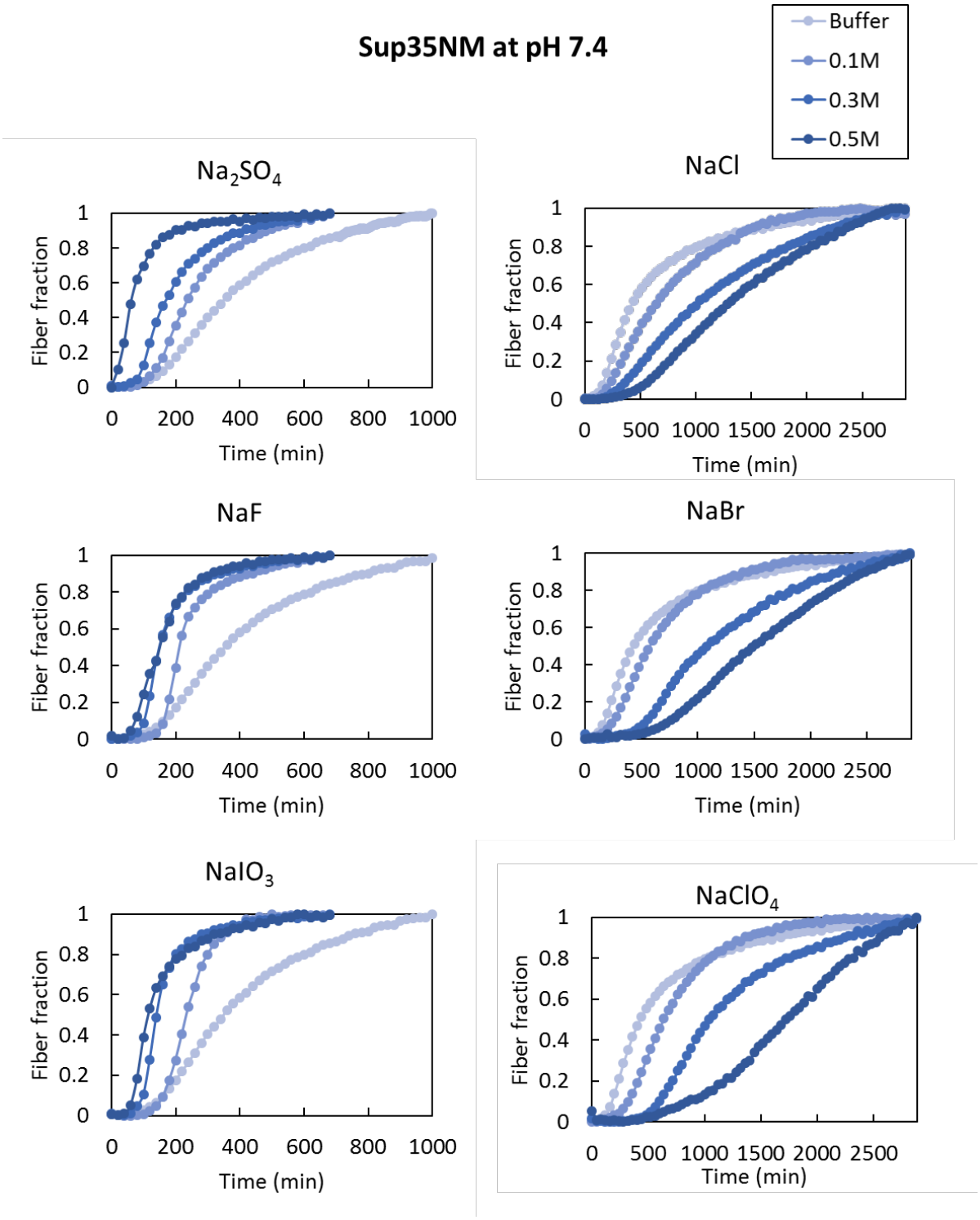

Figure 3.1 – Fibrillation of Sup35NM at pH 7.4 in the presence of sodium salts of SO_4^{2-}, IO_3^-, F^-, Cl^-, Br^-, and ClO_4^- at 37°C. The fiber fraction was determined from relative fluorescence units (RFU) measured at an excitation wavelength of 440nm and emission wavelength of 485nm.

On the other hand, we see that the presence of both kosmotropic and chaotropic anions promotes faster fibrillation of $A\beta_{42}$ at pH 7.4 (Figure 3.2). While we expect the effect of kosmotropes to remain the same, our observation of the effect of chaotropes on $A\beta_{42}$ aggregation is interesting. Here, we see that increasing concentration of chaotropes result in faster aggregation of $A\beta_{42}$. This is opposite to the effect of increasing concentrations of chaotropes on aggregation of Sup35NM where we had seen that as the concentration of chaotropes was increased the aggregation was hindered (Figure 3.1).

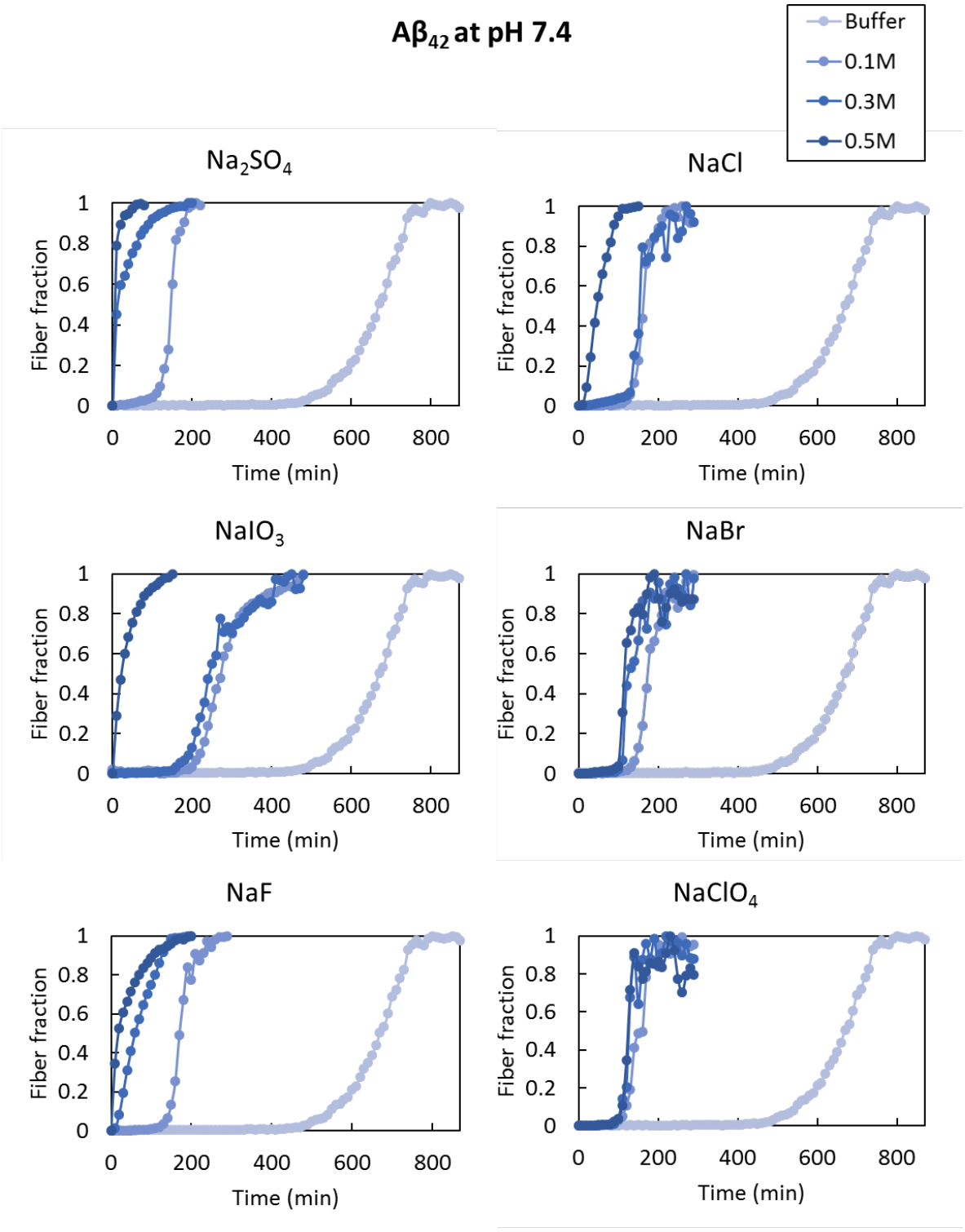

Figure 3.2 – Fibrillation of Aβ$_{42}$ at pH 7.4 in the presence of sodium salts of SO_4^{2-}, IO_3^-, F^-, Cl^-, Br^-, and ClO_4^- at 37°C

While increasing the concentration of chaotropic ions favored faster aggregation for $A\beta_{42}$, however, similar to Sup35NM, the relative effect of anions (at the same concentration) on the kinetics of aggregation of $A\beta_{42}$ still correlated with their position in the Hofmeister series (Figure 3.1 and Figure 3.2). For example, at a concentration of 0.5M the most kosmotropic SO_4^{2-} was the most effective in promoting aggregation while the most chaotropic ClO_4^- was the least effective for Sup35NM and $A\beta_{42}$ both (Figure 3.3 and Figure 3.4).

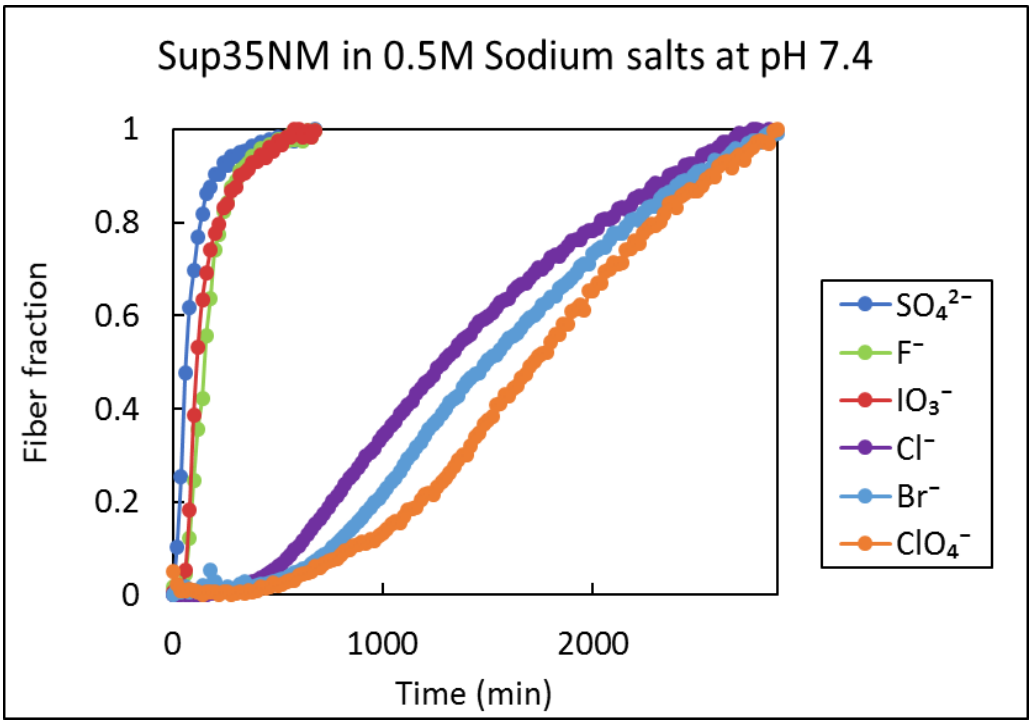

Figure 3.3 – Fibrillation of Sup35NM at pH 7.4 in the presence of 0.5M salt

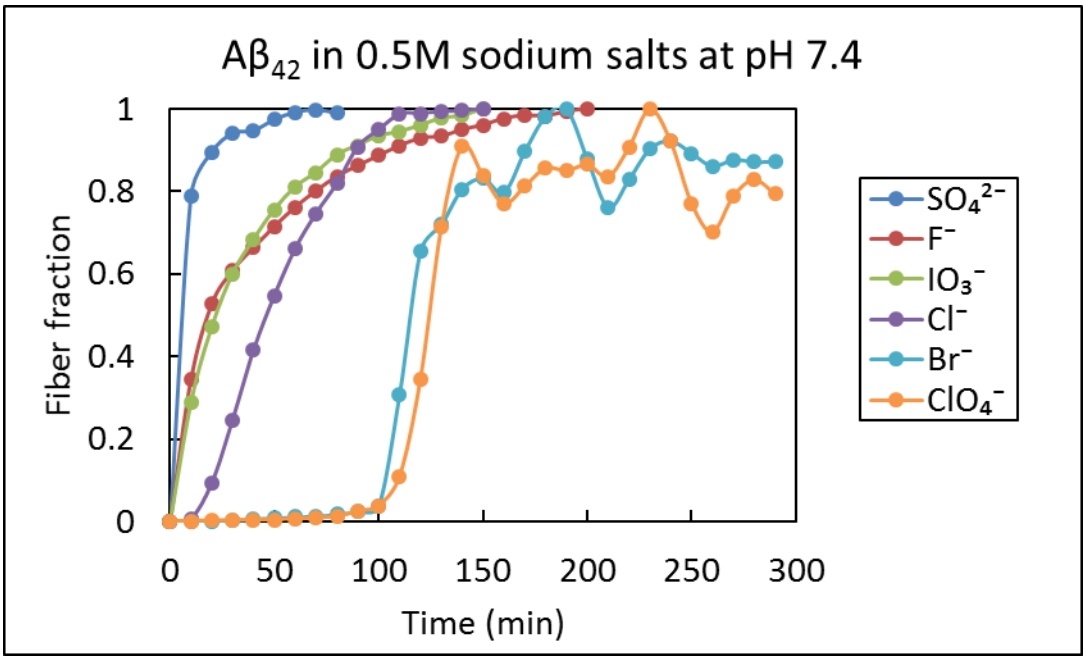

Figure 3.4 – Fibrillation of Aβ42 at pH 7.4 in the presence of 0.5M salt

3.4.2 Electrophoretic mobility of Sup35NM and Aβ42 at pH above pI

Next we performed electrophoretic mobility measurements in the presence of ions to understand how they interact with Sup35NM and Aβ42. We observe that as the concentration of the ions is increased charge screening increases resulting in an overall reduction in electrophoretic mobility. However, chaotropes are able to adsorb to both Sup35NM and Aβ42 ions in spite of the net negative charge on both proteins at pH 7.4. This results in the electrophoretic mobilities in the presence of chaotropes being more negative than in the presence of kosmotropes (see Figure 3.4 and Figure 3.5). Mobility measurements in the presence of SO_4^{2-} are excluded from the reported data since SO_4^{2-} being a divalent ion offers stronger shielding than monovalent ions, and for the same ionic strength of Na_2SO_4, the concentration of SO_4^{2-} is different, making a direct comparison of mobilities in Na_2SO_4 and mobilities in sodium salts of monovalent ions infeasible.

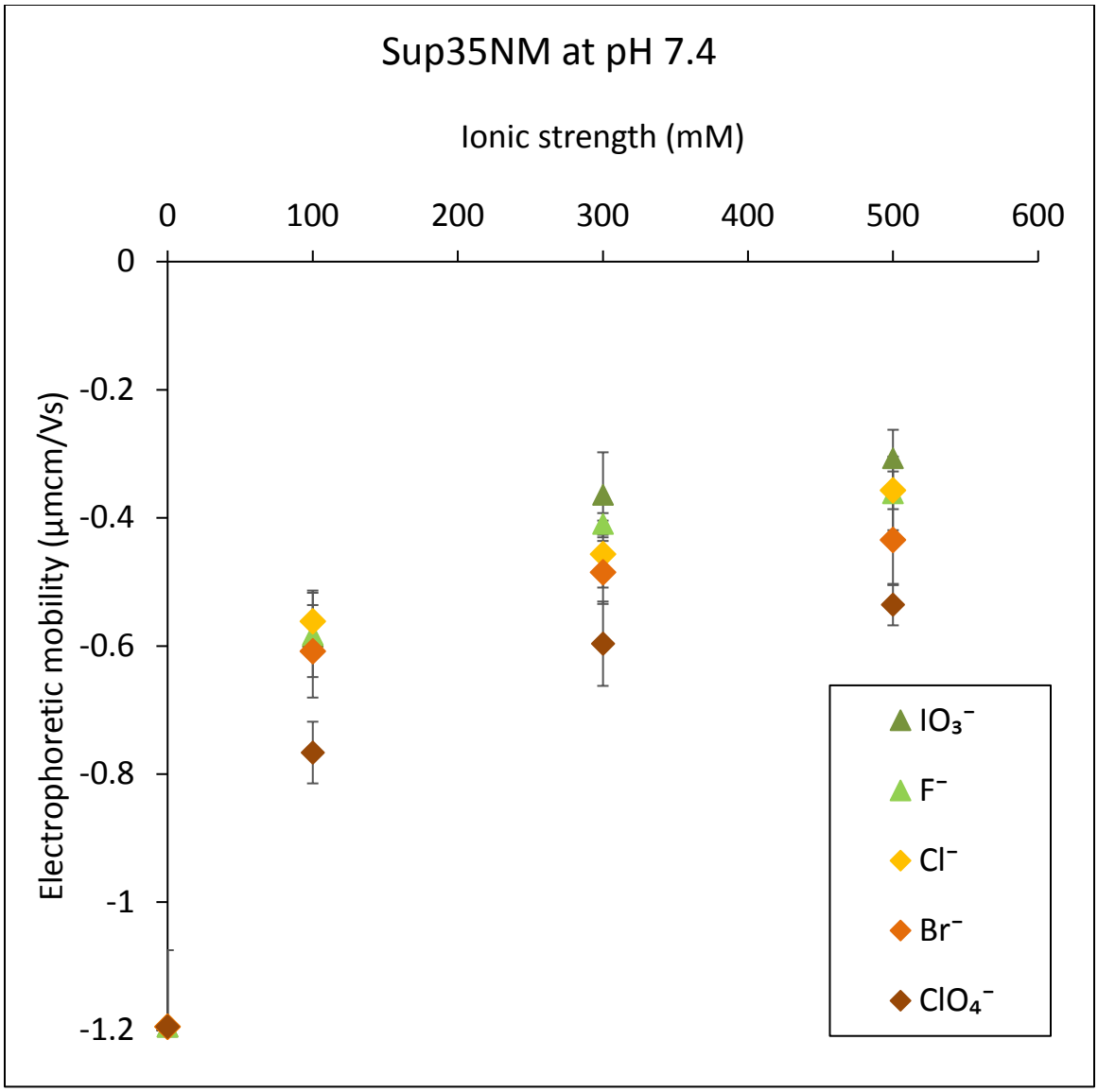

Figure 3.5 – Electrophoretic mobilities of Sup35NM at pH 7.4 in the presence of sodium salts of monovalent anions

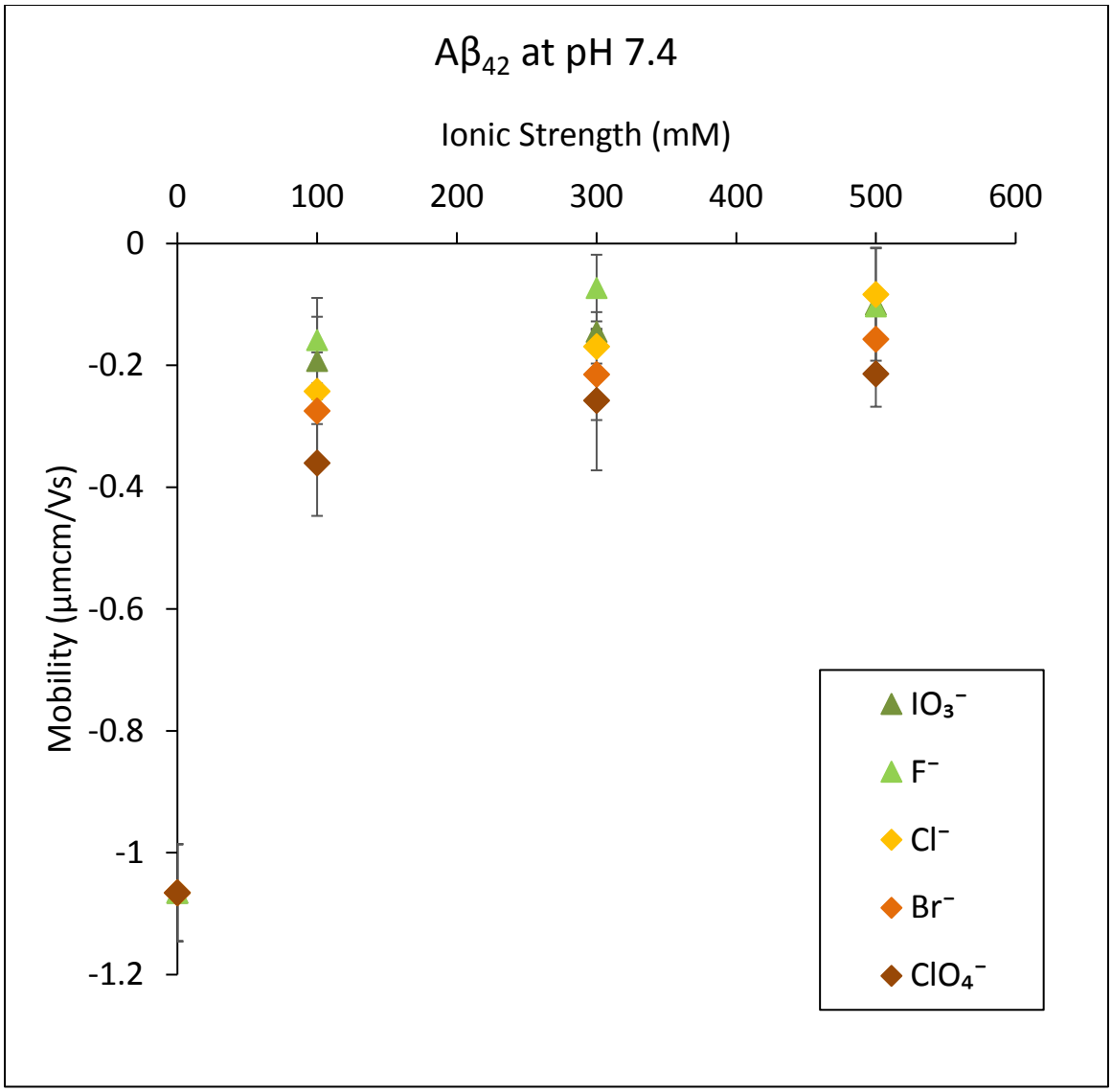

Figure 3.6 – Electrophoretic mobilities of Aβ$_{42}$ at pH 7.4 in the presence of sodium salts of monovalent anions

3.4.3 Fibril formation by Sup35NM and Aβ$_{42}$ at pH below pI

Further, we investigated the effect of anions on the aggregation kinetics of Aβ$_{42}$ and Sup35NM when the charge on the proteins is reversed. In order to do this, we performed aggregation experiments and electrophoretic mobility measurements at pH 4.5 and 3.2.

Due to incomplete dissociation of most of the kosmotropic ions in the acidic pH range we are limited to just SO_4^{2-} and IO_3^- at pH 3.2 and SO_4^{2-}, IO_3^- and $H_2PO_4^-$ at pH 4.5. At a pH of 3.2, we see an inversion in the effect of chaotropes on Sup35NM, while the effect of kosmotropic ions which act by exerting a depletion force is the same. At this pH, chaotropic ions which can interact with specific regions in a polypetide chain, result in more effective charge screening and neutralization, and promote fast fibril formation by Sup35NM.

The effect of both kosmotropes and chaotropes on fibril formation by $A\beta_{42}$ at pH 3.2 is similar to Sup35NM (see Figure 3.6 and Figure 3.7). This reversal of the Hofmeister effect for chatropes on inversion of the net charge on the molecules has been reported for colloidal systems and globular proteins [18-23]

Next, we investigated the consequence of reduction in the net charge on Sup35NM and $A\beta_{42}$ on the effect of ions on their aggregation. While the effect of kosmotropes on both Sup35NM and $A\beta_{42}$ remains the same at pH 4.5, the strong chaotropes (Br^- and ClO_4^-) show a partial reversal in their fibrillation promoting effect at pH 4.5. After a threshold concentration the aggregation becomes slower as the concentration of these ions which adsorb strongly to the proteins is increased (Figure 3.8). Interestingly no such reversal is seen for $A\beta_{42}$ (Figure 3.9).

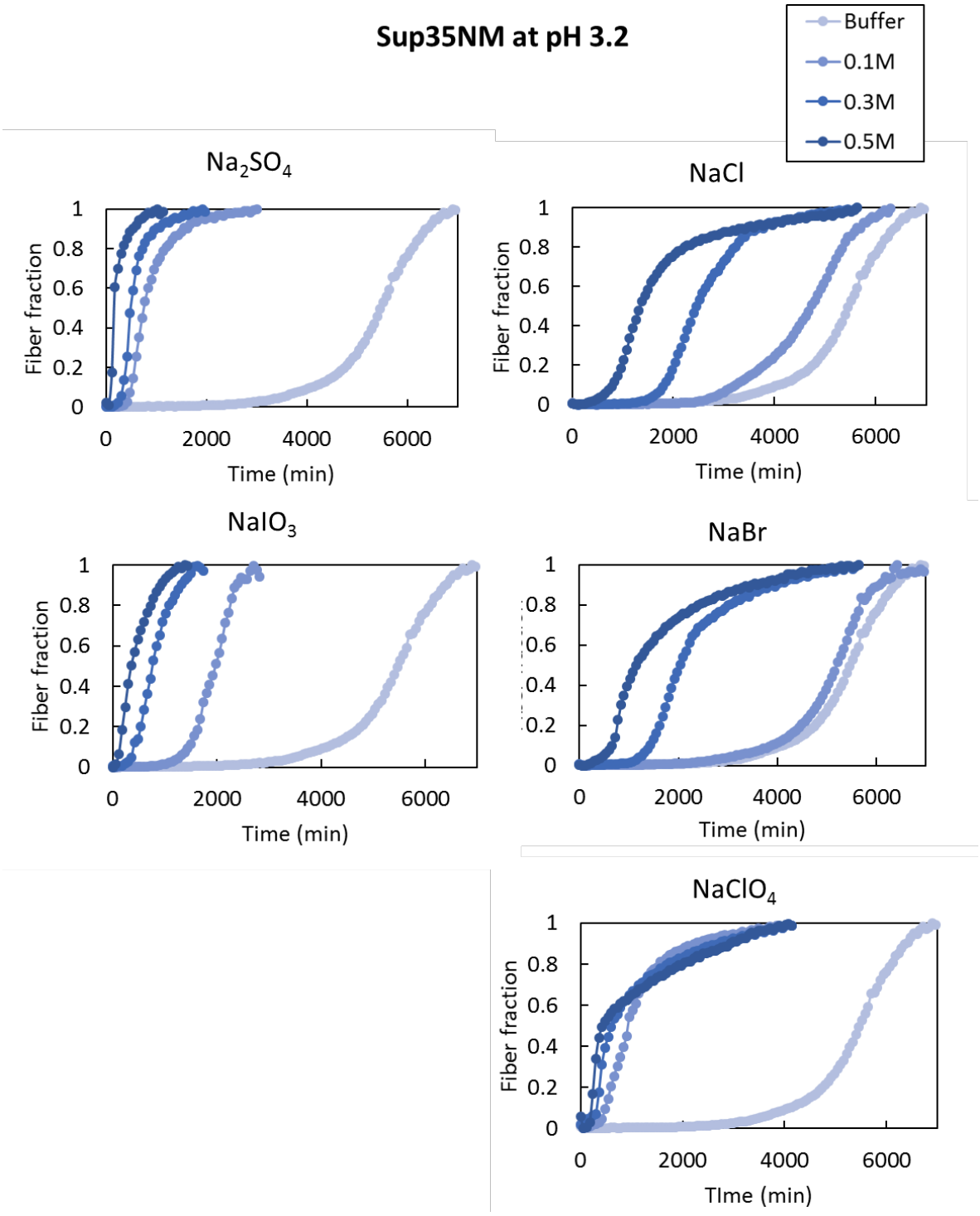

Figure 3.7 – Fibrillation of Sup35NM at pH 3.2 in the presence of sodium salts of SO_4^{2-}, IO_3^-, Cl^-, Br^-, and ClO_4^- at 37ºC

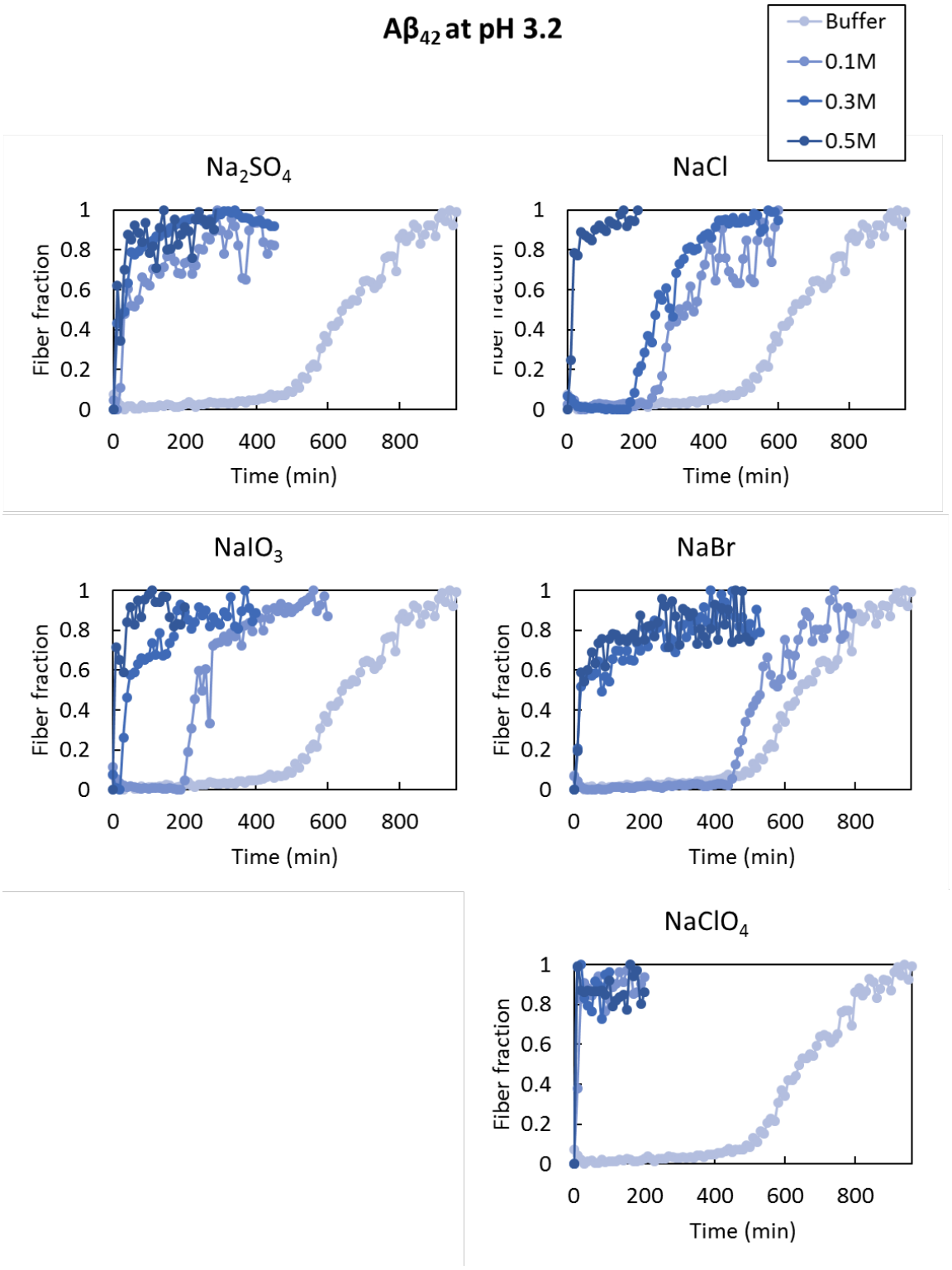

Figure 3.8 – Fibrillation of Aβ$_{42}$ at pH 3.2 in the presence of sodium salts of SO_4^{2-}, IO_3^-, Cl^-, Br^-, and ClO_4^- at 37ºC

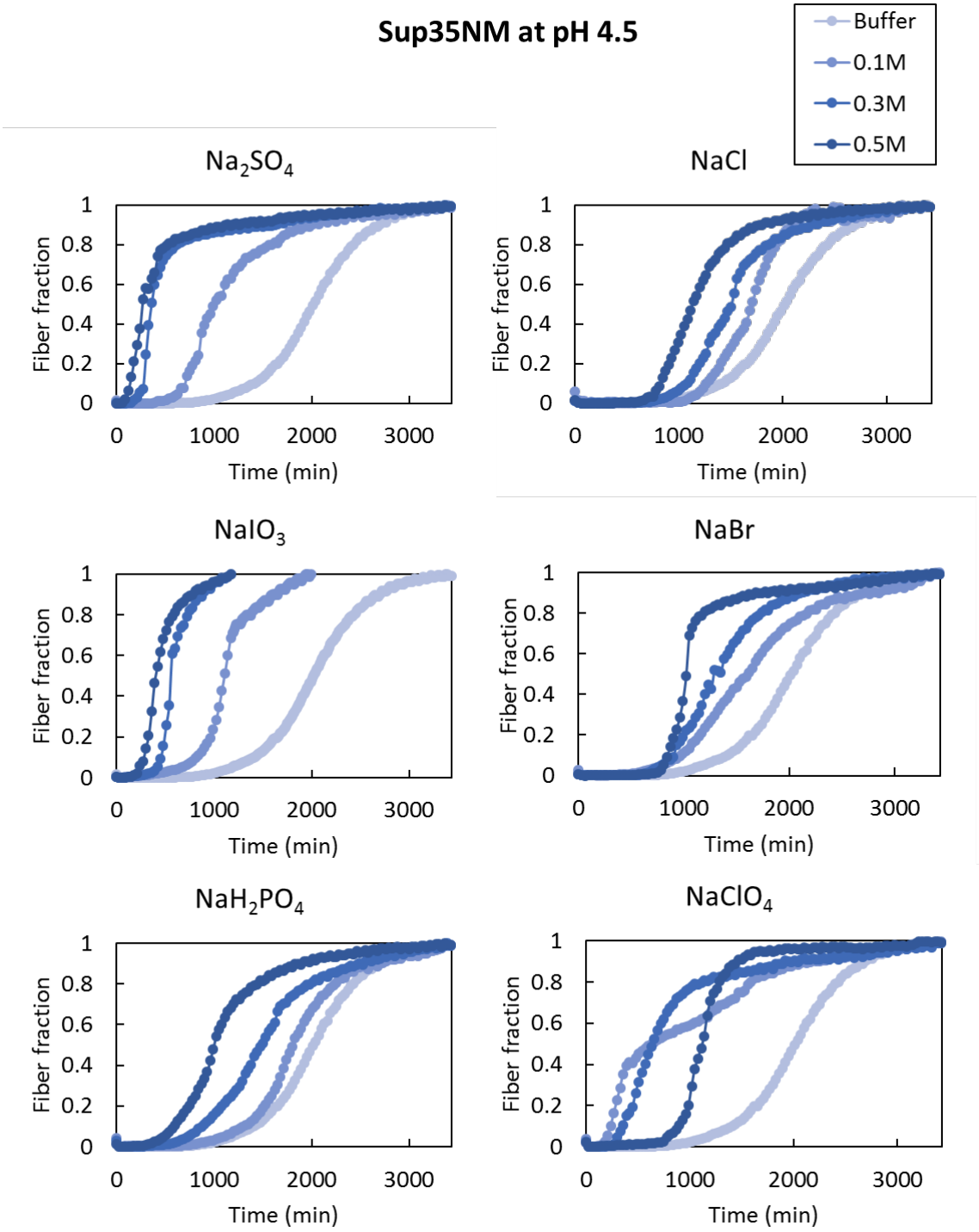

Figure 3.9 – Fibrillation of Sup35NM at pH 4.5 in the presence of sodium salts of SO_4^{2-}, IO_3^-, $H_2PO_4^-$, Cl^-, Br^-, and ClO_4^- at 37°C

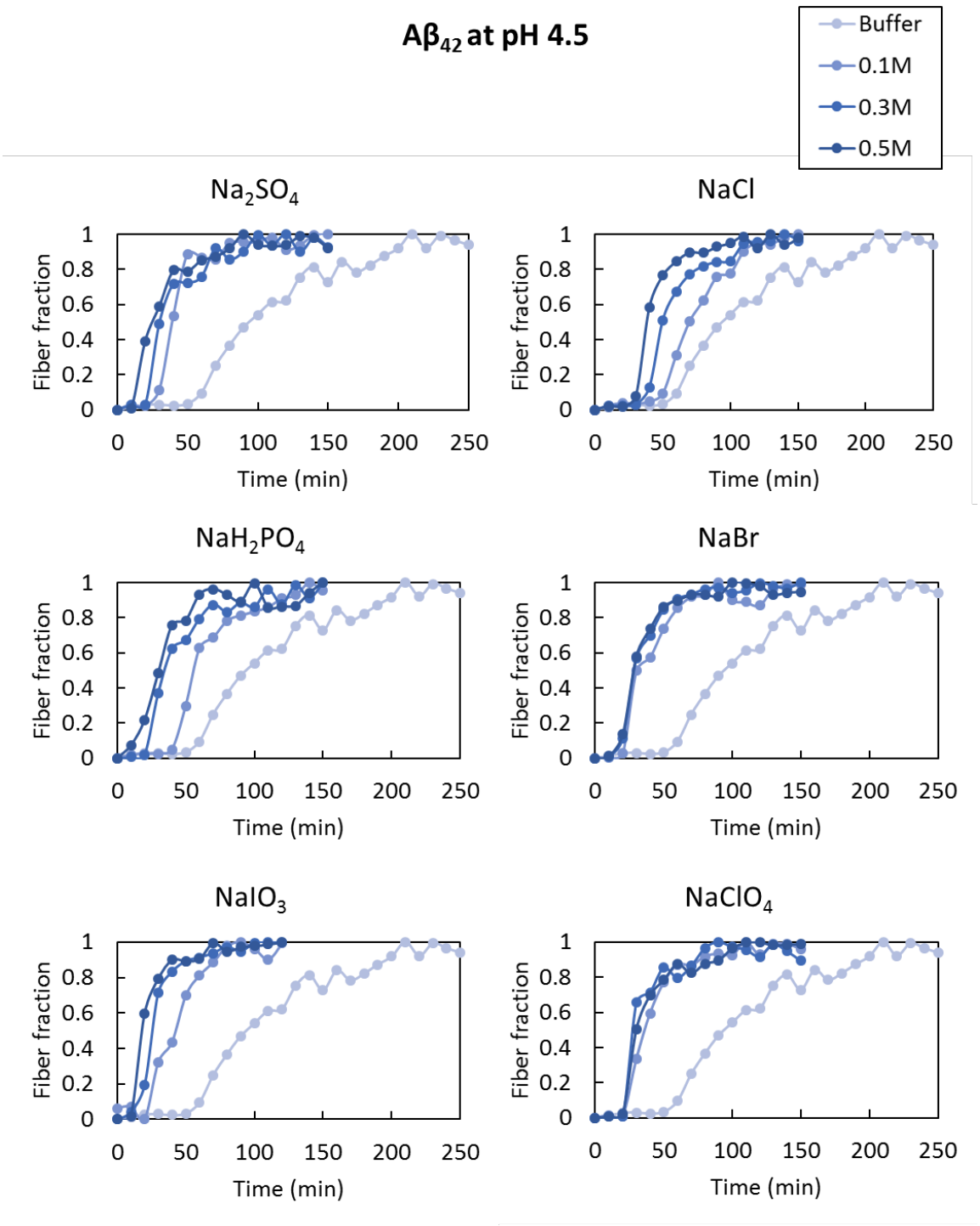

Figure 3.10 – Fibrillation of Aβ42 at pH 4.5 in the presence of sodium salts of SO_4^{2-}, IO_3^-, $H_2PO_4^-$, Cl^-, Br^-, and ClO_4^- at 37ºC

3.4.4 Electrophoretic mobility of Sup35NM and Aβ$_{42}$ at pH below pI

Next, we measured the electrophoretic mobilities of Sup35NM and Aβ$_{42}$ at pH 3.2 and 4.5, where both proteins are positively charged and anions act as counter-ions. Again, we see that as the concentration of the ions is increased charge screening increases resulting in an overall reduction in electrophoretic mobility. Additionally, similar to pH 7.4, the chaotropic anions are able to adsorb better to both Sup35NM and Aβ$_{42}$ than kosmotropes. This results in greater reduction in the effective charge on the proteins in the presence of chaotropes and mobilities being smaller in the presence of chaatropes at pH 3.2 and 4.5 (see Figure 3.10, Figure 3.12, Figure 3.11, and Figure 3.13). At pH 4.5, where the net charge on the protein is less we see that increasing the concentration of Br^- and ClO_4^- results in a reversal in the sign of the mobility and, hence, the charge on Sup35NM. Further increase in the ion concentration adds more negative charges on the protein due to adsorption of more ions resulting in increase in the negative mobilities at higher concentrations of the strong chaotropes. This reversal in the mobilities of Sup35NM in the presence of strong chaotropes at pH 4.5 agrees with our aggregation data (Figure 3.12). Interestingly a charge reversal is also seen in the mobilities of Aβ$_{42}$ at pH 4.5 however, it is not reflected in the aggregation data perhaps because the absolute value of the charge-reversed mobilities are very close to zero. (Figure 3.13 and Figure 3.9).

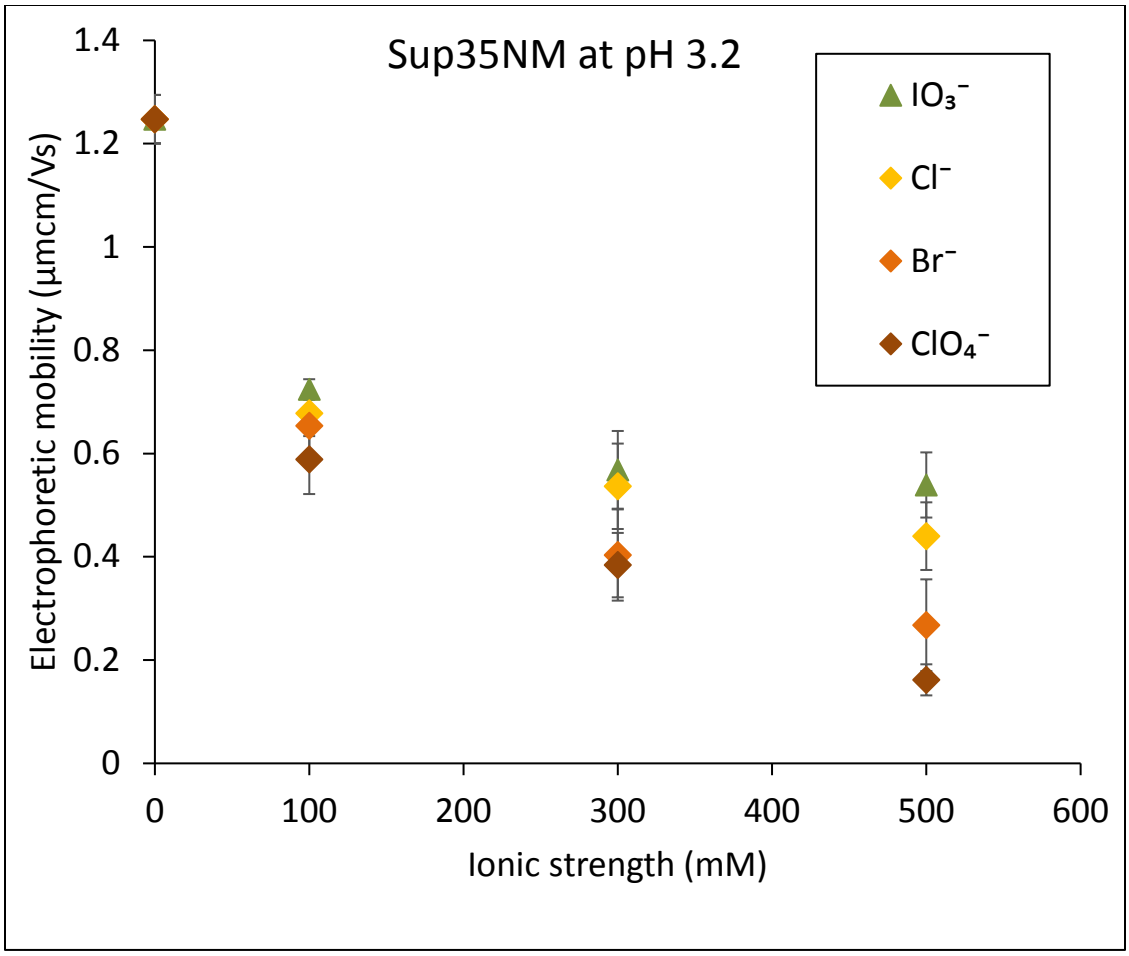

Figure 3.11 – Electrophoretic mobilities of Sup35NM at pH 3.2 in the presence of sodium salts of monovalent anions

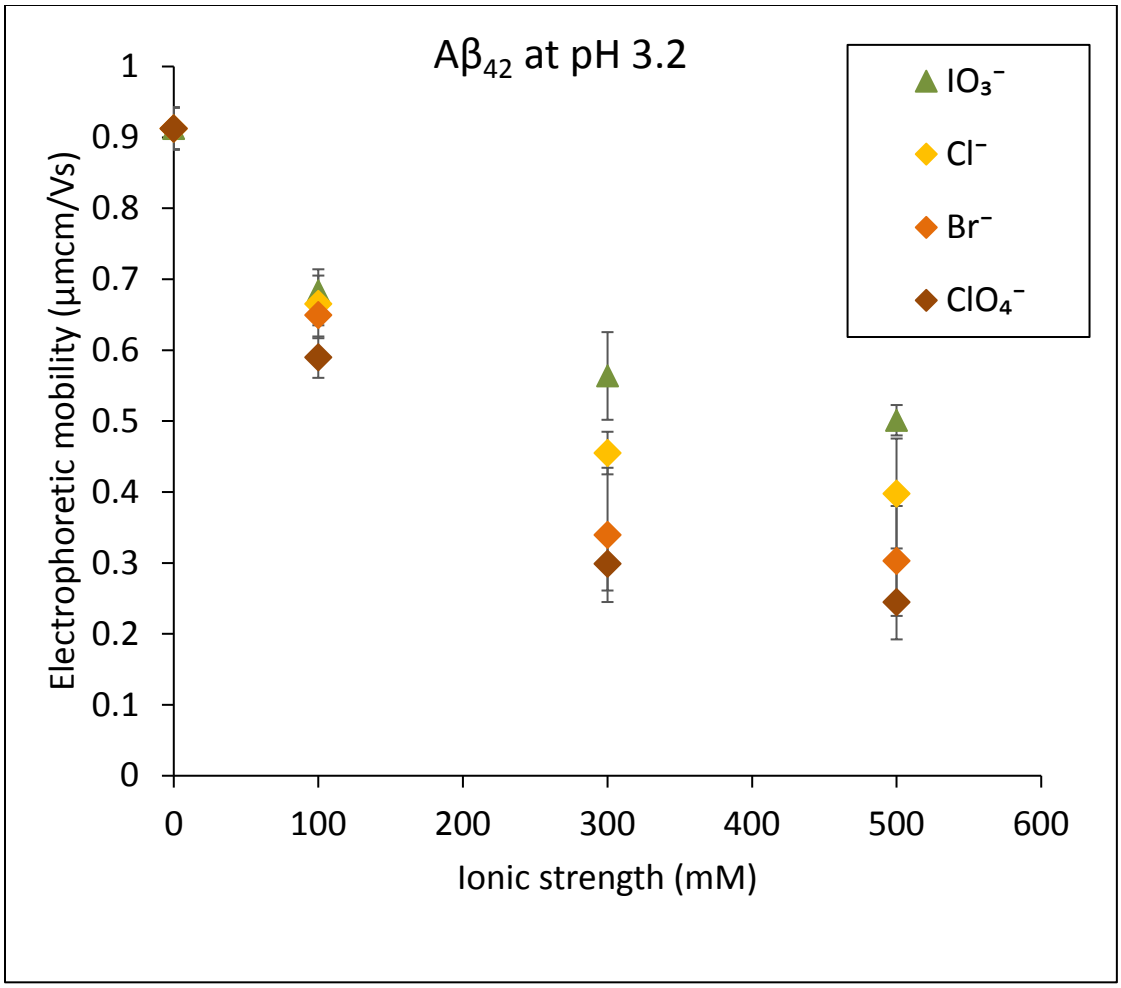

Figure 3.12 – Electrophoretic mobilities of $A\beta_{42}$ at pH 3.2 in the presence of sodium salts of monovalent anions

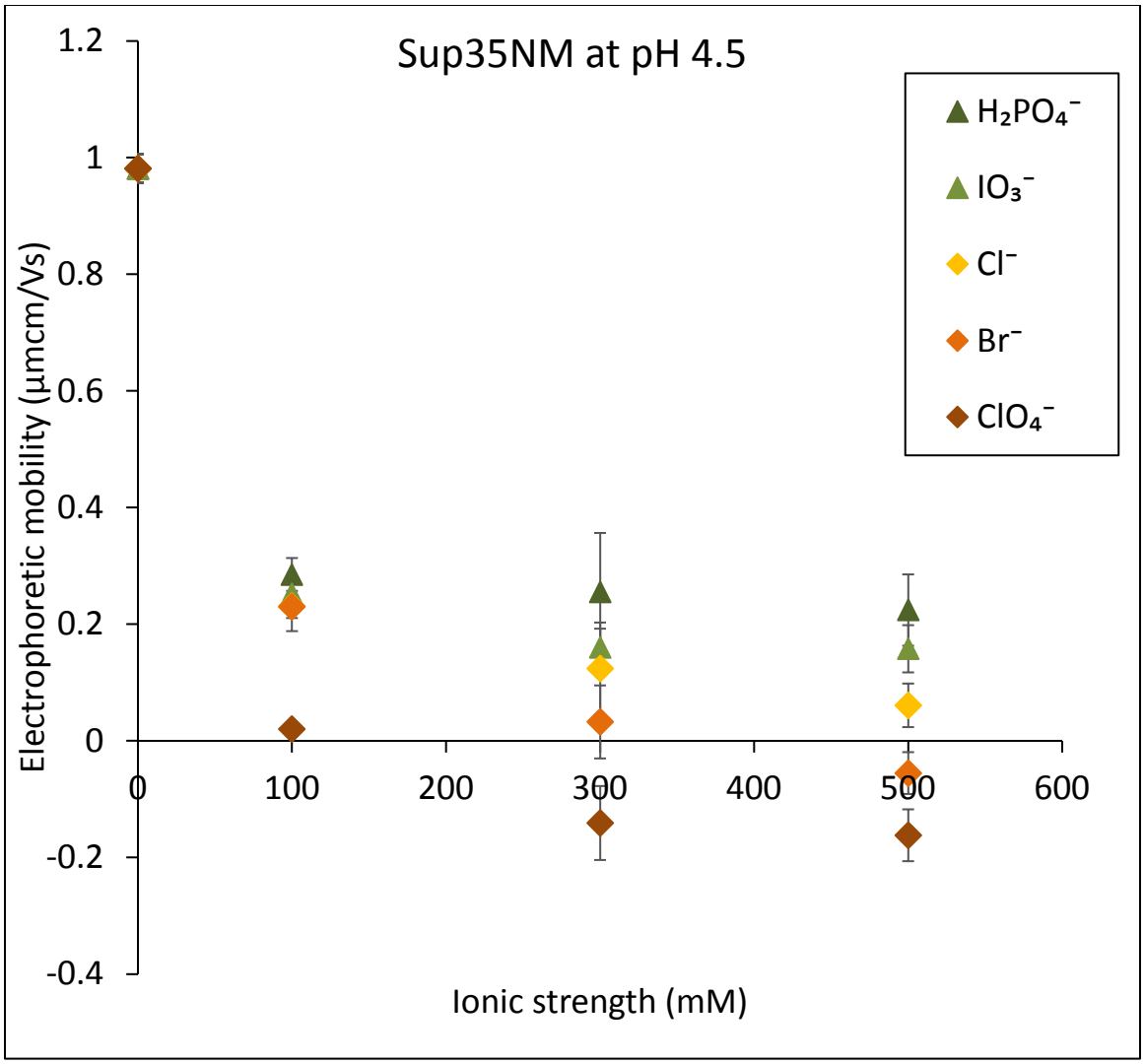

Figure 3.13 – Electrophoretic mobilities of Sup35NM at pH 4.5 in the presence of sodium salts of monovalent anions

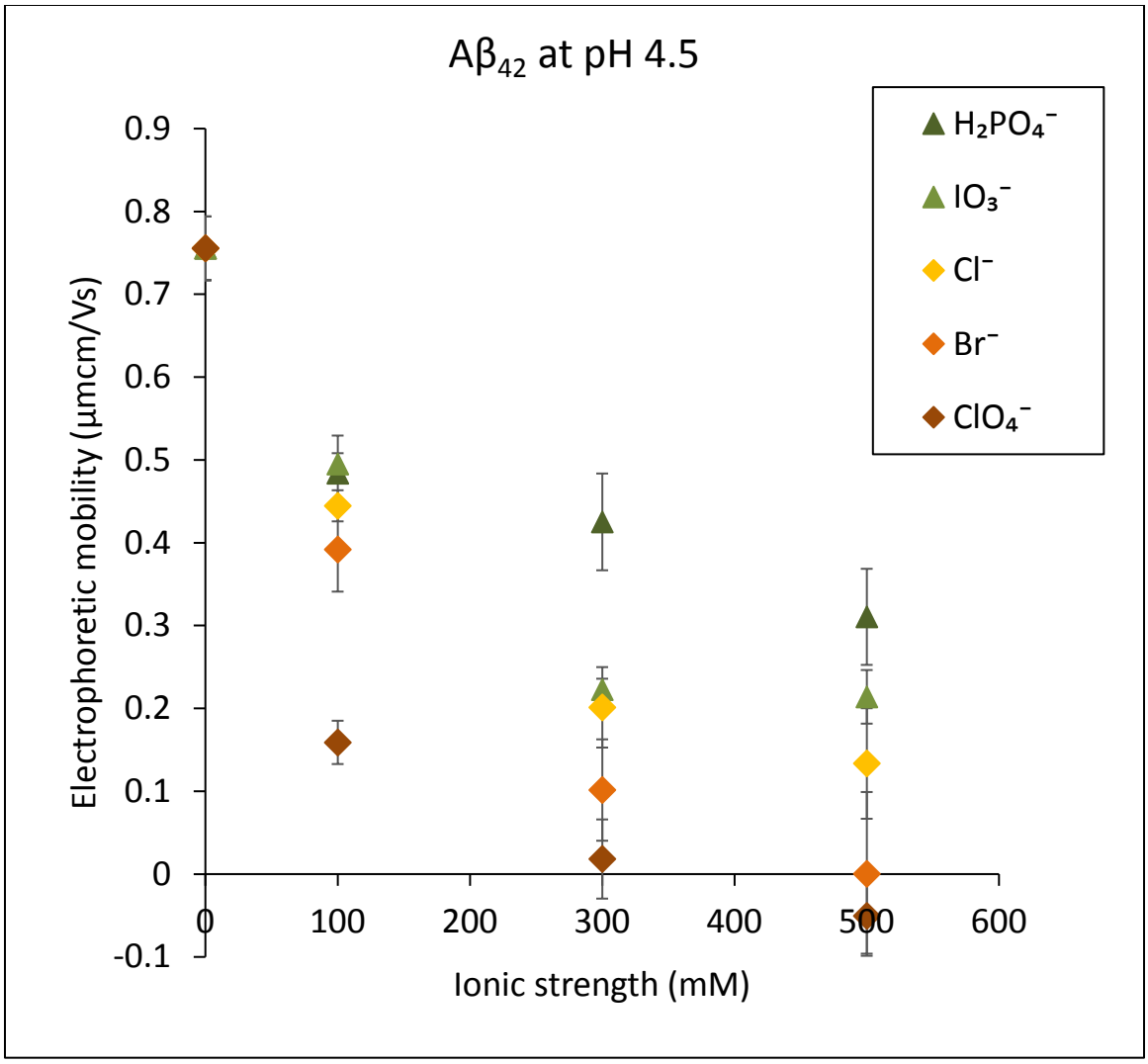

Figure 3.14 – Electrophoretic mobilities of Aβ42 at pH 4.5 in the presence of sodium salts of monovalent anions

3.5 Discussion

The effect of anions on the aggregation of both Sup35NM and Aβ42 can be evaluated in terms of specific and non-specific effects arising from electrostatic and hydrophobic interactions, and preferential interactions or solvent (hydration) effects. The isoelectric points of both Sup35NM and Aβ42 are close to 5.3. Hence, both proteins carry a net positive

charge below a pH of 5.3 and a net negative charge above it. The N and C terminals of the proteins and the polar charged residues can play a role in electrostatic interactions with the ions in solution. These include Lysine (Lys), Arginine (Arg), Histidine (His), Aspartic acid (Asp), and Glutamic acid (Glu). The number of these charged amino acids in both Sup35NM and $A\beta_{42}$, and their amyloid fold forming domains (Sup35N and $A\beta_{15\text{-}42}$) are shown in Table 1. For complete amino acid composition and other relevant properties see Appendix B.

Table 1 – Number of charged amino acid residues in Sup35NM and $A\beta_{42}$, and their amyloid forming domains

Amino acids (pK_a of side chain)	***$A\beta_{1\text{-}42}$***	***$A\beta_{15\text{-}42}$***	***Sup35NM***	***Sup35N***
Arg (12.48)	*1*	*0*	*2*	*2*
Asp (3.65)	*3*	*1*	*9*	*2*
Glu (4.25)	*3*	*1*	*22*	*0*
His (6.0)	*3*	*0*	*1*	*0*
Lys (10.53)	*2*	*2*	*25*	*1*

At a pH of 7.4, Lys and Arg are expected to be protonated and will carry positive charges while Asp and Glu will be deprotonated and will carry negative charges. At a pH of 4.5, His will also be protonated in addition to Lys and Arg. At pH 3.2, Asp and Glu will become protonated and will lose their negative charges. Therefore, the charge distribution on the proteins chages depending on the pH of the solution. Further, the local environment can also affect the pK_a and the charge on individual amino acid side chains. It is important

to note that most of the charged residues in Sup35NM are present in the M domain which does not take part in the amyloid fiber formation. However, as per the proposed parallel in-register structure of Sup35NM fibrils the M-domains of adjacent molecules are in close proximity to each other and can play a crucial role in allowing or hindering the N-domain in forming fibers [13, 24].

Further, the Grand Average of Hydropathicity (GRAVY) scores calculated for Sup35NM and $A\beta_{42}$ indicate that $A\beta_{42}$ with a GRAVY value of 0.205 is much more hydrophobic in nature than Sup35NM with a calculated GRAVY value of -1.596 [25] (Appendix B). Recent work on determining the structure of $A\beta_{42}$ monomer in the fibrillar form has shown that $A\beta_{42}$ fibers consist of two molecules per layer forming dimers arranged in parallel-in-register orientation. The dimer is assembled such that the hydrophobic residues are maximally buried while only the hydrophilic sides chains are exposed to the solvent. This suggests that aggregation of $A\beta_{42}$ is driven by the hydrophobic effect [11, 12].

Besides electrostatic and hydrophobic interactions, competing preferential interactions between the protein, ions, and water can play a crucial role in governing the fibrillation kinetics. While small strongly hydrated kosmotropes are generally considered to act by exerting an excluded volume effect, large weakly hydrated chaotropes are thought to interact directly with hydrophobic regions on a protein [26-31]. Interestingly, in a study of ion interaction with an uncharged 600-residue elastin like polypeptide, chaotropic anions were shown to mainly interact with the polypeptide backbone while no significant binding of the ions to the hydrophobic side chains was detected [32]. In another work, chaotropes were shown to interact with the peptide backbone of a triglycine model peptide [18]. This

suggests that besides the specific residues in a protein the peptide backbone or the length of the protein can have a significant impact on the overall effect of ions on protein stability and aggregation tendency.

Ions can also act by screening electrostatic forces (Debye-Hückel effects). Screening effects are non-specific in nature and depend on the ionic strength of the solution. While electrostatic effects resulting from ion interaction with specific charges on the protein are expected to be dominant at low ionic concentrations, the observed effects at high concentration are due to an interplay of ion-specific Hofmeister effects and non-specific screening effects.

At pH 7.4, both the Sup35NM and $A\beta_{42}$ are negatively charged and anions act as co-ions. Kosmotropes which are excluded from the protein-water interface increase the surface tension and destabilize the monomeric protein resulting in faster fiber formation similar to their effect on globular proteins. Chaotropes, on the other hand, preferentially interact with the hydrophobic regions on the proteins and the polypeptide backbone, and result in stabilization against aggregation. As a result, at a particular ionic strength the relative effects of kosmotropes and chaotropes on aggregation are in the same direction for both Sup35NM and $A\beta_{42}$ and are correlated with the position of the ions in the Hofmeister series. In summary, at the same salt concentration aggregation is the fastest in the presence of the most kosmotropic ion, SO_4^{2-}, and slowest in the presence of the most chaotropic ion, ClO_4^{2-}, as seen in Figure 3.3 and Figure 3.4.

The main difference in the effect of ions on the fibrillation kinetics of Sup35NM and $A\beta_{42}$ at pH of 7.4 is that an increase in the concentration of the salts, promotes the

fibrillation of $A\beta_{42}$ irrespective of whether the anion is a kosmotrope or a chaotrope. On the other hand, increase in the concentration of chaotropic anions hinders the fibrillation of Sup35NM while increase in the concentration of kosmotropes promotes fiber formation. This suggests that the fibrillation of $A\beta_{42}$ is dominated by screening effects and is less sensitive to direct interaction of ions with the protein. On the other hand, interaction of chaotropic ions with Sup35NM disrupts the recognition landscape for templating and hinders fiber formation effectively suggesting that Sup35NM interaction is driven by specific electrostatic interactions.

One possible explanation for this observation invokes a two-step process of nucleus formation where the first step is initial agglomeration of monomers to form a 'pre-organized' oligomeric intermediate followed by conformational conversion or structural reorganization to an organized stable nucleus. Ions can affect these steps through different mechanisms. An increase in ionic strength is likely to promote the agglomeration step through screening effects while ion-specific binding may affect the conformational conversion to form a stable nucleus. Binding of chaotropes to the protein will likely hinder conformational conversion of the oligomer to the nucleus by disrupting the recognition landscape. Since, screening effects due to increase in ionic strength dominate over ion-specific effects, it suggests that the first agglomeration step is the rate limiting step in $A\beta_{42}$ fibrillation.

In the case of $A\beta_{42}$ most of the protein is involved in a cross-beta structure and initial agglomeration is frequently followed by conformational conversion, because once the molecules are brought together, they begin interacting and forming a cross-beta structure. On the other hand, the conformational conversion to the nucleus may be the rate-

limiting step in the aggregation of Sup35NM as the process is highly sensitive to specific ion binding. Sup35NM contains a long M-domain region which is not involved in the amyloid core but needs to be in the proper orientation and conformation that favors nucleus formation. Due to the presence of this long extra domain, initial agglomeration is highly reversible and may not always lead to conformational conversion, which requires interactions between specific residues within the amyloid core domain.

Our observations can also be explained by the previously observed dual 'salting-in' and 'salting-out' behavior of chaotropes [33]. At pH 7.4, $A\beta_{42}$ has only 3 positively charged residues and a much shorter backbone than Sup35NM. It is possible that the sites for chaotrope binding become saturated in $A\beta_{42}$ and a further increase in ionic strength leads to an excluded volume effect resulting in faster fibrillation similar to 'salting-out' of globular proteins by chaotropes at high concentrations. Nevertheless, at pH 7.4 the more chaotropic ions still manage to absorb more effectively to $A\beta_{42}$ resulting in greater negative charge on $A\beta_{42}$ than in the presence of the less chaotropic anions and kosmotropes. This explains why the relative effect on fibrillation still correlates with the position of the ions in the Hofmeister series. On the other hand, Sup35NM has about 27 positively charged residues and a much longer peptide backbone providing more sites for chaotropic anions to bind as compared to $A\beta_{42}$. It is possible that the binding sites on Sup35NM are not completely occupied and an increase in chaotrope concentration results in delayed aggregation due to further stabilization of the monomer similar to 'salting-in' of globular proteins at relatively moderate chaotrope concentrations.

The effect of ions on the fibrillation of Sup35NM and $A\beta_{42}$ at acidic pH values can be explained by electrostatic interactions. At pH less than the pI, the proteins are positively

charged and the anions act as counter-ions. At pH 3.2 and 4.5, kosmotropes act in the same way as at pH 7.4, by exerting depletion forces through an excluded volume effect, chaotropic anions, on the other hand, interact directly with specific residues and neutralize the charge on the protein, reducing repulsion between molecules and promoting fibrillation. Hence, we see a reversal of Hofmeister effect for chaotropic anions when the charge on the proteins is reversed (see sections 3.4.3 and 3.4.4). As we move close to the pI, at pH 4.5 we see that there is charge inversion due to adsorption of an excess of chaotropic anions, resulting in slower fiber formation.

This work shows that ions affect amyloid formation through a complex interplay of specific and non-specific effects comprising of electrostatic and hydrophobic interactions, and preferential interactions (Hofmeister effects). Through a comparison of two amyloid forming proteins, namely, Sup35NM and $A\beta_{42}$ we have shown that the properties of the proteins such as the types of residues (charge and hydrophobicity) and polypeptide chain length play a crucial role in determining the effect of ions on stability and aggregation. Additionally, the main differences in the effect of ions on aggregation of Sup35NM and $A\beta_{42}$ may suggest crucial differences in the aggregation mechanism.

3.6 Conclusions and future work

Chapter 3 presents a detailed investigation of the effect of ions on the aggregation of amyloids. We demonstrate that the effect of ions on amyloid aggregation is a complex interplay of the different interactions which depend on many factors such as the effective charges on the protein, the length of the protein, and its surface polarity. We have shown that while the overall effect of ions on the aggregation of the two proteins, Sup35NM and

$A\beta_{42}$, is the same, there are important differences in the absolute effects which point to differences in the rate limiting steps in the aggregation of these proteins. The widely different properties of Sup35NM and $A\beta_{42}$ such as difference in sizes, hydrophobicity, charged residues, and the length of the amyloidogenic domains may contribute to the differences in the aggregation of these proteins. Despite all these differences, the overall effect of anions on their aggregation is the same, which demonstrates the universality of ion-specific effects on proteins.

As an extension of this work, $A\beta_{42}$ aggregates produced in the presence of ions can be analyzed by TEM/AFM to understand the effect of ions on the length and diameter of $A\beta_{42}$ fibers. At pH 7.4 we see that $A\beta_{42}$ aggregation kinetics is primarily determined by the ionic strength, while at a particular ionic strength the kinetics correlates to the position of the ions along the Hofmeister series. It will be interesting to check whether at the same ionic strength $A\beta_{42}$ aggregates formed in the presence of kosmotropes are smaller in diameter and length on average, and if the ones formed in the presence of chaotropes possess a larger average diameter and length like Sup35NM aggregates formed under similar conditions [1]. Confirming if ions (kosmotropes vs chaotropes) have a similar effect on $A\beta_{42}$ fiber structure will imply that ions can be used as universal regulators of strain *in vitro*, although, the absolute effects are determined by a complex interplay of ion-specific effects and ionic strength. It will also be interesting to see how the $A\beta_{42}$ amyloid fiber structure changes with increase in ionic strength. Along the same lines, the thermal stability and frangibility of the $A\beta_{42}$ strains can also be analyzed by SDS-PAGE and SDD-AGE analysis.

Furthermore, the structure, stability, and frangibility of the Sup35NM and Aβ_{42} aggregates formed at pH values below the isoelectric points can be analyzed to understand the effect of ions on aggregation when they act as counter-ions. When the protein is positively charged the kinetics in the presence of chaotropes is primarily determined by the charge screening and neutralization. While the properties of the fibers formed in the presence of kosmotropes are expected to be the same at pH 3.2 and 4.5 as at pH 7.4, the properties of the fibers formed in the presence of chaotropes can be expected to be determined by either the kinetics of aggregation (screening and neutralization effects) or by the ionic character. Investigating this can also help in determining whether strain conformation and type is determined by the kinetics or other ion-specific effects.

Finally, the presence of a relatively large highly charged M-domain in Sup35NM may interfere in the aggregation process, especially during the structural reorganization stage during nucleus formation where the N-domain forms inter and intramolecular contacts resulting in the formation of the amyloid core. Therefore, it will be interesting to see how the addition of the M-domain of Sup35 to Aβ_{42} might affect its aggregation behavior. More specially, the effect of ions on the aggregation of Aβ_{42} fused with the M-domain of Sup35 can be investigated and compared to their effect on the aggregation of Sup35NM. The amyloid forming region of Aβ_{42} comprises of residues from 15-42. The M-domain of Sup35 can also be fused to the amyloid core-forming residues of Aβ_{42} and a comparative study of the aggregation behavior of these fusion proteins in the presence of ions can be performed to improve our understanding of the contribution of the amyloidogenic and non-amyloidogenic domains of these proteins on their aggregation properties.

3.7 References

1. Rubin, J., H. Khosravi, K.L. Bruce, M.E. Lydon, S.H. Behrens, Y.O. Chernoff, and A.S. Bommarius, *Ion-specific effects on prion nucleation and strain formation.* J Biol Chem, 2013. **288**(42): p. 30300-8.

2. Yeh, V., J.M. Broering, A. Romanyuk, B. Chen, Y.O. Chernoff, and A.S. Bommarius, *The Hofmeister effect on amyloid formation using yeast prion protein.* Protein Science, 2010. **19**(1): p. 47-56.

3. Klement, K., K. Wieligmann, J. Meinhardt, P. Hortschansky, W. Richter, and M. Fandrich, *Effect of different salt ions on the propensity of aggregation and on the structure of Alzheimer's abeta(1-40) amyloid fibrils.* J Mol Biol, 2007. **373**(5): p. 1321-33.

4. Tanaka, M., P. Chien, N. Naber, R. Cooke, and J.S. Weissman, *Conformational variations in an infectious protein determine prion strain differences.* Nature, 2004. **428**(6980): p. 323-328.

5. Hofmeister, F., *On the understanding of the effects of salts.* Arch. Exp. Pathol. Pharmakol.(Leipzig), 1888. **24**: p. 247-260.

6. Sharma, A., K.L. Bruce, B. Chen, S. Gyoneva, S.H. Behrens, A.S. Bommarius, and Y.O. Chernoff, *Contributions of the Prion Protein Sequence, Strain and Environment to the Species Barrier.* Journal of Biological Chemistry, 2015.

7. Marek, P.J., V. Patsalo, D.F. Green, and D.P. Raleigh, *Ionic strength effects on amyloid formation by amylin are a complicated interplay among Debye screening, ion selectivity, and Hofmeister effects.* Biochemistry, 2012. **51**(43): p. 8478-90.

8. Raman, B., E. Chatani, M. Kihara, T. Ban, M. Sakai, K. Hasegawa, H. Naiki, M. Rao Ch, and Y. Goto, *Critical balance of electrostatic and hydrophobic interactions is required for beta 2-microglobulin amyloid fibril growth and stability.* Biochemistry, 2005. **44**(4): p. 1288-99.

9. Jain, S. and J.B. Udgaonkar, *Salt-induced modulation of the pathway of amyloid fibril formation by the mouse prion protein.* Biochemistry, 2010. **49**(35): p. 7615-24.

10. Munishkina, L.A., J. Henriques, V.N. Uversky, and A.L. Fink, *Role of protein−water interactions and electrostatics in α-synuclein fibril formation.* Biochemistry, 2004. **43**(11): p. 3289-3300.

11. Colvin, M.T., R. Silvers, Q.Z. Ni, T.V. Can, I. Sergeyev, M. Rosay, K.J. Donovan, B. Michael, J. Wall, S. Linse, and R.G. Griffin, *Atomic Resolution Structure of Monomorphic Abeta42 Amyloid Fibrils.* J Am Chem Soc, 2016. **138**(30): p. 9663-74.

12. Walti, M.A., F. Ravotti, H. Arai, C.G. Glabe, J.S. Wall, A. Bockmann, P. Guntert, B.H. Meier, and R. Riek, *Atomic-resolution structure of a disease-relevant Abeta(1-42) amyloid fibril.* Proc Natl Acad Sci U S A, 2016. **113**(34): p. E4976-84.

13. Shewmaker, F., R.B. Wickner, and R. Tycko, *Amyloid of the prion domain of Sup35p has an in-register parallel beta-sheet structure.* Proc Natl Acad Sci U S A, 2006. **103**(52): p. 19754-9.

14. Gorkovskiy, A., K.R. Thurber, R. Tycko, and R.B. Wickner, *Locating folds of the in-register parallel β-sheet of the Sup35p prion domain infectious amyloid.* Proceedings of the National Academy of Sciences of the United States of America, 2014. **111**(43): p. E4615-E4622.

15. Lührs, T., C. Ritter, M. Adrian, D. Riek-Loher, B. Bohrmann, H. Döbeli, D. Schubert, and R. Riek, *3D structure of Alzheimer's amyloid-β(1–42) fibrils.* Proceedings of the National Academy of Sciences of the United States of America, 2005. **102**(48): p. 17342-17347.

16. Allen, K.D., R.D. Wegrzyn, T.A. Chernova, S. Müller, G.P. Newnam, P.A. Winslett, K.B. Wittich, K.D. Wilkinson, and Y.O. Chernoff, *Hsp70 Chaperones as Modulators of Prion Life Cycle Novel Effects of Ssa and Ssb on the Saccharomyces cerevisiae Prion [PSI+]*. Genetics, 2005. **169**(3): p. 1227-1242.

17. Walsh, D.M., E. Thulin, A.M. Minogue, N. Gustavsson, E. Pang, D.B. Teplow, and S. Linse, *A facile method for expression and purification of the Alzheimer's disease-associated amyloid beta-peptide.* FEBS J, 2009. **276**(5): p. 1266-81.

18. Paterova, J., K.B. Rembert, J. Heyda, Y. Kurra, H.I. Okur, W.R. Liu, C. Hilty, P.S. Cremer, and P. Jungwirth, *Reversal of the hofmeister series: specific ion effects on peptides.* J Phys Chem B, 2013. **117**(27): p. 8150-8.

19. Bostrom, M., F.W. Tavares, S. Finet, F. Skouri-Panet, A. Tardieu, and B.W. Ninham, *Why forces between proteins follow different Hofmeister series for pH above and below pI.* Biophys Chem, 2005. **117**(3): p. 217-24.

20. Salis, A. and B.W. Ninham, *Models and mechanisms of Hofmeister effects in electrolyte solutions, and colloid and protein systems revisited.* Chem Soc Rev, 2014. **43**(21): p. 7358-77.

21. Schwierz, N., D. Horinek, and R.R. Netz, *Reversed anionic Hofmeister series: the interplay of surface charge and surface polarity.* Langmuir, 2010. **26**(10): p. 7370-9.

22. Lopez-Leon, T., A.B. Jodar-Reyes, J.L. Ortega-Vinuesa, and D. Bastos-Gonzalez, *Hofmeister effects on the colloidal stability of an IgG-coated polystyrene latex.* J Colloid Interface Sci, 2005. **284**(1): p. 139-48.

23. López-León, T., M.J. Santander-Ortega, J.L. Ortega-Vinuesa, and D. Bastos-González, *Hofmeister effects in colloidal systems: influence of the surface nature.* The Journal of Physical Chemistry C, 2008. **112**(41): p. 16060-16069.

24. Wickner, R.B., H.K. Edskes, F. Shewmaker, and T. Nakayashiki, *Prions of fungi: inherited structures and biological roles.* Nature reviews microbiology, 2007. **5**(8): p. 611-618.

25. Gasteiger, E., C. Hoogland, A. Gattiker, S.e. Duvaud, M.R. Wilkins, R.D. Appel, and A. Bairoch, *Protein identification and analysis tools on the ExPASy server*. 2005: Springer.

26. Zhang, Y. and P.S. Cremer, *Interactions between macromolecules and ions: the Hofmeister series.* Current Opinion in Chemical Biology, 2006. **10**(6): p. 658-663.

27. Arakawa, T. and S. Timasheff, *The stabilization of proteins by osmolytes.* Biophysical journal, 1985. **47**(3): p. 411-414.

28. Collins, K.D., *Ions from the Hofmeister series and osmolytes: effects on proteins in solution and in the crystallization process.* Methods, 2004. **34**(3): p. 300-311.

29. Collins, K.D., *Sticky ions in biological systems.* Proceedings of the National Academy of Sciences, 1995. **92**(12): p. 5553-5557.

30. Arakawa, T. and S.N. Timasheff, *Preferential interactions of proteins with salts in concentrated solutions.* Biochemistry, 1982. **21**(25): p. 6545-6552.

31. Kita, Y., T. Arakawa, T.-Y. Lin, and S.N. Timasheff, *Contribution of the surface free energy perturbation to protein-solvent interactions.* Biochemistry, 1994. **33**(50): p. 15178-15189.

32. Rembert, K.B., J. Paterova, J. Heyda, C. Hilty, P. Jungwirth, and P.S. Cremer, *Molecular mechanisms of ion-specific effects on proteins.* J Am Chem Soc, 2012. **134**(24): p. 10039-46.

33. Kunz, W., *Specific ion effects in colloidal and biological systems.* Current Opinion in Colloid & Interface Science, 2010. **15**(1): p. 34-39.

CHAPTER 4. COMPUTATIONAL MODELING OF AMYLOID AGGREGATION KINETICS

4.1 Abstract

Amyloid aggregation is a complex process involving many steps such as primary nucleation, elongation, and fragmentation. Many empirical and mechanism based models have been used to fit aggregation data obtained for different amyloid/prion proteins. Performing global fitting analysis of aggregation data is crucial to determine the most appropriate mechanism for a system. Here, we have performed a half time analysis to match the experimentally observed dependence of aggregation kinetics on the protein concentration and determine the most appropriate model for fitting our aggregation data. Global fitting analysis was then done to evaluate the model. We find that existing mechanism schemes are not suitable for fitting Sup35NM aggregation data. Even the best performing scheme, provided relatively poor fits to the aggregation data which suggests that some mechanistic details may be missing from or different in the model when compared to the actual aggregation mechanism of Sup35NM. In this chapter, we evaluate a simulation model which offers advantages such as ease of making modifications and including new process steps. We also discuss limitations of the model and potential sources of discrepancies between model predictions and experimental kinetic data collected using Thioflavin T binding assay and the model.

4.2 Introduction

Amyloid aggregation is a complex process comprising of a number of steps which result in the assembly of monomeric proteins into amyloid fibers. The simplest mechanistic explanation of the process of amyloid formation generally consists of a two-step pattern of initial nucleation corresponding to a lag phase followed by a fiber elongation phase to form a mature fiber [1]. When the fibril mass fraction for an unseeded aggregation reaction is plotted with respect to time a sigmoidal curve is usually obtained. This behavior is generally modeled using mathematical empirical functions such as the logistic function (equation 1), which captures the near sigmoidal shape of amyloid aggregation [2, 3].

$$F(t) = F_0 + \frac{A}{1 + \exp\left[-k\left(t - t_{1/2}\right)\right]} \quad (1)$$

Here, F_0 is the baseline, A is the amplitude, k is the elongation rate constant, and $t_{1/2}$ is the time at 50% aggregation. The lag time is given by $t_{lag} = t_{1/2} - \frac{2}{k}$

However, while the logistic model is easy to apply and parameterize the data, it is not based upon any mechanism and cannot be used to get mechanistic insights into the aggregation kinetics.

The simplest non-empirical kinetic models that have been used for fitting amyloid aggregation data include two-step mechanisms for fibrillation of human calcitonin, and human insulin, and the Finke-Watzky (F-W) 2-step mechanism [4-6]. These mechanisms de-convolute aggregation into a slow conformational conversion of cellular protein to the amyloid/prion form followed by an autocatalytic reaction resulting in typically fast

formation of more of the amyloid/prion form. These models share a very similar mathematical form, a result of the autocatalytic component of these mechanisms. However, it should be noted that these models do not incorporate association of molecules which is central to a process like amyloid formation involving polymerization of monomeric protein. More complex models based on a nucleation-polymerization mechanism have been proposed and used to fit amyloid aggregation data, however, recent work has shown the importance of secondary processes like fragmentation and fiber-assisted nucleation on the aggregation process [7-13]. Analytical solutions to models consisting of secondary processes like fragmentation or fiber catalyzed secondary nucleation have been obtained and used to fit aggregation data [14-18]. However, due to the complex nature of the aggregation process and differences in the aggregation mechanism of different proteins, different models are usually required to fit aggregation data for different proteins. Here, we have developed a simulation model for amyloid aggregation process which primarily consists of four main process steps: primary nucleation, elongation, breakage and secondary nucleation. We have then attempted to use the model to perform global fitting of Sup35NM aggregation data. The model is then modified to simulate the mechanism found to match the experimentally observed dependence of aggregation kinetics on protein concentration and improve the overall fitting.

4.2.1 General mechanism of amyloid aggregation

The process of amyloid aggregation starts with the formation of several primary nuclei from monomers (M), which then act as templates for addition of more monomeric protein molecules. Sequential and stepwise addition of monomers results in fiber elongation generating a pool of fibers of different sizes (P_i). At any stage after the formation

of primary nuclei, secondary processes like breakage/fragmentation and fiber-assisted nucleus formation generate more fiber ends or surfaces for the monomer to attach. While secondary nucleation can occur in both *in vivo* and *in vitro* systems by similar mechanisms, breakage generally occurs in *in vitro* systems due to agitation which causes shear, and *in vivo* systems by the action of chaperones which break down larger aggregates or fibers [19-23]. This process can be represented in a schematic as shown below in Figure 4.1

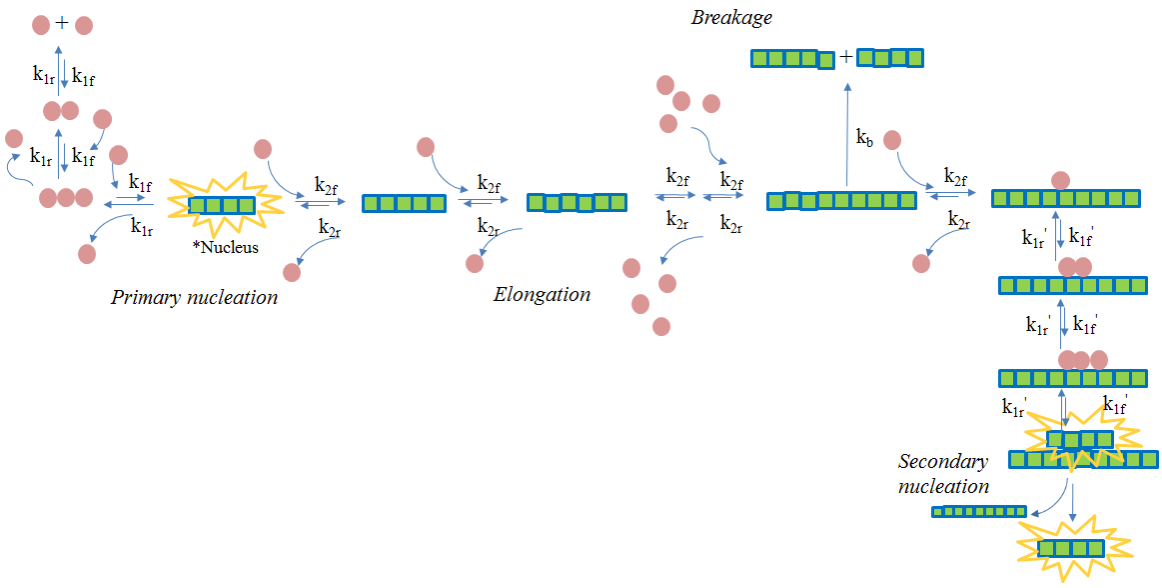

Figure 4.1 – General scheme of amyloid aggregation comprising of four fundamental processes, namely, primary nucleation, elongation, breakage and secondary nucleation. k_{1f} and k_{2f} are the rates of monomer addition before and after nucleus formation, k_{1r} and k_{2r} are the rate of monomer dissociation before and after nucleus formation, k_b is the breakage or fragmentation rate, and k_{1f}' and k_{1r}' are the rates of forward and backward reactions for fiber-catalyzed nucleus formation.

The main assumptions are as follows: 1) rate of monomer association, k_{1f}, is less than the rate of monomer dissociation, k_{1r}, prior to nucleus formation 2) rate of monomer association, k_{2f}, is greater than the rate of monomer dissociation, k_{2r}, after nucleus formation, 3) one monomer is added to a polymer at time, 4) there is no end-to-end

association of polymers, and 5) all steps, with the exception of fragmentation, are reversible.

The above scheme was then simplified as shown below in order to reduce the number of parameters (Figure 4.2). Primary and secondary nucleation were considered to involve simultaneous association of monomers to form a stable nucleus followed by sequential addition of monomers resulting in fiber elongation. Breakage can occur for any fiber of the size larger than the nucleus.

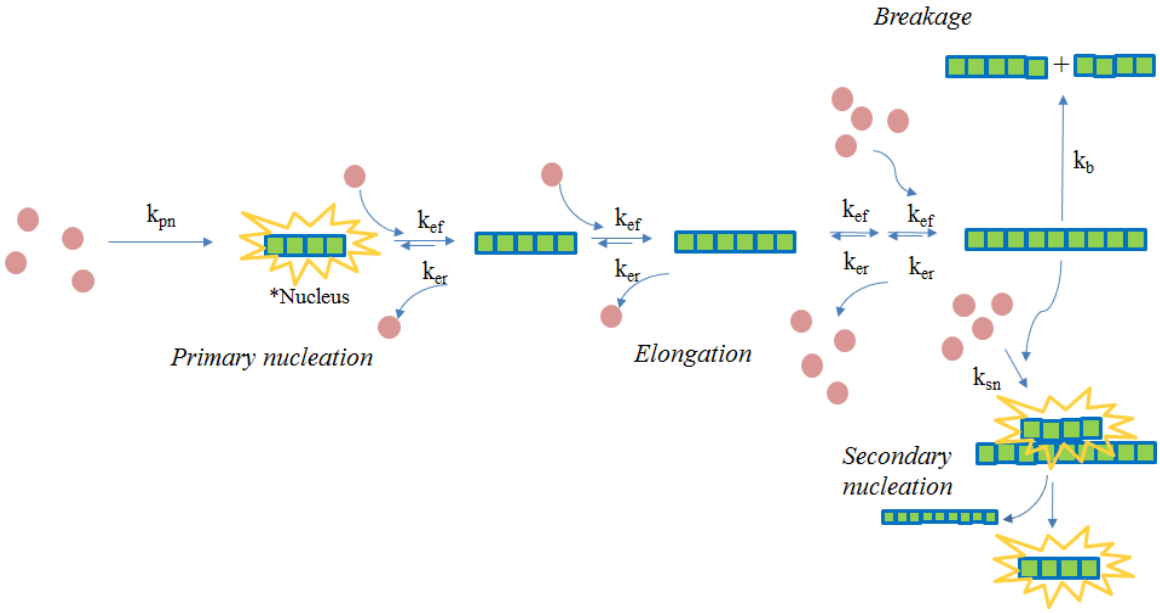

Figure 4.2 – Simplified scheme of amyloid aggregation. Here, k_{pn} is the primary nucleation rate constant, k_{ef} is the rate constant for monomer association, k_{er} is the rate constant for monomer dissociation, k_b is the breakage or fragmentation rate constant and k_{sn} is the secondary nucleation rate constant

The above scheme can be summarized in the following reactions.

Primary nucleation

$$n_c M \xrightarrow{k_{pn}} P^*_{n_c} \tag{2}$$

Fiber elongation:

$$M + P^*_{n_c} \xrightarrow{k_{ef}} P_{n_c+1} \tag{3}$$

……..……..

$$M + P_i \xrightarrow{k_{ef}} P_{i+1} \tag{4}$$

$$P_{i+1} \xrightarrow{k_{er}} P_i + M \tag{5}$$

Breakage of polymer of size i at position j:

$$P_i \xrightarrow{k_b} P_j + P_{i-j} \tag{4}$$

Fiber-catalyzed secondary nucleation

$$n_c M \xrightarrow{k_{sn}[F_m]} P^*_{n_c} \tag{5}$$

Here, M is the concentration of monomer, * indicates a nucleus, n_c is the size of the nucleus, P_i is the concentration of polymer of size, F_m is the fiber mass concentration, k_{pn} is the primary nucleation rate constant, k_{ef} is the monomer association rate constant, k_{er} is the monomer dissociation rate constant, k_b is the breakage/fragmentation rate constant, and k_{sn} is the secondary nucleation rate constant.

This system can then be described by the following population balance equations.

The rate of change of nuclei concentration:

$$\frac{dp_{n_c}}{dt} = k_{pn}[p_1]^{n_c} - k_{ef}[p_1][p_{n_c}] + k_{er}[p_{n_c+1}] + 2 \times \sum_{j=n_c+1}^{nMax} k_b[p_j] + k_{sn}[F_m][p_1]^{n_c} \quad (6)$$

Where $nMax$ is the maximum aggregate size, and $F_m = \sum_{j=n_c}^{nMax} j[p_j]$.

The rate of change of concentration of fibers of size $i > n_c$:

$$\frac{dp_i}{dt} = k_{ef}[p_1][p_{i-1}] - k_{ef}[p_1][p_i] + k_{er}[p_{i+1}] - k_{er}[p_i] - k_b \times (i-1) \times [p_i] + 2 \times \sum_{j=i+1}^{nMax} k_b[p_j] \quad (7)$$

The rate of change of monomer concentration:

$$\frac{dp_1}{dt} = 2 \times \sum_{j=n_c+1}^{nMax} k_b[p_j] - k_{pn}[p_1]^{n_c} - \sum_{j=n_c}^{nMax-1} k_{ef}[p_j][p_1] + \sum_{j=n_c+1}^{nMax} k_{er}[p \quad (8)$$

$$- k_{sn}[F_m]\,[p_1]^{n_c}$$

4.3 Material and Methods

4.3.1 Expression and purification of Sup35NM

Sup35NM was expressed and purified as previously described in section 3.3.1.

4.3.2 Fibrillation assays using Thioflavin T

Fibrillation assays were performed as previously described in section 3.3.3. Thioflavin T assay was performed for a range of concentrations of Sup35NM: 0.25µM, 0.5 µM, 0.75 µM, 1 µM, 2.5 µM, 5 µM, 7.5 µM, 10 µM, 15 µM, 20 µM, and 25 µM, in the presence of PBS at 37ºC in a 96-well plate with linear shaking at 18Hz in a BioTek Synergy H4 Hybrid Multi-Mode Microplate Reader (Winooski, VT). Fluorescence readings were taken every 10 minutes using an excitation wavelength of 440 nm and emission wavelength of 485 nm.

4.3.3 Computational modelling of aggregation kinetics

The system of equations was modelled as a system of matrices consisting of the concentration of each species at a particular time and the time derivative as follows:

$$X_u = [p_1@t_u \quad \cdots \quad p_{max}@t_u] \quad (9)$$

$$\frac{dX}{dt} = \begin{bmatrix} \frac{dp_1}{dt} \\ \vdots \\ \frac{dp_{max}}{dt} \end{bmatrix} \tag{10}$$

which is expressed as a linear combination of X based on equations (8), (9) and (10).

The time derivative is then numerically integrated to determine the concentration of all species at all times.

$$XT = \begin{bmatrix} p_1@t_0 & \cdots & p_{max}@t_0 \\ \vdots & \ddots & \vdots \\ p_1@t_{fin} & \cdots & p_{max}@t_{fin} \end{bmatrix} \tag{11}$$

Detailed description of the matrix implementation is shown in Appendix C.

The simulation is then used to fit experimental data with rate constant parameters.

4.4 Results

4.4.1 Fitting aggregation data with model

The model was able to successfully fit aggregation data collected for individual concentrations. An example fit is shown in Figure 4.3 below.

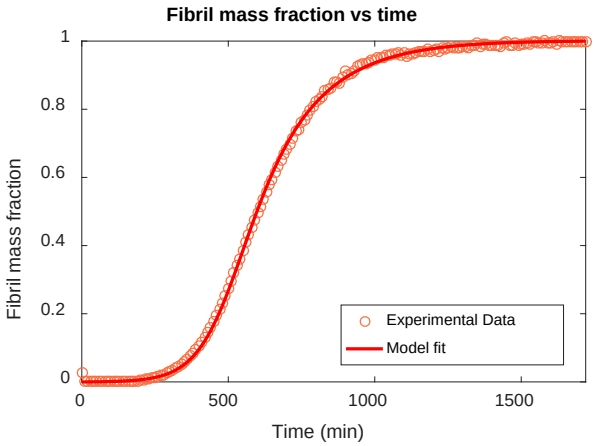

Figure 4.3 – Model fit to aggregation data for 2.5 µM Sup35NM

However, a single experimental curve does not contain enough information to reliably determine all the free parameters (rate constants). To remedy this problem, we turned to simultaneous fits of data. But the same model comprising primary nucleation, elongation, breakage/fragmentation, and fiber-catalysed secondary nucleation was not able to fit the aggregation data obtained for several different Sup35NM concentrations simultaneously. Notably, the model overpredicts the sensitivity of the aggregation lag time on the overall protein concentration, see Figure 4.4.

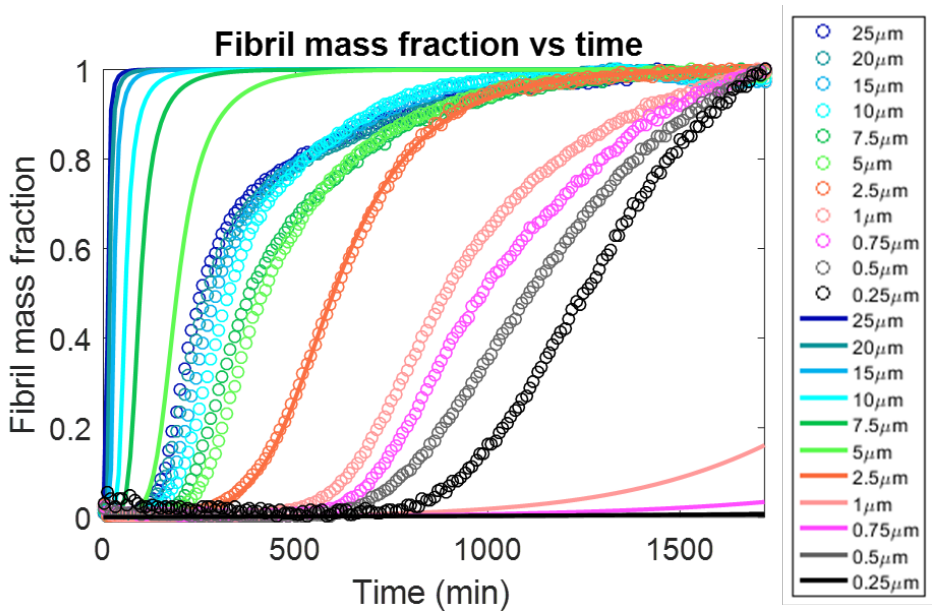

Figure 4.4 – Aggregation data obtained for different concentrations of Sup35NM and model simulations obtained if the model is used to fit the aggregation data obtained for 2.5 μM Sup35NM. Experimental data is shown in circles and model simulations in solid lines.

Such a mismatch in the experimental data and the model simulation suggested that we were not using the appropriate model for fitting the experimental data. Generally, a scaling exponent (γ), obtained by plotting the logarithm of aggregation half times against the logarithm of protein concentration, is used as an indicator of the mechanism/model which is closest to the experimental data [17]. We next, obtained the γ for our data and model previously used as shown in Figure 4.5

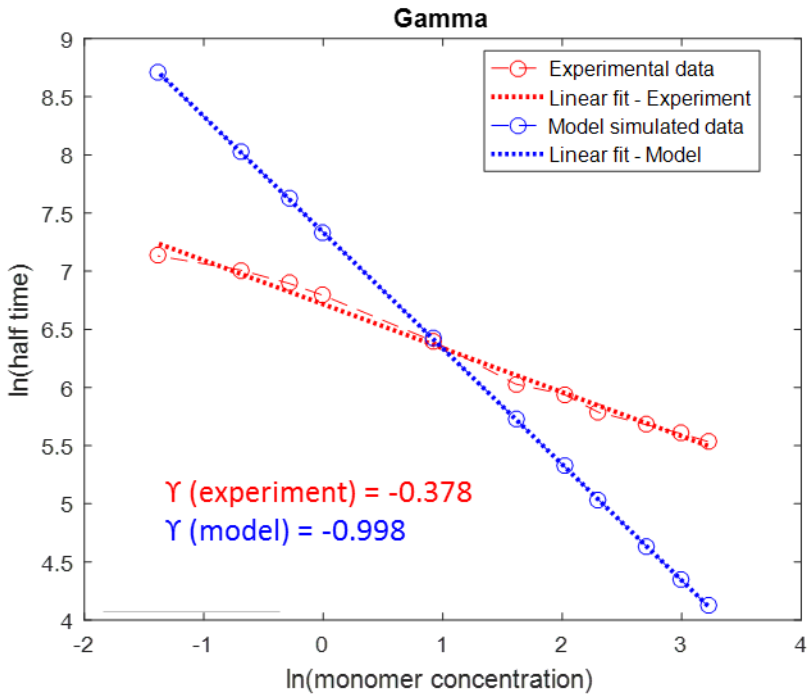

Figure 4.5 – Scaling exponent for experimental data and model

We see that the γ value of the model does not match the γ value of the experimental data. So, we then compared the γ value of our experimental data to the expected γ values for different models for which analytical solutions have been made available [17]. We found the γ value for our system seems to lie in the range of γ values expected for a saturating elongation and fragmentation model (Table 2).

Table 2 – Models and their expected scaling exponent values

Model	**Scaling exponent (γ)**
Nucleation-elongation	-1
Secondary nucleation	-1.5
Fragmentation	-0.5
Fragmentation and secondary nucleation	-1.5 to -0.5
Multistep secondary nucleation	-1.5 to -0.5
Saturating elongation	-0.5
Saturating elongation and secondary nucleation	-1.5 to -0.5
Saturating elongation and fragmentation	-0.5 to 0

Saturating elongation describes a special situation which occurs at monomer concentrations above a certain threshold concentration where the diffusion of monomers to the fibril ends is no longer rate-limiting; rather, the conformational conversion of the monomer after attachment to a fibril end becomes the rate limiting step [17]. The rate of change of polymer number and mass concentrations are then described by equations 14 and 15.

$$\frac{dP}{dt} = k_n m(t)^{n_c} + k\_M(t) \tag{12}$$

$$\frac{dM}{dt} = 2k_{+}P(t)\frac{m(t)}{1+\frac{m(t)}{K_E}} \tag{13}$$

Here, P(t) is the total polymer number concentration, M(t) is the total polymer mass concentration, m(t) is the monomer concentration, k_+ is the elongation rate constant, k_- is the breakage rate constant and K_E is the crossover concentration above which elongation is rearrangement-limited. Note that the mathematical form of equation (15) is similar to the Michaelis-Menten equation for enzymatic reactions. Analytical solutions to the eight models listed in Table 2 have been obtained by Knowles and co-workers [17] who have also developed an online platform for fitting amyloid aggregation data, named AmyloFit (http://www.amylofit.ch.cam.ac.uk). We then used the saturating elongation and fragmentation model in AmyloFit to fit our aggregation data and compared it to fits obtained by incorporating the saturating elongation scenario in our simulation model. We were able to obtain similar results with both the tools (see Figure 4.6)

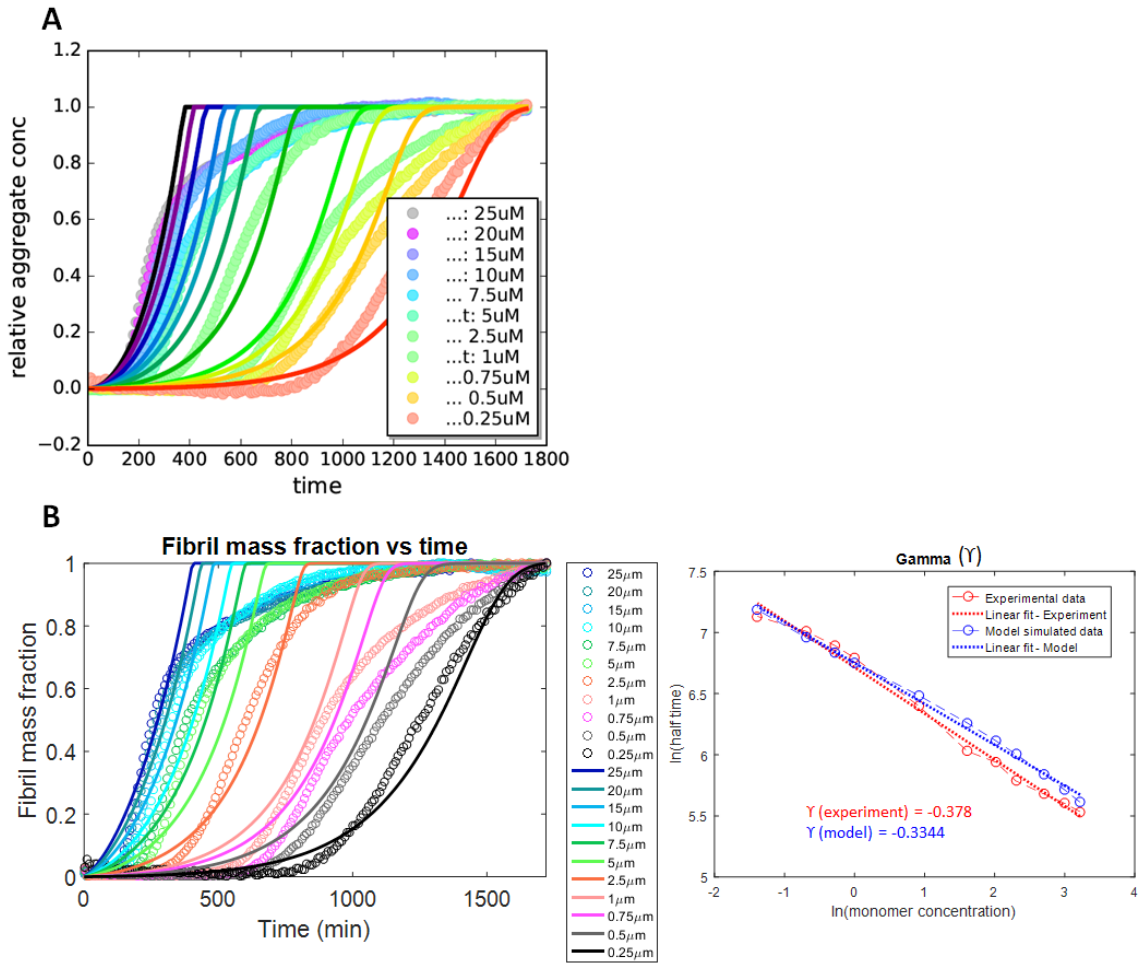

Figure 4.6 – Aggregation data fitted to saturating elongation and fragmentation model using A) AmyloFit and B) Simulation model

From the above figure, we can see that while both the tools perform equally well, the saturating elongation and fragmentation model does not represent the experimental data very well. The model is especially not able to fit the aggregation curves towards the end of the aggregation period and the ascent to the plateau is much sharper for the models than for the experimental data. The predicted sharp ascent to the plateau was found to be insensitive to the chosen maximum allowable aggregate size (maximum number of monomers in an aggregate). The problem, therefore, was not an artifact due to the cut-off limit imposed on the maximum aggregate size.

4.5 Discussion

Global fitting of amyloid aggregation data is necessary to arrive at the most appropriate mechanistic model for a given protein. While most models can fit aggregation kinetics at a single concentration, only the most accurate model can reproduce the aggregation behavior at different concentrations simultaneously. Here, we have performed global fitting of Sup35NM aggregation data at different concentrations using the most appropriate model as indicated by calculation of the scaling exponent, γ, which is generally used as a guide for determining the correct model. We find that while the model suggested by the half time analysis (saturating elongation and fragmentation) matches the expected dependence of half times of aggregation on the protein concentration, it is still unable to fit our aggregation data well. Our simulation model performs as well as the publicly available online tool AmyloFit; however, it appears that the model lacks crucial mechanistic details making it insufficient. There is a considerable mismatch between the model and the experimental data, especially towards the end of the aggregation where the model over-predicts the aggregation rate considerably.

It is interesting to note that $A\beta_{42}$ and $A\beta_{40}$ peptide which only differ by 2 amino acids have been shown to aggregate by different mechanisms. A model comprising of primary nucleation, elongation, and fiber catalyzed secondary nucleation with a primary and secondary nucleus size of two has been successfully used to fit aggregation data for $A\beta_{42}$, while a model with a two-step secondary nucleation process was found to fit $A\beta_{40}$ data globally [8, 10]. It is highly likely that Sup35NM, which is a much larger protein with very different properties may aggregate through a different mechanism. We have discussed in the Chapter 3 that ions affect the aggregation of Sup35NM and $A\beta_{42}$ differently which

points to differences in their aggregation mechanisms. A three stage mechanism comprising of conformation conversion, nucleation and elongation was found to fit insulin aggregation data [12]. Therefore, different amyloidogenic proteins appear to aggregate through different mechanisms and it is plausible that Sup35NM may aggregate through its own unique mechanism. Logically, the next step would be to test models accounting for other permutations and combinations of the individual sub-processes and use them to perform global fitting of the aggregation data.

Other possible reasons for the model not being able to fit the aggregation data include crowding due to high concentration of large aggregates especially for high concentrations. This can lead to diffusional limitations as well as excluded volume effects. Diffusional limitations due to crowding may dominate over excluded volume effects if the kinetic bottleneck is the process of diffusion and collision between the monomer and fibril end. Such a situation is likely for proteins which have a high tendency to aggregate. For such proteins, macromolecular crowding is much less efficient in accelerating peptide self-association. Diffusion of monomeric protein in a solution of protein polymers of different sizes is a complicated process. At high concentrations, amyloids can form a polymer gel like network which can obstruct diffusion of monomeric protein. Another plausible reason for the mismatch could be the dependence of the length of aggregate/polymer on their diffusivities and hence the rate constants. And finally, it is possible that crowding and entanglement of polymers to form a gel could interfere with binding of the dye to the aggregates resulting in a non-linear dependence of the fluorescent signal with the fiber concentration.

It is important to note here that analytical solutions are available only for the models listed in Table 2. These models represent a subset of the mechanisms that can occur. The lack of analytical solutions to other combinations of processes points to the difficulty in obtaining analytical solutions to these systems which become more and more complex as more steps are introduced. However, our simulation model presents certain advantages over analytical models which are listed below:

1) Any step/process/limiting situation such as two-step secondary nucleation, saturating elongation, etc., can be incorporated in the model relatively easily.
2) Any combination of sub-processes can be modelled.
3) The model provides population balance distributions which can be verified using other techniques such as TEM/AFM analysis of aggregates formed over the course of the reaction. This can provide an additional verification of the model.
4) The model allows us to vary the primary and secondary nucleus size, and the smallest detectable size independently. Therefore, data collected using other dyes can also be used for fitting and to ensure the validity of the model.

4.6 Conclusions and future work

Here, we have developed a tool for modelling of amyloid aggregation kinetics using a simulation approach. The model offers many advantages over analytical models which make it a versatile tool for testing any mechanism. A closed form solution, which can be difficult to obtain for complex mechanisms, is not required for such a simulation model. The model also provides a distribution of different species with respect to time which is not provided by an analytical solution based model.

We find that the most suitable model suggested by half time analysis is inadequate for fitting our Sup35NM aggregation data as it overpredicts that rate of aggregation especially towards the end of the aggregation process. Analytical solution based models have been successfully used to fit $A\beta_{42}$ and $A\beta_{40}$ aggregation data collected at different concentrations simultaneously, and the most appropriate mechanisms for the aggregation of these peptides have been established [8, 10]. Therefore, fitting $A\beta_{42}$ and/or $A\beta_{40}$ aggregation data with our simulation model, tailored to the mechanism of aggregation of these peptides, can provide a sanity check for our model. If the model can predict and fit aggregation of amyloid beta peptides, then it will indicate that such a simulation based implementation of amyloid aggregation is at par with existing analytical models.

The current inability of the available analytical models and our simulation model to fit Sup35NM aggregation data indicates that a crucial detail is missing in the mechanism. The next logical step is to test different combinations of the underlying processes to fit the data. Another approach would be to resort to our general amyloid aggregation scheme and introduce reversibility back in the nucleation process. The aggregation process can be considered to consist of a stepwise process of monomer addition (forward reaction) and monomer dissociation (reverse reaction) till an aggregate of the size of nucleus is formed, after which the rate of monomer association is more favorable than the rate of monomer dissociation. Alternatively, the nucleation process can be modelled as a simultaneous association of monomers to form an intermediate of the size of nucleus, which can dissociate into its constituent monomers, followed by conformational conversion of the intermediate to the nucleus. Similarly, the effect of introduction of an additional step

involving conformational conversion cellular monomer to the amyloid form before or after attachment to the fiber can be investigated.

Finally, other phenomena such as crowding and formation of a gel like network of polymers can also result in a mismatch between the experimental data and the model simulation due to diffusional limitations. The dependence of rate constants on some these effects can also be incorporated into the model to improve fitting.

Once an appropriate model has been determined, global fitting of aggregation data obtained in the presence of different ions can provide useful insights such as whether the presence of co-solutes such as ions results in a change in the mechanism of aggregation. If there is no change in mechanism, then fitting experimental data collected in the presence of varying concentration of ions can tell us how the rates of reactions of the underlying fundamental processes are affected by the presence of different ions along the Hofmeister series. This can provide a clue to the mechanism of action of the ions. Further, the effect of shaking on the aggregation kinetics can also be studied to de-convolute the effect of shaking on breakage of fibers and fiber-catalyzed secondary nucleation.

Such a model can be a very powerful tool in determining the appropriate mechanism of aggregation of a particular protein using global fitting analysis. Once the most correct model is determined, it can be used to understand the effect of different environmental conditions on the aggregation mechanism and/or kinetics. It can also be used to determine fundamental differences in the aggregation mechanism of different proteins.

4.7 References

1. Shorter, J. and S. Lindquist, *Prions as adaptive conduits of memory and inheritance.* Nature Reviews Genetics, 2005. **6**(6): p. 435-450.

2. Nielsen, L., R. Khurana, A. Coats, S. Frokjaer, J. Brange, S. Vyas, V.N. Uversky, and A.L. Fink, *Effect of environmental factors on the kinetics of insulin fibril formation: elucidation of the molecular mechanism.* Biochemistry, 2001. **40**(20): p. 6036-6046.

3. Hellstrand, E., B. Boland, D.M. Walsh, and S. Linse, *Amyloid β-protein aggregation produces highly reproducible kinetic data and occurs by a two-phase process.* ACS chemical neuroscience, 2009. **1**(1): p. 13-18.

4. Morris, A.M., M.A. Watzky, J.N. Agar, and R.G. Finke, *Fitting neurological protein aggregation kinetic data via a 2-step, minimal/"Ockham's razor" model: the Finke-Watzky mechanism of nucleation followed by autocatalytic surface growth.* Biochemistry, 2008. **47**(8): p. 2413-2427.

5. Gibson, T.J. and R.M. Murphy, *Inhibition of insulin fibrillogenesis with targeted peptides.* Protein Science, 2006. **15**(5): p. 1133-1141.

6. Kamihira, M., A. Naito, S. Tuzi, A.Y. Nosaka, and H. Saitô, *Conformational transitions and fibrillation mechanism of human calcitonin as studied by high-resolution solid-state 13 C NMR.* Protein Science, 2000. **9**(5): p. 867-877.

7. Arosio, P., T.P. Knowles, and S. Linse, *On the lag phase in amyloid fibril formation.* Phys Chem Chem Phys, 2015. **17**(12): p. 7606-18.

8. Cohen, S.I., S. Linse, L.M. Luheshi, E. Hellstrand, D.A. White, L. Rajah, D.E. Otzen, M. Vendruscolo, C.M. Dobson, and T.P. Knowles, *Proliferation of amyloid-β42 aggregates occurs through a secondary nucleation mechanism.* Proceedings of the National Academy of Sciences, 2013. **110**(24): p. 9758-9763.

9. Cohen, S.I., M. Vendruscolo, C.M. Dobson, and T.P. Knowles, *From macroscopic measurements to microscopic mechanisms of protein aggregation.* J Mol Biol, 2012. **421**(2-3): p. 160-71.

10. Meisl, G., X. Yang, E. Hellstrand, B. Frohm, J.B. Kirkegaard, S.I. Cohen, C.M. Dobson, S. Linse, and T.P. Knowles, *Differences in nucleation behavior underlie the contrasting aggregation kinetics of the Aβ40 and Aβ42 peptides.* Proceedings of the National Academy of Sciences, 2014. **111**(26): p. 9384-9389.

11. Nicoud, L., S. Lazzari, D. Balderas Barragan, and M. Morbidelli, *Fragmentation of amyloid fibrils occurs in preferential positions depending on the environmental conditions.* J Phys Chem B, 2015. **119**(13): p. 4644-52.

12. Lee, C.C., A. Nayak, A. Sethuraman, G. Belfort, and G.J. McRae, *A three-stage kinetic model of amyloid fibrillation.* Biophys J, 2007. **92**(10): p. 3448-58.

13. Sorci, M., R.A. Grassucci, I. Hahn, J. Frank, and G. Belfort, *Time-dependent insulin oligomer reaction pathway prior to fibril formation: Cooling and seeding.* Proteins: Structure, Function, and Bioinformatics, 2009. **77**(1): p. 62-73.

14. Cohen, S.I., M. Vendruscolo, M.E. Welland, C.M. Dobson, E.M. Terentjev, and T.P. Knowles, *Nucleated polymerization with secondary pathways. I. Time evolution of the principal moments.* J Chem Phys, 2011. **135**(6): p. 065105.

15. Cohen, S.I., M. Vendruscolo, C.M. Dobson, and T.P. Knowles, *Nucleated polymerization with secondary pathways. II. Determination of self-consistent solutions to growth processes described by non-linear master equations.* The Journal of chemical physics, 2011. **135**(6): p. 08B611.

16. Cohen, S.I., M. Vendruscolo, C.M. Dobson, and T.P. Knowles, *Nucleated polymerization with secondary pathways. III. Equilibrium behavior and oligomer populations.* J Chem Phys, 2011. **135**(6): p. 065107.

17. Meisl, G., J.B. Kirkegaard, P. Arosio, T.C. Michaels, M. Vendruscolo, C.M. Dobson, S. Linse, and T.P. Knowles, *Molecular mechanisms of protein aggregation from global fitting of kinetic models.* Nat Protoc, 2016. **11**(2): p. 252-72.

18. Knowles, T.P., C.A. Waudby, G.L. Devlin, S.I. Cohen, A. Aguzzi, M. Vendruscolo, E.M. Terentjev, M.E. Welland, and C.M. Dobson, *An analytical solution to the kinetics of breakable filament assembly.* Science, 2009. **326**(5959): p. 1533-7.

19. Allen, K.D., R.D. Wegrzyn, T.A. Chernova, S. Müller, G.P. Newnam, P.A. Winslett, K.B. Wittich, K.D. Wilkinson, and Y.O. Chernoff, *Hsp70 Chaperones as Modulators of Prion Life Cycle Novel Effects of Ssa and Ssb on the Saccharomyces cerevisiae Prion [PSI+]*. Genetics, 2005. **169**(3): p. 1227-1242.

20. Hartl, F.U. and M. Hayer-Hartl, *Converging concepts of protein folding in vitro and in vivo.* Nat Struct Mol Biol, 2009. **16**(6): p. 574-81.

21. Muchowski, P.J. and J.L. Wacker, *Modulation of neurodegeneration by molecular chaperones.* Nature Reviews Neuroscience, 2005. **6**(1): p. 11-22.

22. Dunstan, D.E., P. Hamilton-Brown, P. Asimakis, W. Ducker, and J. Bertolini, *Shear flow promotes amyloid-{beta} fibrilization.* Protein Eng Des Sel, 2009. **22**(12): p. 741-6.

23. Hill, E.K., B. Krebs, D.G. Goodall, G.J. Howlett, and D.E. Dunstan, *Shear flow induces amyloid fibril formation.* Biomacromolecules, 2006. **7**(1): p. 10-13.

CHAPTER 5. CONCLUSIONS, PERSPECTIVES, AND FUTURE RECOMMENDATIONS

Proteins are an important class of functional biomolecules. Most of the biological functions in the human body are performed by proteins. Proteins in the form of enzymes, vaccines, antibodies etc. also comprise a large sector of the biopharmaceutical industry. The functionality of protein molecules is integrally tied to their structure. Therefore, proper folding into their functional folded state is crucial for optimal biological activity and to maintain the efficacy of protein based pharmaceutical products. The deleterious effects of improper folding and aggregation of proteins have been discussed earlier in this thesis. To effectively prevent misfolding/unfolding and aggregation it is crucial to understand these adverse processes as well as the factors which promote or inhibit them. This thesis explores the influence of ions on the aggregation behavior of amyloids. The insights from this work not only aid towards a better understanding of amyloid aggregation but also can be useful to predict and prevent aggregation of proteins during production, storage, and transport in the biopharmaceutical industry. Ions are ubiquitous in biology and are also important components of many solutions like buffers and stabilizer solutions that are frequently used in the biopharmaceutical industry where ion-specific effects may give rise to problems like aggregation [1]. The co-existence of ions with biological proteins as well as biopharmaceutical products makes it important to study the influence of ions on protein aggregation. Moreover, ions can pass the blood-brain barrier (BBB) and affect the amyloidogenic proteins present in the central nervous system that are involved in neurodegenerative diseases. For example, lithium carbonate, which was prescribed as a

drug for mood disorders, has been shown to cross the BBB. This highlights the importance of studying the effect of ions on amyloid formation [2].

Building on the previous work by our group on ion-specific effects on amyloid aggregation and strain formation [3], we have shown in Chapter 2 of this thesis that ions can also regulate cross-species prion transmission. The results presented in this work highlight the relative contributions of protein sequence, prion strain, and environment on species barrier. We have shown that ions present during co-aggregation have a systematic influence on the barrier while ions used to form the donor or seed amyloid can affect the barrier specificity. An important follow up question that arises from this investigation is *whether the resulting morphology of the aggregates formed after seeding is dictated by the environment of aggregation or the seed strain*. Such an investigation would reveal how faithfully the amyloid seed conformation is adopted and propagated when the environment of aggregation is altered from the conditions which were initially used to form the seed.

Chapter 3 of this thesis entails a systematic investigation of the effect of ions on amyloid aggregation by two different amyloid proteins, Sup35NM and Amyloid β-42. We show that ions can have varied effects on amyloid formation by these proteins. pH of the solution also plays an important role in determining the how ions interact with proteins in solution, thereby affecting the aggregation kinetics. While ion-protein interactions follow expectations per the relative positions of the ions in the Hofmeister series for both proteins, the absolute effects on the aggregation kinetics of the two proteins are not always similar. This suggests that there may be differences in the mechanisms of aggregation of these proteins. An interesting question which arises from this study is *what is the degree to which amyloid conformation and morphology are determined by the ionic strength of the solution*

vs the identity of the ions (or the environment)? Investigation of the morphology of the amyloids formed by Sup35NM and $A\beta_{42}$ in the presence of varying concentrations of different ions and at varied pH values can shed light onto this question. If ion identity/character is the primary determinant of the morphology then we can expect the morphology to be different in the presence of kosmotropic and chaotropic ions (as previously observed for Sup35NM [3]). On the other hand, if the morphology is primarily determined by ionic strength then we can expect changes in the amyloid morphology to be related to increase or decrease in ionic strength irrespective of ion identity/character. It would also be worthwhile to investigate the effect of other environmental factors which affect the aggregation kinetics to ascertain the primary determinant of amyloid structure. For example, the effect of temperature on various amyloidogenic proteins has been widely studied and increase in temperature has been reported to promote faster kinetics [4-6]. Interestingly, however, Sup35NM aggregates with a 'strong' phenotype and low thermal stability were formed at a low temperature of 4ºC (which is expected to result in slow kinetics), whereas Sup35NM aggregates with a 'weak' phenotype and high thermal stability were observed at a high temperature of 37ºC (which is expected to result in fast kinetics) [6]. These are contrary to our group's previous observations that fast Sup35NM aggregation kinetics correlated with a 'strong' phenotype and low thermal stability and vice versa [3]. While phenotype and thermal stability may be related to morphology such that we expect aggregates with a 'strong' phenotype and low thermal stability to have smaller and shorter fibers and vice versa, it is still necessary to image the aggregates to ascertain their morphology. Therefore, a similar detailed investigation of the effect of other factors such as temperature, agitation, other non-ionic co-solutes etc. on kinetics and

morphology and physiochemical properties of aggregates might conclusively answer the question that we have posed above.

Moreover, a plausible explanation for the differences in the aggregation behavior of Sup35NM and $A\beta_{42}$ proposed in Chapter 3 favors a non-classical two-step nucleation process over the classical one-step process of nucleation. While experimental corroboration of either nucleation process is an extremely challenging task, it may be possible to provide some confirmation with the help of a computational model that fits the aggregation data. Computational models based on the kinetics of aggregation have been used to ascertain the most likely aggregation mechanisms of different proteins [7, 8]. In this work, we have also attempted to develop a computational model for Sup35NM aggregation kinetics. While amyloid aggregation in the most general sense is considered to follow a nucleation-polymerization mechanism, there may be subtle differences in the individual processes like nucleation, elongation, and secondary processes for different amyloidogenic proteins. Kinetic models that successfully fit aggregation data can be used to gain insights into the most likely mechanism of aggregation. Here, we have developed a simulation based model which can be modified to suit any mechanism. A logical future step would be to include the two-step process of nucleus formation involving agglomeration of monomers to form a pre-defined oligomer followed by conformation conversion to form the nucleus [9]. Modification of the nucleation step of our best performing model mechanism, saturated elongation and fragmentation, into a two-step nucleation process may reduce the mismatch between the experimental data and the model.

Finally, a rewarding activity would be to compile the effects of ions of the Hofmeister series on amyloidogenic as well as non-amyloidogenic proteins in a form

similar to the Hofmeister phase diagram for colloidal particles [10]. This would entail literature search for previously observed effects as well as a similar systematic analysis of the effect of ions on other proteins as performed in this work. This would help to cluster proteins with similar behavior together which might help uncover other patterns or similarities and, thus, aid in understanding some of these ion-specific effects which are not yet clearly understood in the context of complex protein molecules. It could also be used to make predictions which can be verified through experiments.

In summary, this thesis advances the understanding of the effect of ions on aggregation of amyloids/prions and cross-species prion transmission through detailed investigations as described in Chapters 2 and 3, and provides a modelling framework for fitting amyloid aggregation data as discussed in Chapter 4. The significance of this work is two fold. Primarily it provides a better understanding of the fundamentals of amyloid formation and propagation, which may one day help in the development of more effective drugs/therapies for amyloid/prion diseases. Moreover, this knowledge can be applied to prevent the formation of protein aggregates in the biopharmaceutical industry and help in the development of safer biopharmaceuticals.

References

1. Lo Nostro, P. and B.W. Ninham, *Hofmeister phenomena: an update on ion specificity in biology.* Chemical reviews, 2012. **112**(4): p. 2286-2322.

2. Ehrlich, B.E. and J.M. Diamond, *Lithium, membranes, and manic-depressive illness.* Journal of Membrane Biology, 1980. **52**(3): p. 187-200.

3. Rubin, J., H. Khosravi, K.L. Bruce, M.E. Lydon, S.H. Behrens, Y.O. Chernoff, and A.S. Bommarius, *Ion-specific effects on prion nucleation and strain formation.* J Biol Chem, 2013. **288**(42): p. 30300-8.

4. Nicoud, L., S. Lazzari, D. Balderas Barragan, and M. Morbidelli, *Fragmentation of amyloid fibrils occurs in preferential positions depending on the environmental conditions.* J Phys Chem B, 2015. **119**(13): p. 4644-52.

5. Sabaté, R., A. Villar-Piqué, A. Espargaró, and S. Ventura, *Temperature dependence of the aggregation kinetics of Sup35 and Ure2p yeast prions.* Biomacromolecules, 2011. **13**(2): p. 474-483.

6. Tanaka, M., P. Chien, N. Naber, R. Cooke, and J.S. Weissman, *Conformational variations in an infectious protein determine prion strain differences.* Nature, 2004. **428**(6980): p. 323-328.

7. Cohen, S.I., S. Linse, L.M. Luheshi, E. Hellstrand, D.A. White, L. Rajah, D.E. Otzen, M. Vendruscolo, C.M. Dobson, and T.P. Knowles, *Proliferation of amyloid-β42 aggregates occurs through a secondary nucleation mechanism.* Proceedings of the National Academy of Sciences, 2013. **110**(24): p. 9758-9763.

8. Meisl, G., X. Yang, E. Hellstrand, B. Frohm, J.B. Kirkegaard, S.I. Cohen, C.M. Dobson, S. Linse, and T.P. Knowles, *Differences in nucleation behavior underlie the contrasting aggregation kinetics of the Aβ40 and Aβ42 peptides.* Proceedings of the National Academy of Sciences, 2014. **111**(26): p. 9384-9389.

9. Serio, T.R., A.G. Cashikar, A.S. Kowal, G.J. Sawicki, J.J. Moslehi, L. Serpell, M.F. Arnsdorf, and S.L. Lindquist, *Nucleated conformational conversion and the replication of conformational information by a prion determinant.* Science, 2000. **289**(5483): p. 1317-21.

10. Schwierz, N., D. Horinek, and R.R. Netz, *Reversed anionic Hofmeister series: the interplay of surface charge and surface polarity.* Langmuir, 2010. **26**(10): p. 7370-9.

APPENDIX A. SEQUENCE ALIGNMENTS

The N-domains of Sup35 protein from *Saccharomyces cerevisiae*, *Saccharomyces paradoxus*, and *Saccharomyces bayanus* were aligned using ClustalW.

```
SC              MSDSNQGNNQQNYQQYSQNGNQQQGNNRYQGYQAYNAQAQ-PAGGYYQNYQGYSGYQQGG 59
SP              MSDSNQGNNQQSYQQYGQNSNQQQGNNRSQGYQAYNAQSQ-PAGGYYQNYQGYSGYQQGS 59
SB              MSDSNQGNNQQNYQQYGQNFNQQQGNNKFQGYQAYNAQAQQPAGGYYQNPQGYAGYQQGG 60
                ********** .**** .** ******* : ********* :* ******* *** :***** .

SC              Y-QQYNPDAGYQQQYNPQGGYQQYNPQGGYQQQFNPQGGRGNYKNFNYNNNLQGYQAGFQ 118
SP              Y-QQHNPDAGYQQQYNPQGGYQQYNPQGGYQQQFNPQGGRGNYKNFNYNNNAQGYQAGFQ 118
SB              YDQQFNPEAGYQQQYNAQG---------GYQQQFNPQGGRGNYKSFNYSNNQQGFQAGFQ 111
                * ** .** :******** .**         *************** .*** .** ** :*****

SC              PQSQG 123
SP              PQSQG 123
SB              PQSQG 116
                *****
```

Figure A.1 – Sequence alignment of Sup35N from *S. cerevisiae*, *S. paradoxus*, and *S. bayanus*

APPENDIX B. COMPARISON OF SUP35NM AND AMYLOID BETA -42 AMINO ACID COMPOSITION

Table 3 – Amino acid composition and some properties of Sup35NM and $A\beta_{42}$ and their amyloidogenic domains calculated using ProtParam

	$A\beta_{1-42}$	$A\beta_{15-42}$	Sup35NM	Sup35N
Ala	4	3	16	6
Arg	1	0	2	2
Asn	1	1	27	20
Asp	3	1	9	2
Cys	0	0	0	0
Gln	1	1	41	35
Glu	3	1	22	0
Gly	6	5	23	21
His	3	0	1	0
Ile	3	3	3	0
Leu	2	2	8	1
Lys	2	2	25	1
Met	1	1	2	1
Phe	3	2	4	3
Pro	0	0	14	6
Ser	2	1	15	5
Thr	0	0	11	0
Trp	0	0	0	0
Tyr	1	0	20	20
Val	6	5	10	0
Total number of residues	42	28	253	123
pI	5.31	6.07	5.3	7.81
Aliphatic Index	97.38	132.14	34.74	8.05
GRAVY	0.205	1.086	-1.596	-1.915

APPENDIX C. MATRIX IMPLEMENTATION OF THE AGGREGATION SIMULATION MODEL

The initial matrix implementation of the model comprising of nucleation, elongation, and fragmentation and its MATLAB code was developed by Harrison B. Rose. Below is a matrix implementation of the initial model plus secondary nucleation. The case of saturating elongation has been discussed at the end of this section.

Rate constant of formation of n_i from size below plus monomer and nucleation

$$k_1(length) = \begin{cases} 0, & length < n_c \\ p_1 k_{ef}, & length \geq n_c \end{cases}$$

$$\frac{\mathrm{dx}}{\mathrm{dt}}_{\mathrm{Q1}} = \begin{bmatrix} \frac{\mathrm{dp_1}}{\mathrm{dt}} \\ \frac{\mathrm{dp_2}}{\mathrm{dt}} \\ \frac{\mathrm{dp_3}}{\mathrm{dt}} \\ \frac{\mathrm{d}p_4}{\mathrm{dt}} \\ \vdots \\ \frac{\mathrm{dp_{max-1}}}{\mathrm{dt}} \\ \frac{\mathrm{d}p_{\mathrm{max}}}{\mathrm{dt}} \end{bmatrix}$$

$$= \begin{bmatrix} \times \mathrm{p_1} & \times \mathrm{p_2} & \times \mathrm{p_3} & \times \mathrm{p_4} & & \times \mathrm{p_{max-2}} & \times \mathrm{p_{max-1}} \\ \vec{0} & \vec{0} & \vec{0} & \vec{0} & \cdots & \vec{0} & \vec{0} \\ k_1(1) & 0 & 0 & 0 & \cdots & 0 & 0 \\ 0 & k_1(2) & 0 & 0 & \cdots & 0 & 0 \\ 0 & 0 & k_1(3) & 0 & \cdots & 0 & 0 \\ \vdots & \vdots & \vdots & \vdots & \ddots & \vdots & \vdots \\ 0 & 0 & 0 & 0 & \cdots & k_1(max-2) & 0 \\ 0 & 0 & 0 & 0 & \ldots & 0 & k_1(max-1) \end{bmatrix} \begin{bmatrix} \mathrm{p_1} \\ \mathrm{p_2} \\ \mathrm{p_3} \\ \mathrm{p_4} \\ \vdots \\ \mathrm{p_{max-1}} \end{bmatrix}$$

$$+ \begin{bmatrix} 0 \\ 0 \\ \vdots \\ p_1^{n_c} * (k_{pn} + F_m * k_{sn}) \\ \vdots \\ 0 \end{bmatrix}$$

Rate constant of formation of n_i by breakage of all sizes > n_c

$$k_b(location, length) = 2 * \begin{cases} \mathrm{k_b}\left(-\mathrm{abs}\left(\mathrm{location} - \frac{\mathrm{length}}{2}\right) + \frac{\mathrm{length}}{2}\right), & location > 1 \\ (k_b + k_{er})\left(-\mathrm{abs}\left(\mathrm{location} - \frac{\mathrm{length}}{2}\right) + \frac{\mathrm{length}}{2}\right), & location = 1 \end{cases}$$

$$\frac{\mathrm{dx}}{\mathrm{dt}_{\mathrm{Q2}}} = \begin{bmatrix} \frac{dp_1}{dt} \\ \frac{dp_2}{dt} \\ \frac{dp_3}{dt} \\ \frac{dp_4}{dt} \\ \vdots \\ \frac{dp_{max-1}}{dt} \\ \frac{dp_{max}}{dt} \end{bmatrix}$$

$$= \begin{bmatrix} \overset{\times p_1}{\widehat{0}} & \overset{\times p_2}{\widehat{k_b(1,2)}} & \overset{\times p_3}{\widehat{k_b(1,3)}} & \overset{\times p_4}{\widehat{k_b(1,4)}} & \cdots & \overset{\times p_{max-1}}{\widehat{k_b(1,max-1)}} & \overset{\times p_{max}}{\widehat{k_b(1,max)}} \\ 0 & 0 & k_b(2,3) & k_b(2,4) & \cdots & k_b(2,max-1) & k_b(2,max) \\ 0 & 0 & 0 & k_b(3,4) & \cdots & k_b(3,max-1) & k_b(3,max) \\ 0 & 0 & 0 & 0 & \cdots & k_b(4,max-1) & k_b(4,max) \\ \vdots & \vdots & \vdots & \vdots & \ddots & \vdots & \vdots \\ 0 & 0 & 0 & 0 & \cdots & 0 & k_b(max-1,max) \\ 0 & 0 & 0 & 0 & \ldots & 0 & 0 \end{bmatrix} \begin{bmatrix} p_1 \\ p_2 \\ p_3 \\ p_4 \\ \vdots \\ p_{max-1} \\ p_{max} \end{bmatrix}$$

Rate constant of loss of p_i by breakage to smaller sizes

$$k_2(length) = \sum_{location=1}^{length=i} k_b(location, length)$$

Note that we count only up to the floor (rounding down) of half of the polymer length, so as not to double-count breakage events

$$\frac{\mathrm{dx}}{\mathrm{dt}_{\mathrm{Q3}}} = \begin{bmatrix} \frac{\mathrm{dp}_1}{\mathrm{dt}} \\ \frac{\mathrm{dp}_2}{\mathrm{dt}} \\ \frac{\mathrm{dp}_3}{\mathrm{dt}} \\ \frac{\mathrm{dp}_4}{\mathrm{dt}} \\ \vdots \\ \frac{\mathrm{dp}_{\mathrm{max}-1}}{\mathrm{dt}} \\ \frac{\mathrm{dp}_{\mathrm{max}}}{\mathrm{dt}} \end{bmatrix} = \begin{bmatrix} \overset{\times \mathrm{p}_1}{\widehat{0}} & \overset{\times p_2}{\widehat{0}} & \overset{\times p}{\widehat{0}} & \overset{\times \mathrm{p}_4}{\widehat{0}} & \cdots & \overset{\times \mathrm{p}_{\mathrm{max}-1}}{\widehat{0}} & \overset{\times \mathrm{p}_{\mathrm{max}}}{\widehat{0}} \\ 0 & k_2(2) & 0 & 0 & \cdots & 0 & 0 \\ 0 & 0 & k_2(3) & 0 & \cdots & 0 & 0 \\ 0 & 0 & 0 & k_2(4) & \cdots & 0 & 0 \\ \vdots & \vdots & \vdots & \vdots & \ddots & \vdots & \vdots \\ 0 & 0 & 0 & 0 & \cdots & k_2(max-1) & 0 \\ 0 & 0 & 0 & 0 & \ldots & 0 & k_2(\mathrm{max}) \end{bmatrix} \begin{bmatrix} \mathrm{p}_1 \\ \mathrm{p}_2 \\ \mathrm{p}_3 \\ \mathrm{p}_4 \\ \vdots \\ \mathrm{p}_{\mathrm{max}-1} \\ \mathrm{p}_{\mathrm{max}} \end{bmatrix}$$

Rate constant of loss by formation of polymer of one size above

$$k_3(length) = \begin{cases} p_1^{n_c-1} * (k_{pn} + k_{sn} F_M), & length = n_c - 1 \\ p_1 k_e, & length \geq n_c \end{cases}$$

$$\frac{\mathrm{dx}}{\mathrm{dt}_{\mathrm{Q4}}} = \begin{bmatrix} \frac{\mathrm{dp}_1}{\mathrm{dt}} \\ \frac{\mathrm{dp}_2}{\mathrm{dt}} \\ \frac{\mathrm{dp}_3}{\mathrm{dt}} \\ \frac{\mathrm{dp}_4}{\mathrm{dt}} \\ \vdots \\ \frac{\mathrm{dp}_{\mathrm{max}-1}}{\mathrm{dt}} \\ \frac{\mathrm{dp}_{\mathrm{max}}}{\mathrm{dt}} \end{bmatrix} = \begin{bmatrix} \overset{\times \mathrm{p}_1}{\overbrace{2 * k_3(1)}} & \overset{\times \mathrm{p}_2}{\widehat{0}} & \overset{\times p_3}{\widehat{0}} & \overset{\times \mathrm{p}_4}{\widehat{0}} & \cdots & \overset{\times \mathrm{p}_{\mathrm{max}-1}}{\widehat{0}} & \overset{\times \mathrm{p}_{\mathrm{max}}}{\widehat{0}} \\ 0 & k_3(2) & 0 & 0 & \cdots & 0 & 0 \\ 0 & 0 & k_3(3) & 0 & \cdots & 0 & 0 \\ 0 & 0 & 0 & k_3(4) & \cdots & 0 & 0 \\ \vdots & \vdots & \vdots & \vdots & \ddots & \vdots & \vdots \\ 0 & 0 & 0 & 0 & \cdots & k_3(max-1) & 0 \\ 0 & 0 & 0 & 0 & \ldots & 0 & 0 \end{bmatrix} \begin{bmatrix} \mathrm{p}_1 \\ \mathrm{p}_2 \\ \mathrm{p}_3 \\ \mathrm{p}_4 \\ \vdots \\ \mathrm{p}_{\mathrm{max}-1} \\ \mathrm{p}_{\mathrm{max}} \end{bmatrix}$$

Here,

k_{pn} is the primary nucleation rate constant,

k_{ef} is the monomer association rate constant,

k_{er} is the monomer dissociation rate constant,

k_b is the breakage rate constant

k_{sn} is the secondary nucleation rate constant,

F_m is fiber mass fraction

n_c is the nucleus size

The special case of saturating elongation can be implemented by replacing k_e with $\frac{k_e}{1+\frac{n_1}{K_e}}$, where K_e is the crossover concentration above which structural organization of the monomer for attachment to the fiber becomes rate limiting.